UNCLASSIFI[redacted]
SECURITY CLASSIFI[redacted]HIS PAGE

DTIC FILE COPY

REPORT DOCUMENTATION PAGE

1a.	1b. RESTRICTIVE MARKINGS
2a. / 2b. **AD-A218 372**	3. DISTRIBUTION / AVAILABILITY OF REPORT UNLIMITED Approved for public release, distribution unlimited
4. PERFORMING ORGANIZATION REPORT NUMBER(S) SEI-88-11-15-WB	5. MONITORING ORGANIZATION REPORT NUMBER(S) AFOSR-TR. 90-0201
6a. NAME OF PERFORMING ORGANIZATION Techno-Sciences, Inc. / 6b. OFFICE SYMBOL (If applicable)	7a. NAME OF MONITORING ORGANIZATION
6c. ADDRESS (City, State, and ZIP Code) 7833 Walker Drive, Suite 620 Greenbelt, Maryland 20770	7b. ADDRESS (City, State, and ZIP Code) AFOSR/NA Bolling AFB DC 20332-6448
8a. NAME OF FUNDING / SPONSORING ORGANIZATION Air Force Office of Scientific Research / 8b. OFFICE SYMBOL (If applicable) NA	9. PROCUREMENT INSTRUMENT IDENTIFICATION NUMBER F49620-87-C-0103
8c. ADDRESS (City, State, and ZIP Code) Bldg. 410 Bolling AFB, DC 20332-6448	10. SOURCE OF FUNDING NUMBERS PROGRAM ELEMENT NO. 61102F / PROJECT NO. 2312 / TASK NO. A1 / WORK UNIT ACCESSION NO

11. TITLE (Include Security Classification)
Nonlinear Dynamics and Control of Flexible Structures

12. PERSONAL AUTHOR(S)
W. Bennett, H. Kwatny, G. Blankenship, O. Akhrif

13a. TYPE OF REPORT	13b. TIME COVERED	14. DATE OF REPORT (Year, Month, Day)	15. PAGE COUNT
Annual	FROM 9/87 TO 8/88	11/15/88	62

16. SUPPLEMENTARY NOTATION

17 COSATI CODES			18. SUBJECT TERMS (Continue on reverse if necessary and identify by block number)
FIELD	GROUP	SUB-GROUP	Multibody dynamics, Nonlinear, feedback/control

19. ABSTRACT (Continue on reverse if necessary and identify by block number)

See Reverse

DTIC ELECTE FEB 26 1990 S D Cx B

20. DISTRIBUTION / AVAILABILITY OF ABSTRACT	21. ABSTRACT SECURITY CLASSIFICATION
☒ UNCLASSIFIED/UNLIMITED ☐ SAME AS RPT ☑ DTIC USERS	UNCLASSIFIED

22a. NAME OF RESPONSIBLE INDIVIDUAL	22b. TELEPHONE (Include Area Code)	22c. OFFICE SYMBOL
Lt. Col. George Haritos	(202) 767-[redacted]0463	AFOSR/NA

DD FORM 1473, 84 MAR — 83 APR edition may be used until exhausted. All other editions are obsolete.

SECURITY CLASSIFICATION OF THIS PAGE
UNCLASSIFIED

ABSTRACT

The unprecedented requirements for rapid retargeting and precision pointing for spaced-based directed energy weapon platforms is the prime driver behind the reported modeling and control study. The combination of such requirements demand a comprehensive dynamic model of the nonlinear multibody dynamics of typical space platforms for such weapon including the interaction with the platform structural flexure effecting principal weapon system effective Line-Of-Sight. This report describes the first year effort of a three year project which focuses on: (1) the development of comprehensive; generic nonlinear dynamical models for typical space-based plat forms, (2) the development of high performance, nonlinear control laws for rapid slewing and precesion pointing of primary weapon system payload apertures, and (3) the design of a series of laboratory experiments to verify and test the control laws developed. The validation of the analytical models and the required control theory for the resulting class of nonlinear system is described in this report. Simulation results are given for a simplified benchmark model of a space-based laser slewing control and consideration for compensation for structural flexure effecting optical LOS using optical steering mirrors is discussed.

DISCLAIMER NOTICE

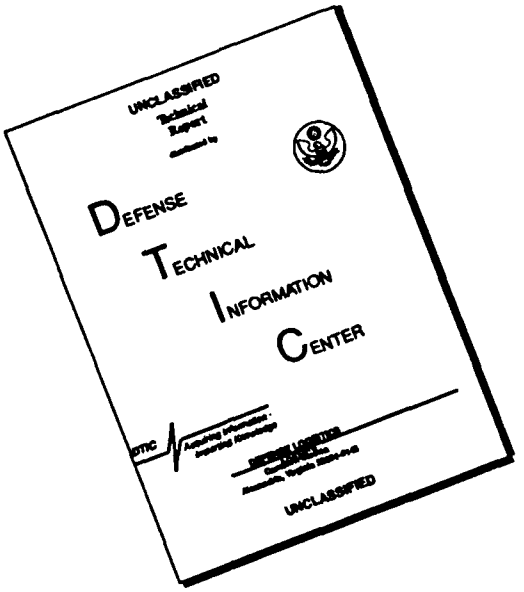

THIS DOCUMENT IS BEST QUALITY AVAILABLE. THE COPY FURNISHED TO DTIC CONTAINED A SIGNIFICANT NUMBER OF PAGES WHICH DO NOT REPRODUCE LEGIBLY.

distribution unlimited. SEI-87

Nonlinear Dynamics and Control of Flexible Structures

Annual Report

Sept. 1, 1987 – Aug. 31, 1988
for AFOSR Contract F49620-87-C-0103

W.H. Bennett, H.G. Kwatny, G.L. Blankenship, O. Akhrif

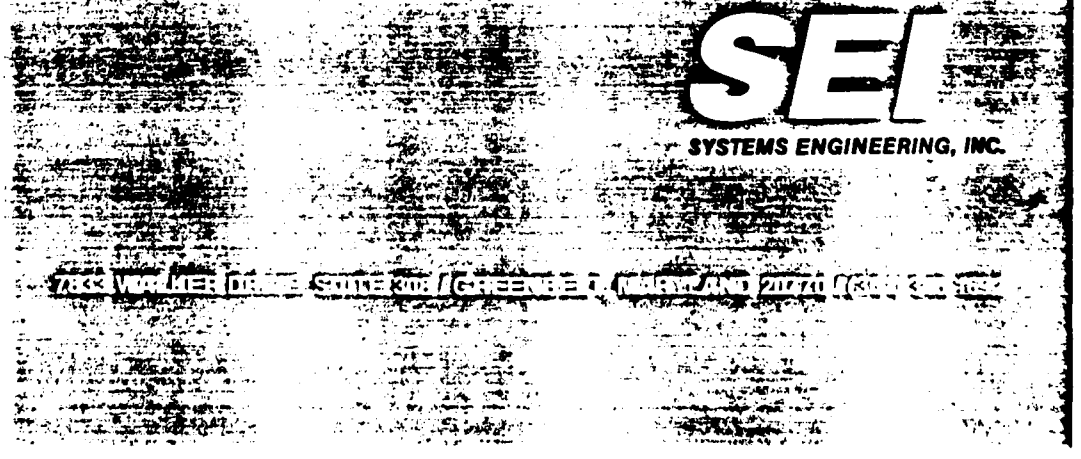

SEI-88-11-15-WB

Nonlinear Dynamics and Control of Flexible Structures

Annual Report

Sept. 1, 1987 – Aug. 31, 1988
for AFOSR Contract F49620-87-C-0103

W.H. Bennett, H.G. Kwatny, G.L. Blankenship, O. Akhrif

SYSTEMS ENGINEERING, INC.
Greenbelt, MD 20770

with appendix by T.A.W. Dwyer, III

Submitted to
Air Force Office of Scientific Research
Directorate of Mathematical and Information Sciences
Bolling Air Force Base, DC 20332-6448
Attn: Ltn. Col. James M. Crowley

Date: Nov. 15, 1988

Foreword

This report contains details of the first year of a three year research study on nonlinear modeling and control of flexible space structures with application to rapid slewing and precision pointing of space-based directed energy weapons. The project is funded by SDIO/IST and managed by AFOSR/SDIO (AFSC). Results reported herein are for the period 1 Sept. 1987 - 31 Aug. 1988.

The project is managed by Ltn. Col. James M. Crowley/AFOSR/NM and Dr. Anthony Amos/AFOSR/NA. We wish to thank both of these individuals for their insight and direction on this project.

1 Research Objectives and Project Summary

The primary research objectives of the first year effort in nonlinear modeling and control of flexible space structures has been in two areas. First, we have considered nonlinear modeling of a generic class of multibody systems with elastic interactions with primary focus on a generic model for structural interactions effecting laser system *line-of-sight (LOS)* pointing for a *Space-Based Laser (SBL)* weapon. Second, we have developed practical extensions and applications of the theory of nonlinear control system synthesis based on the ideal of effective global linearization by feedback transformation. Our approach to nonlinear control has been based on the ideal of *Partial Feedback Linearization (PFL)* with respect to a principal system output representing optical system pointing.

During the performance period 1 September, 1987 - 31 August, 1988 we performed an extensive literature survey of available dynamic models and control system issues relating to primary system performance for a space-based Directed Energy Weapon (DEW). Critical requirements for precision line-of-sight (LOS) pointing and tracking together with requirements for rapid slewing of spacecraft primary body together with possible articulated weapon system aperture have been isolated as important control problems relating to system performance (see Figure 1.1). Additionally, beam quality and jitter is related to probably of kill and is largely effected by controlling alignment of elements within the beam expander. Our efforts have focused on developing a generic collection of models for SBL type systems including provisions for: 1) a primary body with attitude control components including either reaction wheels or control moment gyros and reaction jets, 2) a secondary body representing the beam expander base structure, and 3) a continuum beam representing structural support for the secondary mirror of the beam expander. The modeling approach is readily adaptable to the generic problem of rapid slewing and precision pointing of a multibody system subject to elastic deformation. We have developed a series of generic models of increasing complexity to study the critical nonlinear dynamics effecting LOS pointing and optical system alignment for a benchmark SBL system. A computer simulation was developed and preliminary system tradeoffs are detailed in this report.

In the area of nonlinear control design for rapid slewing and precision pointing we have demonstrated the potential for decoupling control synthesis wherein the flexible dynamics of the weapon system secondary mirror support structure can be decoupled from the effective weapon system LOS by the introduction of nonlinear feedback. The generic class of such transformations obtained for the SBL slewing models we have investigated have a special structure which permits the decoupling/linearizing transformation to be implemented simply by using multiple actuators. One way in which this may be used to advantage is in the integration of continuous mode (e.g. reaction wheels, CMG's, etc.) and discontinuous (on/off) actuation (e.g. jets). In particular, continuous actuation can be used to effect the exact linearizing transformation and decoupling of the structural flexure from the LOS while reaction jets can be used for large angle slewing control. This has significant advantages for rapid slewing.

We have also identified the potential for the application of low cost accelerometers as the primary sensors for implementing the feedback linearizing control laws. The primary benefits

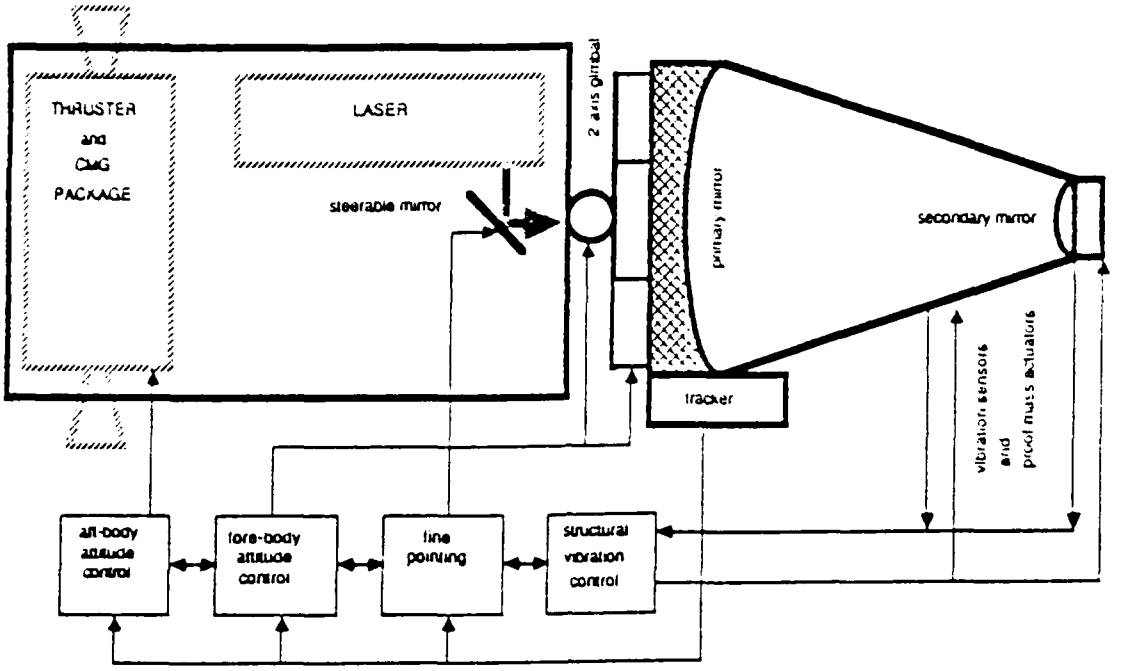

Figure 1.1: Generic Space-Based Laser System with Multiple Control Systems

which may accrue from the use of a relatively large number of accelerometers mounted on certain critical structural components are 1) a reduction in the sensitivity of the decoupling control to detailed knowledge of the elastic stiffness and damping properties of the structure and 2) simplified computational requirements for on-line implementation of the nonlinear decoupling control.

A critical observation in our studies of control architectures for SBL systems is the integration of a variety of actuators for spacecraft attitude control (e.g. thruster jets, momentum wheels, CMG's, etc.), multibody articulation, optical system components (e.g. steering and deformable focusing mirrors), and structural vibration control (e.g. proof mass devices, embedded piezoelectrics, etc.) to achieve principal system performance objectives. In this report we give several examples including simulation results demonstrating options for the integration of various actuators to achieve optical system LOS decoupling from structural deformation using optical components.

A critical feature of the control integration problem for rapid slewing is the relative levels of control authority and control bandwidth achievable from the above spectrum of actuator technologies. The system requirements study [Gea88] presents a comprehensive assessment of engineering design requirements for control of SBL type systems and motivates requirements for 1) torque shaping for deformation control, and 2) actuator sizing for slewing control. In a series of papers and a technical report which we have included as an appendix, Prof. Dwyer describes a design approach for deformation shaping of torques required for feedback linearization. In the second year effort we will study the application of these methods for implementing rapid slewing with available torque actuators.

List of Technical Publications In conjunction with this project we have prepared the following papers for presentation at technical conferences:

1. "A Computer Algorithm for Causal Spectral Factorization", Wm. H. Bennett and Ing Yan, *Proc. 1988 NAECON*, Dayton, Ohio in May, 1988.

2. "Computation and Implementation of Precision Control for Flexible Space Structures", Wm. H. Bennett, *Proc. 1988 ComCon: Advances in Communications and Control Systems*, Baton Rouge, LA, October 1988.

3. "Nonlinear Dynamics and Control Issues for Flexible Space Platforms", H.G. Kwatny and Wm. H. Bennett, *Proc. 27th IEEE Conference on Decision and Control* Austin, TX, December 1988.

4. "Boresight Disturbance Modeling of a Space-based Electromagnetic Rail Gun", T. A. W. Dwyer, III and J.W. Wade, *Proc. 1988 American Control Conference*, Atlanta, GA, June, 1988.

5. "Slew Induced Deformation Shaping", T. A. W. Dwyer, III. *Proc. 27th IEEE Conference of Decision and Control*, Austin, TX, December 1988.

6. "Nonlinear Modeling and Estimation of Slew Induced Structural Deformation", T. A. W. Dwyer, *Proc. ASME Winter Annual Meeting*, Chicago, IL., Nov. 1988.

We have also organized an invited session on Nonlinear Modeling and Control of Aerospace Systems at the 1988 IEEE Control Decision Conference.

Professional Personnel The principal investigator for this project is Dr. William H. Bennett and co-principal investigators are Drs. Harry G. Kwatny and Gilmer L. Blankenship from TSI and Prof. Thomas A. W. Dwyer at University of Illinois. We would also like to acknowledge the parttime support from Ms. Oussima Akhrif who is currently a Ph. D. candidate within the Electrical Engineering Department of the University of Maryland.

Contents

List of Figures

List of Tables

2 Status of the Research Effort: Initial Conclusions

The performance requirements of space-based directed energy weapons as well as other large aperture optical systems will place unprecedented demands on the control precision for such critical mission objectives as optical systems pointing and tracking and retargeting maneuvers. System requirements for rapid retargeting typically involve large angle slewing maneuvers involving the spacecraft bus together with large optical system structures which may or may not be articulated as part of slewing. Such maneuvers will involve nonlinear kinematics and gyroscopic coupling, which is further complicated by coupling with the deformation of the optical train support structure.

Our objective is to demonstrate the feasibility and benefits of advanced nonlinear control design methods for rapid slewing and precision pointing of spaced-based platforms subject to structural flexure effecting primary system LOS and focusing. Our primary focus comes from requirements for rapid retargeting of space based laser systems. To be meaningful, such an analysis must be based on models of realistic scale. At the same time, the precise configuration of potential systems is not yet known. Since various system configurations including space and laboratory experimental systems are anticipated the focus of our FY88 effort was on modeling a generic class of multibody systems with elastic structural interactions which can be used to study qualitative nonlinear behavior of such systems.

In this report we describe a framework for the systematic modeling of multibody flexible structures. It should be noted that multibody dynamics, including modeling, is an area of intense current research. The approach described here is focused to address the issues relevant to control system design. Among these are three general considerations:

- Different views of the same system are appropriate at different stages of design.
- Models must provide insights into the system qualitative behavior and must also provide useful vehicles for computation.
- The models must interface easily to standard structural design and analysis tools for ease of data transfer.

The primary goal of the modeling effort is to provide a basis for design and analysis of control systems for rapid slewing, precision pointing, and structural vibration control. In the first year effort we have focused on nonlinear methods for the first two control system design requirements. Our methods are based on a blend of state-of-the-art methods for nonlinear control system design based on modern methods of differential geometry and *Exact Feedback Linearization (EFL)* and well proven methods of linear system control system synthesis and design based on frequency response methods. The balance of considerations for state-space or internal dynamical modeling and input-output or transfer function models has proven increasingly important in providing a quantifiable basis for robust control system design for linear systems. The methods of nonlinear EFL, however, are primarily based on state space models. In this report we indicate how the input-output characterization of an important class of nonlinear systems can play an important role in control system design for rapid slewing.

The primary goal of this project for the next year is the design of a series of laboratory experiments to demonstrate the viability of the nonlinear control methods described in this report. One central issue in practical applications and laboratory experiments is the extent to which modeling assumptions can effect results. This report describes the basis for the nonlinear control methods of EFL and shows that in principal they are based on "exact cancelation" of certain critical nonlinear terms. Thus we have included a survey of methods for robust nonlinear control system design for a variety of methods related to EFL in Section 7. In the Research Progress and Forecast Report [BBK88] we discussed the relationship between nonlinear control based on EFL and control systems using the idea of a "sliding mode" (sometimes called Variable Structure Control). These methods implement a high gain control which can be inherently robust under certain conditions by utilizing discontinuous (switching) controllers. We believe the integration of discontinuous and continuous mode control actuation is an important—indeed essential—feature of rapid slewing control.

3 Evolution Equations of Lagrangian Dynamics

The formalism of Lagrangian dynamics begins with the identification of the configuration space, i.e. the generalized coordinates, associated with the dynamical system of interest. Once the configuration manifold, M, is specified we have the natural definition of velocity at a point $q \in M$ as an vector, $\dot{q}$, in the tangent space to M at q, often denoted T_qM. We then define the state space as the union of all points $q \in M$ along with their tangent spaces, the so-called tangent bundle (c.f. [AM78, Arn78]) T_qM. The evolution of the system in the state space is characterized using Hamilton's principle of least action by the definition of a Lagrangian $L(q, \dot{q}) : M \times T_qM \rightarrow \Re$. Hamilton's principle says that the motion of a dynamical system between times t_1 and t_2 is a "natural" motion if and only if

$$\delta \int_{t_1}^{t_2} L \, dt = 0, \tag{3.1}$$

or—accounting for the presence of external generalized forces, Q—in its generalized form;

$$\int_{t_1}^{t_2} (\delta L + Q^T \delta q) \, dt = 0. \tag{3.2}$$

For *distributed parameter systems (DPS)*, special care is required to properly characterize the configuration space for modeling the system motions. The principal reasons for this fact follow from the application of the models obtained; viz., the study of time evolutions subject to control forces. First, control systems will inevitably involve the implementation of feedback and we are therefore immediately concerned with stability. An appropriate notion of stability is central to the design of feedback control systems. For Lagrangian systems the natural definition of stability is implicit in the structure of the state space which for DPS is a function space and care must be exercised that the construction (and assumptions) of the state space are consistent with the engineering control problem. Second, it is often necessary to define finite dimensional approximations to DPS for a variety of reasons including computer simulation. Again, our primary concern is in approximating the

time evolution under the influence of control. As we will make clear in the following section, the formulation of such models in a consistent way is inherently bound to the definition of the configuration space. In this section we confine our discussion to the configuration space for continuous systems with one spatial dimension.

The generalized coordinates are chosen so that all "nonworking" or geometric constraints on the motion are eliminated. This is the key to the utility of the Lagrange formalism for constructing the equations of motion. In the case of DPS any "geometric" boundary conditions (which we will denote $\mathcal{G}$) are therefore included as part of the definition of the configuration space. All other boundary conditions necessary to complete the Euler-Lagrange equations result from the application of Hamilton's Principle, (3.1) or (3.2). These are the "natural" boundary conditions (denoted $\mathcal{N}$).

An essential part of the definition of the configuration space in the infinite dimensional case is the specification of the norm. Although all norms are equivalent in finite dimensions, this is certainly not the case in infinite dimensions. We briefly summarize the main issues. Consider functions $v(z)$ defined on the domain $z \in [0,1]$ and let $D^r v(z)$ denote the r^{th} derivative with respect to z. We denote by H^p the completion of the set of the set of functions with p continuous derivatives and which satisfy

$$\|v\|_p^2 = \int_0^\ell \{|D^p v(z)|^2 + \ldots + |v(z)|^2\} dz < \infty \tag{3.3}$$

These are the *Sobolev spaces* [Lio71]. Equivalently, H^p consists of those functions whose first p derivatives belong to the Hilbert space of square integrable functions. Note that $x \in H^i$ implies $x \in H^{i-1}$ for $i = 1, 2, \ldots$.

Let $H^p_{\mathcal{G}}$ denote the completion of the set of functions satisfying (3.3) as well as a prescribed set of boundary conditions designated $\mathcal{G}$. It is not necessarily true that all of the functions in this new space satisfy the boundary conditions. The reason for this is that an arbitrary sequence of functions, all satisfying the given boundary conditions, may converge to a function which does not satisfy the boundary conditions. However, the following proposition is true. Suppose the boundary conditions $\mathcal{G}$ involve derivatives of order s and none higher. Then all of the functions in $H^p_{\mathcal{G}}$ satisfy the boundary conditions provided $p > s$. Thus, a consistent definition of the configuration space is obtained *if the specified norm is compatible with the geometric boundary conditions.*

Hamilton's principle may be used to derive the Euler-Lagrange equations and the natural boundary conditions. The Euler-Lagrange equations are to be solved along with boundary conditions $\mathcal{B} = \mathcal{G} \cup \mathcal{N}$. In general, the Lagrangian will involve derivatives with respect to z of order p and the Euler-Lagrange equations will involve derivatives of order $2p$. In finding solutions $q(t)$ we seek "weak" (sometimes called generalized or distributional[1]) solutions in $H^p_{\mathcal{G}}$ which satisfy Hamilton's principle or "strong" (pointwise, genuine or classical) solutions in $H^{2p}_{\mathcal{B}}$ which satisfy the Euler-Lagrange equations. The results are equivalent (in $H^p_{\mathcal{G}}$) when both problems have solutions. The Euler-Lagrange equations may be given the interpretation of an evolution equation as we sill describe below.

[1]There are several approaches to developing the notion weak and strong solutions and many good reasons for doing so. Thus, the proliferation of terminology carries with it sometimes subtle distinctions (c.f. [SF73, RM57, Sta79]).

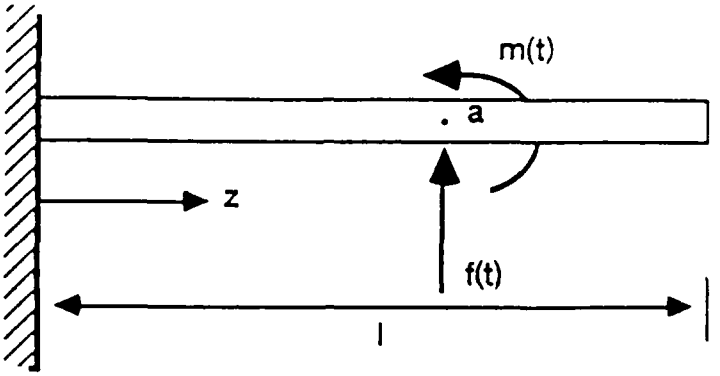

Figure 3.1: Simple Cantilevered Beam

Finite Dimensional Approximation and Computer Simulation Finite dimensional approximations to the system dynamics may be obtained by seeking an approximate solution to the Euler-Lagrange equations or to Hamilton's principle directly. The latter has the advantage that solutions are to be sought in a larger space of admissible functions which provides a wider choice of approximating functions. Perhaps unexpectedly, this turns out to be of fundamental significance in developing numerical solutions to the required evolution dynamics and for computer simulation. Furthermore, important links to the system physics are retained through this modeling process. These observations appear consistent with many standard engineering methods which introduce approximations to continuous, distributed system dynamics by discretization of the variational problem underlying the Lagrangian dyanmics [Mei67]. Indeed, this is the basis for the Finite Element Method (FEM) for evolution dynamics described in [SF73]. The simulation models developed in this study are based on finite dimensional approximation using *collocation by splines* [Aga84, Sta79, Pre75]. Further details of the method will be given in a later section with examples.

Next we consider some simple continuous systems arising in structural mechanics which will illustrate the evolution modeling setup described above.

3.1 Example: Simple Cantilevered Beam

Consider the cantilevered beam undergoing small transverse motions confined to the plane. The beam is excited by a concentrated force, $f(t)$, and moment, $m(t)$, applied at the point $z = a \in (0, 1)$.

Timoshenko Model. Each cross section undergoes a displacement $\eta(z,t)$ and a rotation $\phi(z,t)$. These are the generalized coordinates. The geometric boundary conditions are

$$\mathcal{G}: \ \eta(0,1) = 0 \quad \text{and} \quad \phi(0,1) = 0.$$

Thus, the appropriate configuration space is $H^1_{\mathcal{G}}$. The Lagrangian is

$$L = \int_0^l \left[\tfrac{1}{2}\rho A \left(\frac{\partial \eta}{\partial t}\right)^2 + \tfrac{1}{2}\rho I \left(\frac{\partial \phi}{\partial t}\right)^2 \right] - \left[\tfrac{1}{2} EI \left(\frac{\partial \phi}{\partial z}\right)^2 + \tfrac{1}{2}\kappa GA \left(\frac{\partial \eta}{\partial z} - \phi\right)^2 \right] dz$$

and the virtual work $\delta W = Q^T \delta q$ due to the external forces is

$$\delta W = \int_0^\ell \{f(t)\delta(z-a)\delta\eta + m(t)\delta(z-a)\delta\phi\}dz,$$

where ρ is the mass density, A, the cross section area, I, the moment of inertia, E, the modulus of elasticity, and κG, the effective shear modulus. Upon application of Hamilton's principle, we obtain the partial differential equations

$$\begin{aligned}
\rho A \frac{\partial^2 \eta}{\partial t^2} &= \frac{\partial}{\partial z}\left[\kappa GA\left(\frac{\partial \eta}{\partial z} - \phi\right)\right] + f(t)\delta(z-a), \\
\rho I \frac{\partial^2 \phi}{\partial t^2} &= \frac{\partial}{\partial z}\left[EI\left(\frac{\partial \phi}{\partial z}\right) + \kappa GA\left(\frac{\partial \eta}{\partial z} - \phi\right)\right] + m(t)\delta(z-a),
\end{aligned}$$

and the natural boundary conditions

$$\mathcal{N}: \quad \kappa GA\left(\frac{\partial \eta(\ell,t)}{\partial z} - \phi\right) = 0 \quad \text{and} \quad EI\left(\frac{\partial \phi(\ell,t)}{\partial z}\right) = 0.$$

Thus, we have the evolution equation

$$\begin{bmatrix} \rho A & 0 \\ 0 & \rho I \end{bmatrix} \begin{pmatrix} \ddot{\eta} \\ \ddot{\phi} \end{pmatrix} - \frac{\partial}{\partial z} \begin{bmatrix} \kappa GA \frac{\partial}{\partial z} & -\kappa GA \\ \kappa GA & EI \frac{\partial}{\partial z} \kappa GA \end{bmatrix} \begin{pmatrix} \eta \\ \phi \end{pmatrix} = \begin{pmatrix} f(t) \\ m(t) \end{pmatrix} \delta(z-a)$$

where we interpret $[\eta(\cdot,t), \phi(\cdot,t)]^T$ as an element in $H^2_{\mathcal{B}}$.

Bernoulli-Euler Model. Suppose that we consider the same situation with the additional Bernoulli-Euler assumptions [BK89]. These are

1. rotational inertia is negligible, $\rho I \to 0$,
2. shear deformation is negligible, $\eta_z - \phi \to 0$.

The deformed beam configuration is completely specified by $\eta(z,t)$. The geometric boundary conditions are

$$\mathcal{G}: \ \eta(0,1) = 0 \quad \text{and} \quad \frac{\partial \eta(0,1)}{\partial z} = 0.$$

Notice that the appropriate configuration space is $H^2_{\mathcal{G}}$. The simplified Lagrangian is

$$L = \int_0^\ell \left[\tfrac{1}{2}\rho A\left(\frac{\partial \eta}{\partial t}\right)^2 - \tfrac{1}{2}EI\left(\frac{\partial^2 \eta}{\partial z^2}\right)^2\right] dz$$

and the virtual work expression also simplifies to

$$\begin{aligned}
\delta W &= \int_0^\ell \left\{f(t)\delta(z-a)\delta\eta + m(t)\delta(z-a)\delta\left(\frac{\partial \eta}{\partial z}\right)\right\} dz \\
&= \int_0^\ell \left\{f(t)\delta(z-a) + m(t)\delta^{-1}(z-a)\right\}\delta\eta \, dz. \qquad (3.4)
\end{aligned}$$

The evolution equation is

$$\rho A\ddot{\eta} + \frac{\partial^2}{\partial z^2}\left[EI\frac{\partial^2\eta}{\partial z^2}\right] = f(t)\delta(z-a) + m(t)\delta^{-1}(z-a),$$

which is to be interpreted on H_B^4 with

$$\mathcal{N}: \; EI\frac{\partial^3\eta(\ell,t)}{\partial z^3} = 0 \text{ and } EI\frac{\partial^2\eta(\ell,t)}{\partial z^2} = 0.$$

4 Generic Models for Multibody Flexible Spacecraft

In this section we describe the basis for the formal development of a class of evolution models for multibody systems with elastic interactions. We follow the approach suggested by Baillieul and Levi [BL87]. As will be seen, the formulation captures the essential evolution dynamical structure of the system without requiring detailed knowledge of its internal configuration. As such this framework provides a consistent modeling approach for developing a hierarchy of models with increasing internal complexity and fine structure. The main idea is to isolate a "primary body" and to attach a reference frame to it at a convenient location for measuring attitude and displacement dynamics. The motion of all other spacecraft components will then be measured relative to this frame.

Throughout this report we will use the notational conventions given in Table 4.1. Consider a reference frame fixed in the primary body, with origin located by the position vector $R \in \Re^3$ and angular orientation denoted by $L \in SO(3)$, both relative to a fixed inertial frame (see Figure 4.1). L can be parameterized by the Euler angles[2] ψ, θ, ϕ representing sequential rotations about the axes 3,2,1, respectively:

$$L = \begin{bmatrix} \cos\theta\cos\psi & \cos\theta\sin\theta & -\sin\theta \\ \sin\phi\sin\theta\cos\psi - \cos\phi\sin\psi & \sin\phi\sin\theta\sin\psi + \cos\phi\cos\psi & \sin\phi\cos\theta \\ \cos\phi\sin\theta\cos\psi + \sin\phi\sin\psi & \cos\phi\sin\theta\sin\psi - \sin\phi\cos\psi & \cos\phi\cos\theta \end{bmatrix}. \tag{4.1}$$

A fundamental kinematic relationship is

$$\dot{L}(t) = -\Omega(t)L(t) \tag{4.2}$$

where

$$\Omega = \begin{bmatrix} 0 & -\omega_3 & \omega_2 \\ \omega_3 & 0 & -\omega_1 \\ -\omega_2 & \omega_1 & 0 \end{bmatrix} \tag{4.3}$$

and $\omega = (\omega_1, \omega_2, \omega_3)^T$ is the primary body (inertial) angular velocity as measured in the body coordinates.

[2] We use the so-called NASA standard or 321 convention [Gol82].

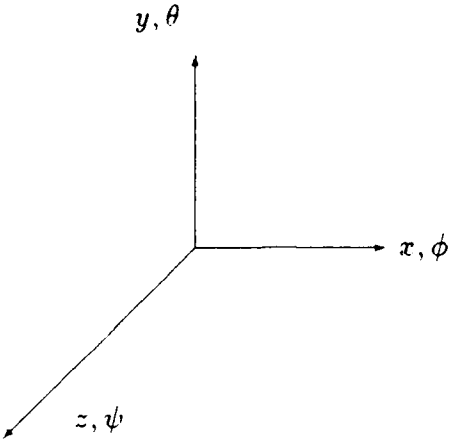

Figure 4.1: Standard Coordinate Frame for Modeling

Notation	Explanation
$x_i,\ i = 1, 2, \ldots$	element of a vector x
x^T	transpose of vector x
$\dot{x} = \frac{dx}{dt}$	time differentiation
$x_z(t,z) = \frac{\partial x}{\partial z}(z,t)$	partial differentiation
$\langle \cdot, \cdot \rangle$	natural (Hilbert space) inner product
$\| \cdot \|$	natural (Hilbert space) norm
δx	differential variation
$x \times y$	vector cross product of x and y

Table 4.1: Standard Notation for Lagrangian Mechanics

Define $\xi \in \Re^3$ as $\xi = (\psi, \theta, \phi)^T$. Then an equivalent relation[3] is

$$\dot{\xi} = \Gamma(\xi)\omega, \quad \Gamma^{-1}(\xi) = \begin{bmatrix} 1 & 0 & -\sin\theta \\ 0 & \cos\psi & \cos\theta\sin\psi \\ 0 & -\sin\psi & \cos\theta\cos\psi \end{bmatrix}. \tag{4.4}$$

The body frame position and orientation can be characterized as a point in the special Euclidian group, $SE(3, \Re)$, each element of which can be represented by a matrix

$$X = \begin{bmatrix} L^T & R \\ 0 & 1 \end{bmatrix}. \tag{4.5}$$

The positions of all other elements of the system are measured relative to the primary body frame. We identify each particle (or element), P, by its "undeformed" position, z, in the primary body frame. Let $u(z,t)$ denote the deformed position of P. Furthermore, we fix a coordinate system in each particle with origin at $u(z,t)$ and aligned—in the undeformed state—with the body axis coordinates. Let $\ell(z,t) \in SO(3)$ denote the orientation of P in the deformed state as measured in the primary body coordinates. Note that in the undeformed state

$$\ell_{undeformed} = \begin{bmatrix} 1 & 0 & 0 \\ 0 & 1 & 0 \\ 0 & 0 & 1 \end{bmatrix} \tag{4.6}$$

and for small relative motions[4]

$$\ell_{small} = \begin{bmatrix} 1 & \psi & -\theta \\ -\psi & 1 & \phi \\ \theta & -\phi & 1 \end{bmatrix}. \tag{4.7}$$

The inertial coordinates $U(z,t)$ of a particle P can be obtained from the body coordinates $u(z,t)$ via the relation

$$U(z,t) = L^T u(z,t) + R. \tag{4.8}$$

Note also that

$$\dot{X}(t) = \begin{bmatrix} L^T(t)\Omega(t) & \dot{R}(t) \\ 0 & 0 \end{bmatrix}. \tag{4.9}$$

Also, a direct computation yields

$$\frac{d}{dt}U = L^T(t)[\Omega u + \dot{u}] + \dot{R}(t) \tag{4.10}$$

[3]Equation (4.4) is essential to the analytic framework for multibody modeling. Alternate parametrizations of $SO(3)$—such as the Cayley-Rodrigues parameters [Dwy84]—can be used to advantage and the general form remains intact.

[4]This is a standard assumption in modeling *small* elastic deformation. A considerably different class of models is obtained using exact (i.e. "geometric") deformation model as in [Pos88]. Since our primary concern in this study is to develop a class of models applicable for flexure modeling affecting precision optical systems we retain the small deformation assumption throughout.

The kinetic energy of the system can be written in terms of the generalized coordinates $q = (\xi, R, u)$ in the form

$$\begin{aligned} T(q,\dot{q}) &= \tfrac{1}{2}\int_S \|\dot{U}\|^2 dm \;= \tfrac{1}{2}\int_S \|L^T[\Omega u + u_t] + \dot{R}\|^2 dm \\ &= \tfrac{1}{2}\int_S \|[\Omega u + u_t]\|^2 + 2\langle \Omega u + u_t, L\dot{R}\rangle + \|\dot{R}\|^2 dm \end{aligned} \tag{4.11}$$

where S denotes that the integral is to be taken over the entire system.

4.1 Lagrange's Equations

In addition to the kinetic energy, $T(q,\dot{q})$, we assume that a potential energy function $V(q)$ is also available. Then Lagrange's equations take the form

$$\begin{aligned} \frac{d}{dt}\frac{\partial T}{\partial \dot{\xi}} - \frac{\partial T}{\partial \xi} + \frac{\partial V}{\partial \xi} &= Q_\xi, \\ \frac{d}{dt}\frac{\partial T}{\partial \dot{R}} - \frac{\partial T}{\partial R} + \frac{\partial V}{\partial R} &= Q_R, \\ \frac{d}{dt}\frac{\delta T}{\delta \dot{u}} - \frac{\delta T}{\delta u} + \frac{\delta V}{\delta u} &= Q_u, \end{aligned} \tag{4.12}$$

where the generalized forces are defined in terms of the *virtual work expression*;

$$\delta W = Q_\xi^T d\xi + Q_R^T dR + Q_u^T \delta u. \tag{4.13}$$

Now, we define the *system angular momentum* with respect to the origin of the body frame

$$H = \int_S u \times [(\omega \times u + u_t) + L\dot{R}]dm = a + \int_S u \times L\dot{R}\, dm. \tag{4.14}$$

With some calculation[5] these equations reduce to

System Angular Momentum

$$\Gamma^T(\xi)[\dot{a} + \omega \times a] + \int_S u(z,t) \times L\ddot{R}\, dm = Q_\xi - \frac{\partial V}{\partial \xi}, \tag{4.15}$$

System Linear Momentum

$$\int_S [\frac{d}{dt}L^T(u_t + \omega \times u) + \ddot{R}]dm = Q_R - \frac{\partial V}{\partial R}, \tag{4.16}$$

$$u_{tt} + \omega \times (\omega \times u) + \dot{\omega} \times u + 2\omega \times u_t + L\ddot{R} = Q_u - \frac{\delta V}{\delta u}. \tag{4.17}$$

Equivalently we obtain

$$\Gamma^T(\xi)[I\dot{\omega} + \omega \times I\omega] + mc \times L\ddot{R} + \Gamma^T(\xi)D\int_S u \times [\omega \times u + u_t]dm + \int_S u \times L\ddot{R}dm = Q_\xi - \frac{\partial V}{\partial \xi} \tag{4.18}$$

[5] Appendix A contains some identities useful for these calculations.

$$m\ddot{R} + mL^T[\omega \times (\omega \times c) + \dot{\omega} \times c] + \int_S L^T[D^2u + L\ddot{R}]dm = Q_R - \frac{\partial V}{\partial R} \tag{4.19}$$

$$D^2u + L\ddot{R} = Q_u - \frac{\delta V}{\delta u} \tag{4.20}$$

where the operator D is defined by

$$D(\cdot) := \frac{d}{dt}(\cdot) + \omega \times (\cdot)$$

Note that, in applications, the integrals in (4.15)-(4.17) or (4.18)-(4.17) would not be evaluated directly. Instead, they are to be replaced by momentum expressions in terms of an appropriate choice of generalized coordinates.

4.2 Generic Models for Slewing and Pointing of Precision Optical Structures

In this section we develop several benchmark generic models for rapid slewing and precision pointing of flexible space structures which are motivated by problems relating to control of precision optical structures subject to elastic interactions. Such problems arise in requirements for rapid retargeting coupled with precision pointing for space-based laser (SBL) systems. The models reflect generic qualitative dynamical properties of such systems. In a subsequent section we develop a simulation model with physical parameters obtained from the benchmark SBL structural model developed in [Lea87].

The models developed in this section focus on primary sources of structural interaction with principal body slewing maneuvers affecting system LOS pointing. Modeling assumptions used to characterize generic responses are based on the initial system level tradeoffs described in the R & D Associates report [Lea87]. This study indicates that the principal source of structural flexure affecting laser LOS is within the beam expanded optical train—the principal structural component being the metering truss supporting the relative position and orientation of the primary and secondary mirrors. Our initial or first-level model assumes the beam expander primary mirror and support is rigidly attached to the spacecraft body and only the metering truss is subject to flexure. In the second model we include provisions for articulation of the SBL beam expander with respect to the SBL system spacecraft body using a gimbaled joint.

4.2.1 Example: Rigid Body With 1-Dimensional Appendage

We consider a single rigid body attached to a flexible appendage as illustrated in Figure 4.2. The system kinetic energy can be expressed as

$$\begin{aligned} T &= \tfrac{1}{2}\int_{rb} \|\Omega u\|^2 + 2\langle \Omega u, L\dot{R}\rangle + \|R\|^2 dm \\ &\quad + \tfrac{1}{2}\int_{fb} \|\Omega u + u_t\|^2 + 2\langle \Omega u + u_t, L\dot{R}\rangle + \|\dot{R}\|^2 dm \\ &= \tfrac{1}{2}\omega_b^T I_b \omega_b - m_b c^T \Omega_b L\dot{R} + \tfrac{1}{2}m_b\|\dot{R}\|^2 \\ &\quad + \tfrac{1}{2}\int_0^\ell \{\|\Omega_b\eta + \eta_t\|^2 + 2\langle \Omega_b\eta + \eta_t, L\dot{R}\rangle + \|\dot{R}\|^2\}\rho A\, dz \end{aligned} \tag{4.21}$$

$$+\tfrac{1}{2}\int_0^\ell \{[\omega_b + \xi_t]^T I[\omega_b + \xi_t]\}\rho\, dz$$

where $c \in \Re^3$ is the location of the rigid body center of mass in the body frame, m_b is the mass of the rigid body, I_b is the inertia tensor of the rigid body in the body frame, and ρ is the mass density of the beam, $\eta(z,t)$ is the position vector of points on the deformed centerline of the beam in the primary body coordinate frame and $\xi(z,t) = (\psi, \theta, \phi)^T(z,t)$ is the beam angular deformation. We have assumed small deformation of the beam so that the angular velocity of the beam section at z is

$$\omega(z,t) = \omega_b + \xi_t(z,t)$$

up to first order in the angular deformation.

The potential energy of the system consists only of the potential energy associated with deformation of the beam. Under Timoshenko beam assumptions [CKEFKP68] the potential energy function is

$$\begin{aligned} V(\xi,\eta) &= \tfrac{1}{2}\int_0^\ell \Big\{GJ(\psi_z)^2 + EI_2(\theta_z)^2 + EI_3(\phi_z)^2 \\ &\quad + \kappa_1 GA(\eta_{1,z} - \theta)^2 + \kappa_2 GA(\eta_{2,z} - \phi)^2 + \mu EA(\eta_{3,z} - 1)^2\Big\}\, dz \qquad (4.22) \\ &= \tfrac{1}{2}\int_0^\ell \Big\{(\xi_z^T K \xi_z) + (\eta_z - P\xi)^T S(\eta_z - \xi)\Big\}\, dz \end{aligned}$$

where the stiffness matrices are defined as

$$K = \mathrm{diag}(GJ, EI_2, EI_3), \quad S = \mathrm{diag}(\kappa_1 GA, \kappa_2 GA, \mu EA),$$

and

$$P = \begin{bmatrix} 0 & 1 & 0 \\ 1 & 0 & 0 \\ 0 & 0 & 0 \end{bmatrix}.$$

The system angular momentum vector is

$$a = I_b\omega_b + \int_0^\ell [A\eta \times (\omega_b \times \eta + \dot\eta) + I\omega]\rho\, dz$$

so that equations (4.15)–(4.17) reduce to

$$\begin{aligned} &\Gamma^T(\xi)(I_b\dot\omega_b + \omega_b \times I_b\omega_b) \\ &\quad + \int_0^\ell [\Gamma^T(\xi)A\eta \times (\eta_{tt} + \omega_b \times (\omega_b \times \eta) + \dot\omega_b \times \eta + 2\omega_b \times \dot\eta) \\ &\quad + A\eta \times L\ddot R + I(\dot\omega + \omega_b \times \omega)]\rho\, dz + mc \times L\ddot R = Q_{\xi_b}, \qquad (4.23) \\ &m\ddot R + mL^T(\omega \times (\omega \times c) + \dot\omega \times c) + \int_0^\ell \rho A(L^T D^2\eta + \ddot R)dz = Q_R, \qquad (4.24) \\ &\rho A(\eta_{tt} + \omega_b \times (\omega_b \times \eta) + \dot\omega_b \times \eta + 2\omega_b \times \dot\eta + L\ddot R) = Q_\eta - S(\eta_{zz} - P\xi_z), \qquad (4.25) \\ &\rho I[\xi_{tt} + \dot\omega_b + \omega_b \times (\omega_b + \xi_t)] = Q_\xi - K\xi_{zz} + P^T S(\eta_z - P\xi). \qquad (4.26) \end{aligned}$$

System Dissipation A simple model of generalized dissipation in the appendage can be obtained by introducing a Rayleigh dissipation function. We formulate such a function based on the assumption that dissipation forces are proportional to beam deformation rates, i.e. generalized coordinate velocities (η_t and ξ_t) and strain rates ($(\eta_1)_{tz} - \theta_t, (\eta_2)_{tz} - \phi_t, \xi_{tz}$).

$$R(\eta_t, \xi_t) = \tfrac{1}{2}\int_0^\ell \{\eta_t^T \Xi_1 \eta_t + \xi_t^T \Xi_2 \xi_t + (\eta_{tz})^T \Xi_3 \eta_{tz} + (\xi_{tz})^T \Xi_4 (\xi_{tz})\} dz \tag{4.27}$$

where $\Xi_i = \mathrm{diag}(\zeta_{i1}, \zeta_{i2}, \zeta_{i3})$. From $R(\eta_t, \xi_t)$ we obtain the generalized dissipative forces

$$\frac{\delta R}{\delta \eta_t} = \Xi_1 \eta_t + \Xi_3(\eta_{tzz} - P\xi_{tz}), \tag{4.28}$$

$$\frac{\delta R}{\delta \xi_t} = \Xi_2 \xi_t + \Xi_3(\eta_{tz} - P\xi_t) + \Xi_4 \xi_{tzz}. \tag{4.29}$$

4.3 Example: Articulated Bodies With Flexible Appendage

We now consider a modification of the previous Example which includes a second body attached to the primary body with a three axis gimbal as illustrated in Figure 2. In addition, the second body carries with it a reaction wheel package. The kinetic energy function is

$$\begin{aligned} T &= \underbrace{\tfrac{1}{2}\omega_p^T I_p \omega_p - m_p c_p^T \Omega_p L \dot{R} + \tfrac{1}{2} m_p \|\dot{R}\|^2}_{\text{primary body}} \\ &\underbrace{+\tfrac{1}{2}\omega_s^T I_s \omega_s - m_s c_s^T \Omega_s L_s \{L\dot{R} + \Omega_p c_{gm}\} + \tfrac{1}{2} m_s \|L\dot{R} + \Omega_p c_{gm}\|^2}_{\text{second body (wheels locked)}} \\ &\underbrace{+\tfrac{1}{2}\omega_3^T I_3 \omega_3 + \omega_s^T I_3 \omega_3}_{\text{reaction wheels}} \\ &+ \tfrac{1}{2}\int_0^\ell \{\|\Omega_p \eta + \eta_t\|^2 + 2\langle \Omega_p \eta + \eta_t, L\dot{R}\rangle + \|\dot{R}\|^2\} \rho A \, dz \\ &+ \tfrac{1}{2}\int_0^\ell \{(\omega_p + \xi_t)^T I (\omega_p + \xi_t)\} \, \rho dz \end{aligned} \tag{4.30}$$

Note that c_p and c_s are the locations of the center of gravity of the primary body and second body (including wheels) in their respective body coordinate frames. The vector c_{gm} denotes the location of the three axis gimbal in the primary body frame. The matrix I_1 is the primary body inertia tensor in the primary body frame, I_2 denotes the second body inertia tensor with reaction wheels, and I_3 is the diagonal matrix of wheel inertias.

4.4 Simulation Example: Slewing in the Plane

Consider a rigid body with a flexible appendage attached which is restrained to motion in the $x \times z$ plane which means that $\phi, \psi = 0$. In addition, we assume that axial beam vibrations are negligible so that $\eta_3 = z$, and that the translational velocity, $\dot{R}$, is also negligible. A control torque T_b is applied to the rigid body.

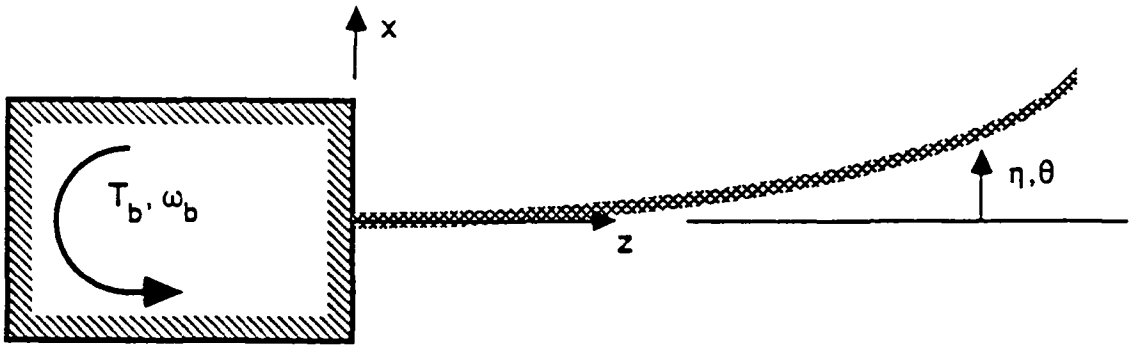

Figure 4.2: Rigid Body with Flexible Appendage

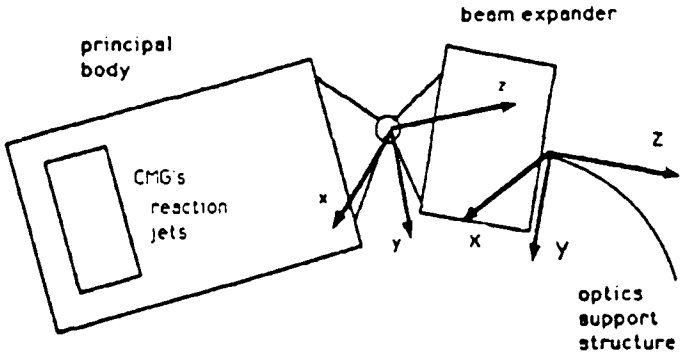

Figure 4.3: Hinged Bodies with Flexible Appendage

The formulation of the equations of motion follows the procedure outlined previously. The system Lagrangian $L = T - V$ can be obtained by reduction of (4.21)-(4.22) under the above assumptions to the form

$$\begin{aligned} L &= \tfrac{1}{2} I_b \omega_b^2 + \tfrac{1}{2} \int_0^\ell \{[\omega_b(z-\eta) + \eta_t]^2 \rho A + (\omega_b + \theta_t)^2 \rho I\} dz \\ &\quad - \tfrac{1}{2} \int_0^\ell \left\{ EI(\theta_z)^2 + \kappa GA(\eta_z - \theta)^2 \right\} dz \end{aligned} \tag{4.31}$$

and the virtual work expression is

$$\delta W = T_b \, \delta\theta_b.$$

Notational conventions for the planar model. In the rest of this section we substitute the symbol η for the first component of the lateral deflection η_1 in an abuse of notation. Whereas θ denotes the rotational deformation of the appendage we denote by θ_b (ω_b) the primary body attitude angle (resp. angular rate).

Notice that the configuration space is $S^1 \times H^1_{\mathcal{G}}$, with generalized coordinates $\theta_b \in S^1$, $(\eta, \theta) \in H^1_{\mathcal{G}}$, and the geometric boundary conditions are

$$\mathcal{G}: \quad \eta(0,t) = 0 \ \text{ and } \ \theta(0,t) = 0.$$

Thus following the previous approach the evolution equations can be written

$$I_b \dot{\omega}_b + \int_0^\ell \{z(\eta_{tt} + \dot{\omega}_b z + \omega_b^2 \eta)\rho A + (\dot{\omega}_b + \theta_{tt})\rho I\} dz = T_b \tag{4.32}$$

$$\rho A(\eta_{tt} + \dot{\omega}_b z + \omega_b^2 \eta) - c_1 \eta_t - c_3(\eta_{tzz} - \theta_{tz}) + \kappa GA(\eta_{zz} - \theta_z) = 0 \tag{4.33}$$

$$\rho I(\dot{\omega}_b + \theta_{tt}) - c_2 \theta_t - c_3(\eta_{tz} - \theta_t) - c_4 \theta_{tzz} + EI\theta_{zz} - \kappa GA(\eta_z - \theta) = 0 \tag{4.34}$$

with natural boundary conditions

$$\mathcal{N}: \ \eta_z(\ell,t) - \theta(\ell,t) = 0 \ \text{ and } \ \theta_z(\ell,t) = 0. \tag{4.35}$$

4.4.1 Finite Dimensional Model for Planar Slewing

From the discussion in Section 3 we some care must be exercised in introducing finite dimensional approximation of the DPS by discretization of the spatial coordinates so that the resulting finite dimensional evolution model approximates the evolution dynamics of the continuous system. One consequence of these remarks is that direct spatial discretization of the DPS evolution equations (4.32)-(4.35) is *not* recommended. Rather the recommended approach is to approximate the system Lagrangian (4.31) by FEM and then develop the finite dimensional evolution model by applying variational arguments to the reduced Lagrangian.

For control system design we are ultimately interested in the stability of certain equilibria of DPS and the asymptotic convergence rates near these equilibria under the influence of exogenous (control) forces. For these purpose useful finite dimensional models must include

some provisions for modeling system dissipation. Our approach is to introduce an approximate Rayleigh dissipation function defined on a finite dimensional subspace of the state space for the DPS which approximates a function of the form

$$R(\eta_t, \theta_t) = \tfrac{1}{2} \int_0^\ell \zeta_1 \eta_t^2 + \zeta_2 \theta_t^2 + \zeta_3 (\eta_{tz} - \theta_t)^2 + \zeta_4 \theta_t^2 \; dz \tag{4.36}$$

which can be obtained directly from (4.27) under the above assumptions.

4.4.2 Reduced Order Modeling by FEM and B-splines.

Our approach to finite dimensional modeling is based on the use of B-splines and the FEM. Recall that a *B-spline* (or basis spline) of order k introduces an approximation to the appropriate distributed parameter of the form,

$$\eta(z,t) \approx \sum_{i=0}^{N+k-1} \hat{\eta}_i(t) B_{i-k}^k(z) \tag{4.37}$$

where N is the number of spline sections (finite elements). The B-splines of increasing order are defined recursively as

$$B_i^k(z) := \left| \frac{z - z_i}{z_{i+k} - z_i} \right| B_i^{k-1}(z) + \left| \frac{z_{i+k+1} - z}{z_{i+k+1} - z_{i+1}} \right| B_{i+1}^{k-1}(z) \tag{4.38}$$

with the order 0 spline defined with continuity from the left;

$$B_i^0(z) := \begin{cases} 1, & \text{if } x_i \le x < x_{i+1} \\ 0, & \text{else} \end{cases} . \tag{4.39}$$

The 'coefficient' functions $\hat{\eta}_i(t)$ are to be eliminated by application of certain interpolation conditions at the *knots* together with the *geometric boundary conditions.*

Remark: For discretization of the system Lagrangian (4.31) and the Rayleigh dissipation (4.36) we see that order 1 B-splines (i.e. linear splines) are all that is required. This is *not* obvious if one attempts to discretize the DPS model (4.32)–(4.35).

The required interpolation conditions are given at N uniformly spaced knots on the spatial interval $0 \le z \le \ell$;

$$\begin{aligned} \eta(\tfrac{\ell}{N}) &= \sum_{i=0}^{N} \hat{\eta}_i B_{i-1}^1(\frac{\ell}{N}) \\ \eta(2\tfrac{\ell}{N}) &= \sum_{i=0}^{N} \hat{\eta}_i B_{i-1}^1(2\frac{\ell}{N}) \\ &\vdots \\ \eta(\ell) &= \sum_{i=0}^{N} \hat{\eta}_i B_{i-1}^1(\ell) \end{aligned} \tag{4.40}$$

together with the geometric boundary condition

$$\eta(0) = \sum_{i=0}^{N} \hat{\eta}_i B^1_{i-1}(0). \tag{4.41}$$

Let $\eta_k = \eta(kL/N)$ for $k = 0, 1, \ldots, N$, and denote

$$\bar{\eta} = \begin{pmatrix} \eta_1 \\ \vdots \\ \eta_N \end{pmatrix}, \quad \tilde{\eta} = \begin{pmatrix} \bar{\eta} \\ \eta_N \end{pmatrix}, \quad \hat{\eta} = \begin{pmatrix} \hat{\eta}_0 \\ \hat{\eta}_1 \\ \vdots \\ \hat{\eta}_N \end{pmatrix}.$$

Then we can write the $N+1$ interpolation conditions in matrix form as

$$\tilde{\eta} = M\hat{\eta}, \tag{4.42}$$

where

$$M = \begin{bmatrix} \bar{B}^T(\frac{\ell}{N}) \\ \bar{B}^T(2\frac{\ell}{N}) \\ \vdots \\ \bar{B}^T(\ell) \\ \bar{B}^T(0) \end{bmatrix}, \tag{4.43}$$

$$\bar{B}(z) = \begin{bmatrix} B^1_{-1}(z) \\ B^1_0(z) \\ \vdots \\ B^1_{N-1}(z) \end{bmatrix}. \tag{4.44}$$

Now we use (4.42) to eliminate $\hat{\eta}$ from (4.37) to obtain,

$$\begin{aligned} \eta(z,t) &\approx \bar{B}^T(z)M^{-1}\tilde{\eta} = [\hat{M}_1, \hat{M}_2] \begin{pmatrix} \bar{\eta} \\ 0 \end{pmatrix} \\ &= \bar{B}^T(z)\hat{M}_1\bar{\eta}(t) \end{aligned} \tag{4.45}$$

Similarly we obtain an approximation to the rotational generalized coordinate as

$$\theta(z,t) \approx \bar{B}^T(z)\hat{M}_1\bar{\theta}(t). \tag{4.46}$$

In the sequel we use the notation

$$\Phi^T(z) := \bar{B}^T(z)\hat{M}_1, \tag{4.47}$$

a $1 \times N$ array. We note that the N-vectors $\bar{\eta}$ and $\bar{\theta}$ represent the spatial solutions at the knots and satisfy the interpolation conditions. The spline is continuous up to its first derivatives.

For this simple model the interpolation conditions and geometric boundary conditions result in a simple relation for the elements of Φ since

$$M = \begin{bmatrix} 0 & \\ \vdots & I_N \\ 1 & 0 \ldots 0 \end{bmatrix}$$

so that

$$\hat{M}_1 = \begin{bmatrix} 0 \ldots 0 \\ I_N \end{bmatrix},$$

thus

$$\Phi^T(z) = [B_0^1(z), B_1^1(z), \ldots, B_{N-1}^1(z)]. \tag{4.48}$$

Now using (4.48) together with (4.45) and (4.46) we can approximate the *System Kinetic Energy*;

$$T = T_{rigid} + T_{flex}, \tag{4.49}$$

$$T_{rigid} = \tfrac{1}{2} I_b \omega_b^2 \tag{4.50}$$

$$T_{flex} \approx \tfrac{1}{2}\dot{\bar{\eta}}^T N_\eta \dot{\bar{\eta}} + \tfrac{1}{2} N_{\omega_b} \omega_b^2 + \omega_b N_{\omega_b\eta}^T \dot{\bar{\eta}} + \tfrac{1}{2}\omega \bar{\eta}^T N_\eta \bar{\eta} + \tfrac{1}{2}\dot{\bar{\theta}}^T N_\theta \dot{\bar{\theta}} + \omega_b N_{\omega_b\theta}^T \dot{\bar{\theta}} \tag{4.51}$$

where

$$N_\eta = \int_0^\ell \rho A \Phi(z) \Phi^T(z)\, dz \tag{4.52}$$

$$N_{\omega_b} = \int_0^\ell (z^2 \rho A + \rho I)\, dz \tag{4.53}$$

$$N_{\omega_b\eta}^T = = \int_0^\ell \rho A z \Phi^T(z)\, dz \tag{4.54}$$

$$N_\theta = \int_0^\ell \rho I \Phi(z) \Phi^T(z)\, dz \tag{4.55}$$

$$N_{\omega_b\theta}^T = \int_0^\ell \rho I \Phi^T(z)\, dz, \tag{4.56}$$

the *System Potential Energy*

$$V \approx \tfrac{1}{2}\bar{\theta}^T K_\theta \bar{\theta} + \tfrac{1}{2}\bar{\eta}^T K_\eta \bar{\eta} + \bar{\eta}^T K_{\eta\theta} \bar{\theta}, \tag{4.57}$$

where

$$K_\eta = \int_0^\ell \kappa G A \Phi_z(z) \Phi_z^T(z)\, dz, \tag{4.58}$$

$$K_\theta = \int_0^\ell \{EI \Phi_z(z) \Phi_z^T(z) + \kappa G A \Phi(z) \Phi^T(z)\}\, dz, \tag{4.59}$$

$$K_{\eta\theta} = -\int_0^\ell \kappa G A \Phi_z(z) \Phi^T(z)\, dz, \tag{4.60}$$

and *System Dissipation Function*

$$R \approx \tfrac{1}{2}\dot{\bar{\eta}}^T B_\eta \dot{\bar{\eta}} + \tfrac{1}{2}\dot{\bar{\theta}}^T B_\theta \dot{\bar{\theta}} + \dot{\bar{\eta}}^T B_{\eta\theta} \dot{\bar{\theta}}, \tag{4.61}$$

where

$$B_\eta = \int_0^\ell \{\zeta_1 \Phi(z) \Phi^T(z) + \zeta_3 \Phi_z(z) \Phi_z^T(z)\}\, dz, \tag{4.62}$$

$$B_\theta = \int_0^\ell \{(\zeta_2 + \zeta_3) \Phi(z) \Phi^T(z) + \zeta_4 \Phi_z(z) \Phi_z^T(z)\}\, dz, \tag{4.63}$$

$$B_{\eta\theta} = -\int_0^\ell \zeta_3 \Phi_z(z) \Phi^T(z)\, dz. \tag{4.64}$$

The parameters ζ_1, ζ_2 represent *external* dissipation (e.g. viscous damping) and ζ_3, ζ_4 model *internal* (e.g. material) dissipation [BK89].

Solving the Lagrange's equations in terms of the finite dimensional generalized coordinates;

$$\begin{aligned} \frac{d}{dt}\frac{\partial T}{\partial \omega_b} - \frac{\partial (T-V)}{\partial \theta_b} + \frac{\partial R}{\partial \omega_b} &= Q_{\theta_b}, \\ \frac{d}{dt}\frac{\partial T}{\partial \dot{\bar{\eta}}} - \frac{\partial (T-V)}{\partial \bar{\eta}} + \frac{\partial R}{\partial \dot{\bar{\eta}}} &= 0, \\ \frac{d}{dt}\frac{\partial T}{\partial \dot{\bar{\theta}}} - \frac{\partial (T-V)}{\partial \bar{\theta}} + \frac{\partial R}{\partial \dot{\bar{\theta}}} &= 0, \end{aligned} \tag{4.65}$$

gives the finite dimensional model evolution equations,

$$[M_\omega + \bar{\eta}^T N_\eta \bar{\eta}]\dot{\omega}_b + N^T_{\omega_b \eta}\ddot{\bar{\eta}} + N^T_{\omega_b \theta}\ddot{\bar{\theta}} + \omega_b \bar{\eta}^T N_\eta \dot{\bar{\eta}} = T_b, \tag{4.66}$$

$$N_\eta \ddot{\bar{\eta}} + \dot{\omega}_b N_{\omega_b \eta} - \omega_b^2 N_\eta \bar{\eta} + K_\eta \bar{\eta} + K_{\eta\theta}\bar{\theta} + B_\eta \dot{\bar{\eta}} + B_{\eta\theta}\dot{\bar{\theta}} = 0, \tag{4.67}$$

$$N_\theta \ddot{\bar{\theta}} + \dot{\omega}_b N_{\omega_b \theta} + K_\theta \bar{\theta} + K^T_{\eta\theta}\bar{\eta} + B_\theta \dot{\bar{\theta}} + B^T_{\eta\theta}\dot{\bar{\eta}} = 0, \tag{4.68}$$

where the effective rigid body inertia for the undeformed elastic appendage state is

$$M_\omega = I_b + N_{\omega_b}.$$

To compute the coefficients of the resulting reduced order model equations in terms of the DPS physical model parameters we must evaluate the integrals in (4.52)-(4.56), (4.58)-(4.60), and (4.62)-(4.64). For initial simulation studies we assume the elastic appendage is a uniform beam and take $\rho I, \rho A, EI, \kappa GA$ constant over $z \in [0, \ell]$. Later this will be modified to model the spatial variation in cross section and moment of inertia associated with a typical pyramidal shaped secondary mirror support structure for typical laser beam expander for a space based laser.

Under these assumptions we can obtain an $N \times N$ matrix

$$\tilde{N} = \int_0^\ell \Phi(z)\Phi^T(z)\, dz$$

with elements of the form

$$[\tilde{N}]_{ij} = \int_0^\ell B^1_{i-1}(z) B^1_{j-1}(z)\, dz, \quad \text{for } i, j = 1, \ldots, N.$$

A straightforward computation[6] obtains the tridiagonal structure of $\tilde{N}$ with elements,

$$[\tilde{N}]_{ij} = \begin{cases} \frac{1}{3}(\frac{\ell}{N}), & \text{for } i = j = N \\ \frac{2}{3}(\frac{\ell}{N}), & \text{for } i = j < N \\ \frac{1}{6}(\frac{\ell}{N}), & \text{for } i = j \pm 1 \\ 0, & \text{else} \end{cases}. \tag{4.69}$$

[6] See Appendix B for details.

Similarly, we obtain the $N \times N$ tridiagonal matrices

$$\tilde{N}' = \int_0^\ell \Phi_z(z)\Phi_z^T(z)\,dz, \tag{4.70}$$

$$\tilde{K}' = \int_0^\ell \Phi_z(z)\Phi^T(z)\,dz, \tag{4.71}$$

with elements given by

$$[\tilde{N}']_{ij} = \begin{cases} (\frac{N}{\ell}), & \text{for } i = j = N \\ 2(\frac{N}{\ell}), & \text{for } i = j < N \\ -(\frac{N}{\ell}), & \text{for } i = j \pm 1 \\ 0, & \text{else} \end{cases}, \tag{4.72}$$

$$[\tilde{K}']_{ij} = \begin{cases} 0, & \text{for } i = j \\ \frac{1}{2}, & \text{for } i = j + 1 \\ -\frac{1}{2}, & \text{for } i = j - 1 \\ 0, & \text{else} \end{cases}. \tag{4.73}$$

With these relations we can express the model coefficient matrices as follows:

$$\begin{aligned} N_\eta &= \rho A\tilde{N} \\ N_\theta &= \rho I\tilde{N} \\ K_\eta &= \kappa GA\tilde{N}' \\ K_\theta &= EI\tilde{N}' + \kappa GA\tilde{N} \\ K_{\eta\theta} &= -\kappa GA\tilde{K}' \\ B_\eta &= \zeta_1\tilde{N} + \zeta_3\tilde{N}' \\ B_\theta &= (\zeta_2 + \zeta_3)\tilde{N} + \zeta_4\tilde{N}' \\ B_{\eta\theta} &= -\zeta_3\tilde{K}'. \end{aligned}$$

Similarly the $1 \times N$ matrices

$$N_{\omega_b\eta}^T = \rho A \int_0^\ell z\Phi^T(z)\,dz, \tag{4.74}$$

$$N_{\omega_b\theta}^T = \rho I \int_0^\ell \Phi^T(z)\,dz, \tag{4.75}$$

can be reduced to the form

$$N_{\omega_b\theta}^T = \rho I\left[\frac{\ell}{N}, \frac{\ell}{N}, \cdots, \frac{\ell}{N}, \frac{\ell}{2N}\right], \tag{4.76}$$

$$[N_{\omega_b\eta}^T]_i = \begin{cases} \rho A(1+i)(\frac{\ell}{N})^2, & \text{for } i = 1, \ldots, N-1 \\ \rho A(\frac{\ell}{N})^2[\frac{N}{2} - \frac{1}{6}], & \text{for } i = N \end{cases}. \tag{4.77}$$

Finally, we obtain by direct integration of (4.53) under the above assumptions that

$$N_{\omega_b} = \rho A\frac{\ell^3}{3} + \rho I\ell. \tag{4.78}$$

5 Normal Forms, Decoupling and Partial Linearization

5.1 Partial Linearization and Stabilization of Nonlinear Systems

Techniques for stabilization of nonlinear systems via feedback control are still very limited and tend to be tailored to specific situations. Among the most promising general approaches are based on global linearization by *Exact Feedback Linearization (EFL)* [HSM83, KC87]. The methods are based on earlier work of Krener [Kre73] and Brockett [Bro78] which demonstrate that a large class of nonlinear dynamical systems can be exactly (i.e. globally linearized) by a combination of nonlinear transformation of the state coordinates and nonlinear state feedback. More recently the connection between these methods and the idea of input-output (or *partial) feedback linearization (PFL)* by construction of a *system inverse* [Hir79] has been articulated in a series of papers by Byrnes and Isidori [BI85, BI84]. These connections have engendered a series of design methods with representative results for specific applications by Kravaris and Chung [KC87] and Fernandez and Hetrick [FH87]. In this section we will summarize these results and then proceed to develop the method for the case of multibody systems from the perspective of Lagrangian mechanics.

Partial linearization derives directly from the Byrnes-Isidori normal form for nonlinear systems. The essentials of the approach are most easily developed for single-input, single output systems and we will present the approach in that context. The theory for extending these results for multi-input, multi-output problems is now complete and references are included.

Consider a nonlinear dynamical system in the form,

$$\dot{x} = f(x) + g(x)u \tag{5.1}$$

$$y = h(x) \tag{5.2}$$

where f, g are smooth C^∞ vector fields on $\Re^n$ and h is a smooth function mapping $\Re^n \rightarrow \Re$. Now if we differentiate (5.2) we obtain

$$\dot{y} = \frac{\partial h}{\partial x}(f(x) + g(x)u). \tag{5.3}$$

In the case that the scalar coefficient of u (viz. $\frac{\partial h}{\partial x}g(x)$) is zero we can differentiate again until a nonzero control coefficient appears. The number of required differentiations is fundamental system invariant which plays a role in constructing system inverse and therefore in partial linearization. The Byrnes-Isidori analysis shows that this integer number is analogous to the *relative degree* for a linear system [BI84].

The above construction can be made precise using the notation of differential geometry which has found application in analytical mechanics [Arn78]. We will need only the notion of Lie derivative and Lie bracket. The Lie (directional) derivative of the scalar function h with respect to the vector field f is

$$L_f(h) = \langle dh, f \rangle := \frac{\partial h}{\partial x} f(x). \tag{5.4}$$

Since the above operation results in a scalar function on $\Re^n$, higher order derivatives can be successively defined

$$L_f^k(h) = L_f(L_f^{k-1}(h)) := \langle dL_f^{k-1}(h), f \rangle. \tag{5.5}$$

Then we can write (5.3) as

$$\begin{aligned} \dot{y} &= \langle dh, f \rangle + \langle dh, g \rangle u \\ &= L_f(h) + L_g(h)u. \end{aligned} \tag{5.6}$$

If $L_g(h) = 0$ then we differentiate again to obtain

$$\begin{aligned} \ddot{y} &= \langle dL_f(h), f \rangle + \langle dL_f(h), g \rangle u \\ &= L_f^2(h) + L_g(L_f(h))u. \end{aligned} \tag{5.7}$$

If $L_g(L_f^{k-1}(h)) = 0$ for $k = 1, \ldots, r-1$, but $L_g(L_f^{r-1}(h)) \neq 0$ then the process terminates with

$$\frac{d^r y}{dt^r} = L_f^r(h) + L_g(L_f^{r-1}(h))u. \tag{5.8}$$

The system (5.8) can be effectively inverted by introducing a feedback transformation of the form

$$u = \frac{1}{L_g(L_f^{r-1}(h))}[v - L_f^r(h)] \tag{5.9}$$

which results in an effective input-output system from $v \rightarrow y$ given by

$$\frac{d^r y}{dt^r} = v,$$

a *linear* system.

The integer $r > 0$ is called the *relative degree* of the nonlinear system (5.1)–(5.2). Note that if we define new state coordinates $z \in \Re^n$ as

$$z_k = L_f^{k-1}(h), \quad k = 1, \ldots, r \tag{5.10}$$

then the nonlinear system (5.8), as obtained from the previous procedure, can be written in the form

$$\dot{z} = \begin{bmatrix} 0 & 1 & 0 & \cdots & 0 \\ 0 & 0 & 1 & \cdots & 0 \\ 0 & 0 & 0 & \cdots & 1 \\ 0 & 0 & 0 & \cdots & 0 \end{bmatrix} z + \begin{bmatrix} 0 \\ 0 \\ \vdots \\ 0 \\ \alpha(x) + \rho(x)u \end{bmatrix}, \tag{5.11}$$

where

$$\alpha(x) = L_f^r(h), \quad \rho(x) = L_g(L_f^{r-1}(h)). \tag{5.12}$$

More generally, using the new coordinates z (5.10) and introducing a nonlinear feedback control of the form

$$u = \frac{(v - \sigma(x))}{\rho(x)} \tag{5.13}$$

where

$$\sigma(x) = \sum_{k=0}^{r-1} \beta_k L_f^k(h) + L_f^r(h), \tag{5.14}$$

$$\rho(x) = L_g(L_f^{r-1}(h)), \tag{5.15}$$

with β_k for $k = 0, \ldots, r-1$ real positive coefficients then the equations (5.6)-(5.7) can be written in 'reduced' form;

$$\dot{z} = \begin{bmatrix} 0 & 1 & 0 & \cdots & 0 \\ 0 & 0 & 1 & \cdots & 0 \\ & & & & \\ 0 & 0 & 0 & \ddots & 0 \\ -\beta_0 & -\beta_1 & -\beta_2 & \ldots & -\beta_{r-1} \end{bmatrix} z + \begin{pmatrix} 0 \\ 0 \\ \vdots \\ 1 \end{pmatrix} v \tag{5.16}$$

$$y = [1, 0, \ldots, 0]\, z. \tag{5.17}$$

Nonlinear System Transmission Zeros Note that the process leading to (5.16)-(5.17) provides an equivalent state space realization for the input-output map of McMillan degree strictly less than n (the dimension of the original state space model (5.1)-(5.2)) *by decoupling a portion of the system dynamics from the output response.* This is depicted in Figure 5.1. Thus the new state coordinates z are a 'partial' state for the system. Thus stabilization of (5.16)-(5.17) cannot guarantee stabilization of the full state model (5.1)-(5.2).

Byrnes and Isidori [BI85] describe the above construction leading to a system *normal form* in the form (5.16)-(5.17) from which complete stability results can be obtained. The main result provides the existence of a transformation of coordinates $x \rightarrow (\xi, z)$, with the state partition in the new coordinates $\xi \in \Re^{n-r}$, $z \in \Re^r$ so that the full state representation in the new coordinates is in *normal form*;

$$\dot{\xi} = F(\xi, z), \tag{5.18}$$

$$\dot{z} = \begin{bmatrix} 0 & I_{r-1} \\ 0 & 0 \end{bmatrix} z + \begin{bmatrix} 0 \\ 1 \end{bmatrix} [\beta(\xi, z) + \tau(\xi, z)u], \tag{5.19}$$

where $\beta(\xi, z) = \alpha(x(\xi, z))$ and $\tau(\xi, z) = \rho(x(\xi, z))$. Thus we can define *zero dynamics* of the original system (5.1)-(5.2) as the autonomous system

$$\dot{\xi} = F(\xi, 0). \tag{5.20}$$

Partial Linearization for Lagrangian Systems Despite the apparent simplicity of determining the zero dynamics from the normal form as above it is, however, quite complex to compute the complete transformation leading to the full state normal form as given above. One approach (if possible) is to obtain the full state exact linearizing transformation via the procedure given by Hunt, Su, and Meyer [HSM83] which requires the solution of a set of simultaneous partial differential equations. However, in many special cases the zero dynamics as well as the required transformations for partial linearizing control can be obtained more directly. In the sequel we discuss the required constructions for Lagrangian systems.

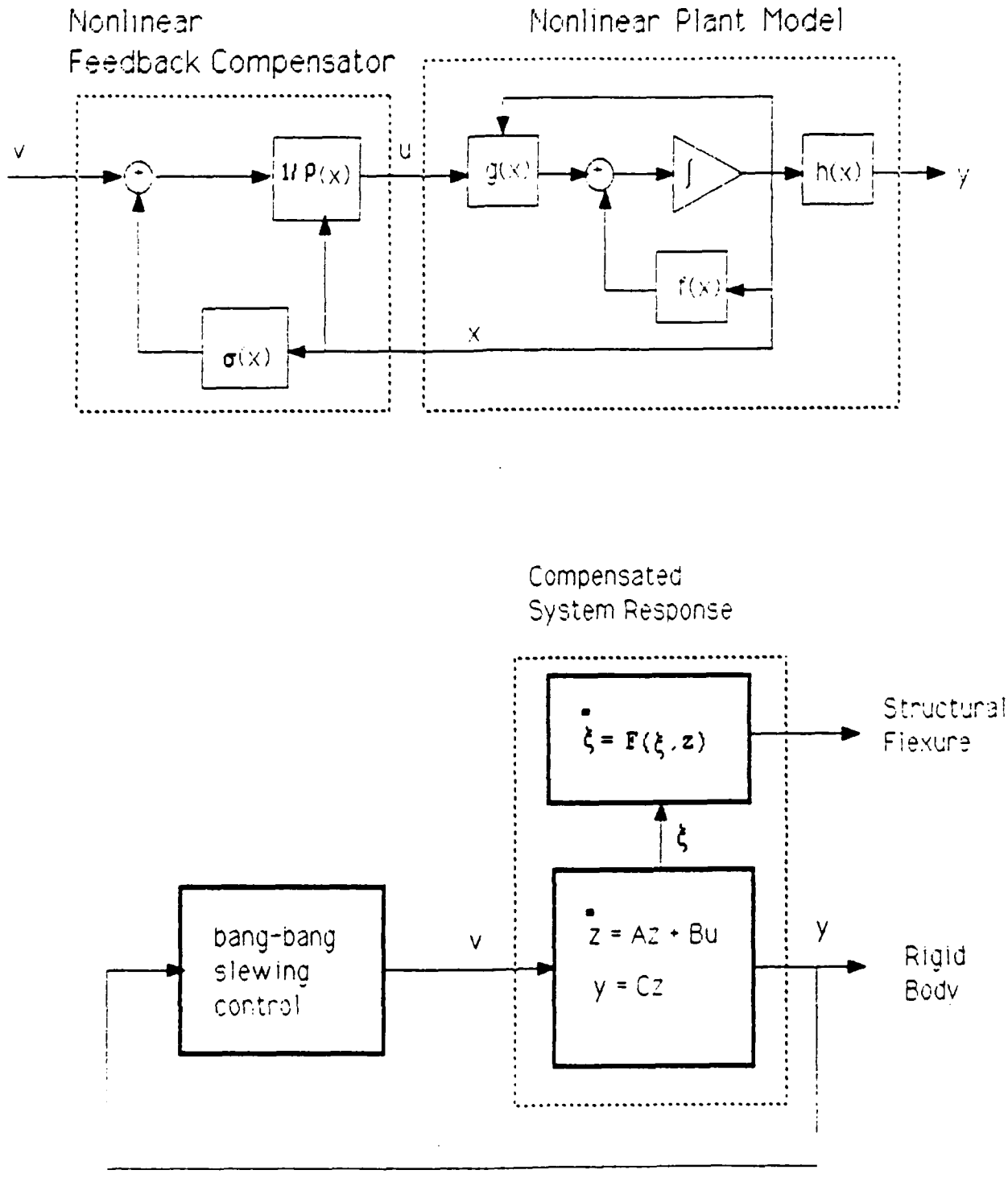

Figure 5.1: Partial Feedback Linearization and Zero Dynamics

Consider the case of a square Lagrangian system with inputs $\tau \in \Re^m$ and outputs $y \in \Re^m$. Suppose that the n generalized coordinates can be partitioned into components $q_1 \in \Re^m$ and $q_2 \in \Re^{n-m}$ so that the equations of motion take the form

$$\frac{d}{dt}\frac{\partial L}{\partial \dot{q}_1} - \frac{\partial L}{\partial q_1} = \tau, \tag{5.21}$$

$$\frac{d}{dt}\frac{\partial L}{\partial \dot{q}_2} - \frac{\partial L}{\partial q_2} = 0, \tag{5.22}$$

$$y = h(q_1, q_2). \tag{5.23}$$

Assume that the origin is an equilibrium point with $\tau = 0$, $h(0,0) = 0$, and that the Jacobian $\partial h / \partial q_1$ is nonsingular on some neighborhood of the origin. Furthermore, we assume that the Lagrangian is a positive definite quadratic form in the generalized velocities. Then the input-output map ($\tau \rightarrow y$) has relative degree 2 (locally), a PLF control exists and the zero dynamics may be computed by a relatively simple coordinate transformation applied to (5.21)–(5.23).

In order to demonstrate these properties we introduce a change of coordinates $(q_1, q_2) \mapsto (y, u)$ via the relations

$$y = h(q_1, q_2), \quad u = q_2 \tag{5.24}$$

Note that the assumption $\det \partial h / \partial q_1 \neq 0$ at the origin assures that this is a valid local coordinates transformation and the inverse relations can be given as

$$q_1 = g(y, u), \quad q_2 = u. \tag{5.25}$$

Since any "point" transformation preserves the Lagrangian structure of the equations, in the new coordinates we can write the variational problem in the form

$$\frac{d}{dt}\frac{\partial \hat{L}}{\partial \dot{y}} - \frac{\partial \hat{L}}{\partial y} = \hat{\Gamma}_y \tau, \tag{5.26}$$

$$\frac{d}{dt}\frac{\partial \hat{L}}{\partial \dot{u}} - \frac{\partial \hat{L}}{\partial u} = \hat{\Gamma}_u \tau, \tag{5.27}$$

where

$$\hat{L}(y, \dot{y}, u, \dot{u}) = L(q_1, \dot{q}_1, q_2, \dot{q}_2)\big|_{q_1 = g(y,u), q_2 = u} \tag{5.28}$$

and

$$\hat{\Gamma}_y = \left[\frac{\partial g}{\partial y}\right]^T, \quad \hat{\Gamma}_u = \left[\frac{\partial g}{\partial u}\right]^T. \tag{5.29}$$

Equations (5.26)–(5.27) reduce to the form

$$\hat{J}_y \ddot{y} + \hat{N} \ddot{u} + \hat{K}_y(y, \dot{y}, u, \dot{u}) = \hat{\Gamma}_y \tau, \tag{5.30}$$

$$\hat{N}^T \ddot{y} + \hat{J}_u \ddot{u} + \hat{K}_u(y, \dot{y}, u, \dot{u}) = \hat{\Gamma}_u \tau. \tag{5.31}$$

Let us define the partitioned matrices $\Sigma_y, \Sigma_u, \Phi_y, \Phi_u$, via the relations

$$\begin{pmatrix} \Sigma_y \\ \Sigma_u \end{pmatrix} = \begin{bmatrix} \hat{J}_y & \hat{N} \\ \hat{N}^T & \hat{J}_u \end{bmatrix}^{-1} \begin{pmatrix} \hat{K}_y \\ \hat{K}_u \end{pmatrix} \tag{5.32}$$

and

$$\begin{pmatrix} \Phi_y \\ \Phi_u \end{pmatrix} = \begin{bmatrix} \hat{J}_y & \hat{N} \\ \hat{N}^T & \hat{J}_u \end{bmatrix}^{-1} \begin{pmatrix} \hat{\Gamma}_y \\ \hat{\Gamma}_u \end{pmatrix}. \tag{5.33}$$

Note the choice of control

$$\tau = \Phi_y^{-1}\{\Sigma_y + v\} \tag{5.34}$$

reduces (5.30)–(5.31) to

$$\ddot{y} = v \tag{5.35}$$

$$\hat{N}^T(y,u)\ddot{y} + \hat{J}_u(y,u)\ddot{u} + \hat{K}(y,\dot{y},u,\dot{u}) = \hat{\Gamma}_u(y,u)\Phi_y^{-1}(y,u)\{\Sigma_y(y,u) + v\} \tag{5.36}$$

where we have explicitly displayed the dependence of the model parameters on the generalized coordinates. Equation (5.35) provides the linearized input-output dynamics and the zero dynamics are obtained from (5.36) upon setting $y(t) = 0$, which implies $\dot{y} = 0, \ddot{y} = 0$, and $v = 0$. Thus, we obtain the zero dynamics in the form

$$\hat{J}_u(0,u)\ddot{u} + \hat{K}(0,0,u,\dot{u}) - \hat{\Gamma}_u(0,u)\Phi_y^{-1}(0,u)\Sigma_y(0,u) = 0 \tag{5.37}$$

which represents an autonomous nonlinear dynamical system in the state coordinates $u, \dot{u}$. We say the system is *locally minimum phase* if the origin in the $(u,\dot{u})$ coordinates is a stable equilibrium for (5.37). If the system is minimum phase then selecting the control v to stabilize the origin of (5.35) guarantees stability of the origin of the dynamical system (5.21)–(5.23). Thus the computational complexity of obtaining the zero dynamics depends on the complexity of the required inverse relation g in (5.25).

In the next section we indicate the importance of this approach to nonlinear control system design for rapid reorientation (slewing) of a flexible space structure.

6 Rapid Slewing Control for Flexible Space Structures

A primary measure of system performance for an SBL weapon system is its retargeting envelope consisting of achievable changes in LOS angle and required minimum slewing time for a given maximum torque capability. For system torque sizing a time-optimal control maneuver is usually assumed. Since the ideal, time-optimal acceleration waveform is a discontinuous, bang-bang control, achievable performance is typically limited by actuator slew rate limiting. For precision optical systems, elastic interactions from spacecraft and optical system support structure may limit achievable slewing times and retargeting angles well before actuator slew rate limiting becomes a factor. Structural excitation will ultimately limit fine pointing precision and optical component alignment and will increase effective system slew times.

In this section we describe the application of PFL and decoupling control for rapid slewing of a flexible space structure. We consider slewing of the system principal LOS while decoupling the system elastic response. Our benchmark problem—as described in a previous section—is motivated by the elastic interactions due to structural deformation in a metering truss of a typical optical beam expander for a SBL system. Initially, we consider LOS defined

in terms of principal body attitude and consider the limits of achievable performance. Next we refine the definition of optical LOS to include relative alignment of optical components subject to structural deformation dynamics. We indicate how to utilize available optical steering mirror components to compensate for structural interaction contributing to a well defined system LOS. Simulation results for a simple planar dynamical model are provided based on the finite element model developed in a previous section and using available system parameters for a typical SBL benchmark.

6.1 Slewing Control for Principal Body LOS

To illustrate the application of nonlinear PFL we focus on the simple planar model for slewing developed in section 3.4 and given by equations (4.32)–(4.35). Consider a typical optical train for a laser beam expander as shown in Figure 6.1. Various options for a support structure for the secondary mirror (metering truss) are considered in the system study [Lea87]. Clearly, flexure response of the metering truss is an issue of dominant concern affecting the optical system alignment including focusing and LOS pointing. The model equations (4.32)–(4.35) can be readily adapted to characterize the principal dynamics of this system under the assumption of planar motion and assuming the metering truss is the primary source of structural flexure affecting LOS pointing.

Initially, we approximate the elastic deformation of the metering truss using a uniform beam model and take the structural parameters $E, I, \rho, A, \kappa G$ as constant over the length of the truss $0 \leq z \leq \ell$. For our simple planar slewing model we take as a model for the system effective optical LOS as θ_{LOS}, given by

$$\theta_{LOS} = \theta_b + \Delta_{LOS} \tag{6.1}$$

where θ_b is the principal body attitude in the $x \times z$ plane and Δ_{LOS} is a relative LOS deflection due to deformation of the metering truss and the resulting dynamic misalignment of the secondary mirror. For the case of planar motion we can model the relative LOS as a perturbation of the body LOS resulting from angular deformation at the secondary mirror of the form,

$$\Delta_{LOS} = 2\{\eta_z(\ell) + \theta(\ell)\}. \tag{6.2}$$

This simple model is summarized in Figure 6.2.

For simulation purposes we introduced a finite element model for this system in section 3.3.1 given by equations (4.66)–(4.68). Our initial considerations for rapid slewing are focused on attitude reorientation of the spacecraft principal body. Thus we define the system output as $y = \theta_b$.

To obtain the PFL transformation we proceed as for Lagrangian systems. In this case the required change of coordinates is trivial since (4.66)–(4.68) are already in the form (5.30)–(5.31) with respect to the system output $y = \theta_b$ and $u = (\bar{\eta}, \bar{\theta})^T$. Thus the linearizing feedback torque can be given immediately from (5.34).

To illustrate the simplicity of the computations, we identify the model equations (4.66)–(4.68) in the form

$$J_\theta(u)\ddot{\theta}_b + N^T\ddot{u} + K_\theta = T_b \tag{6.3}$$

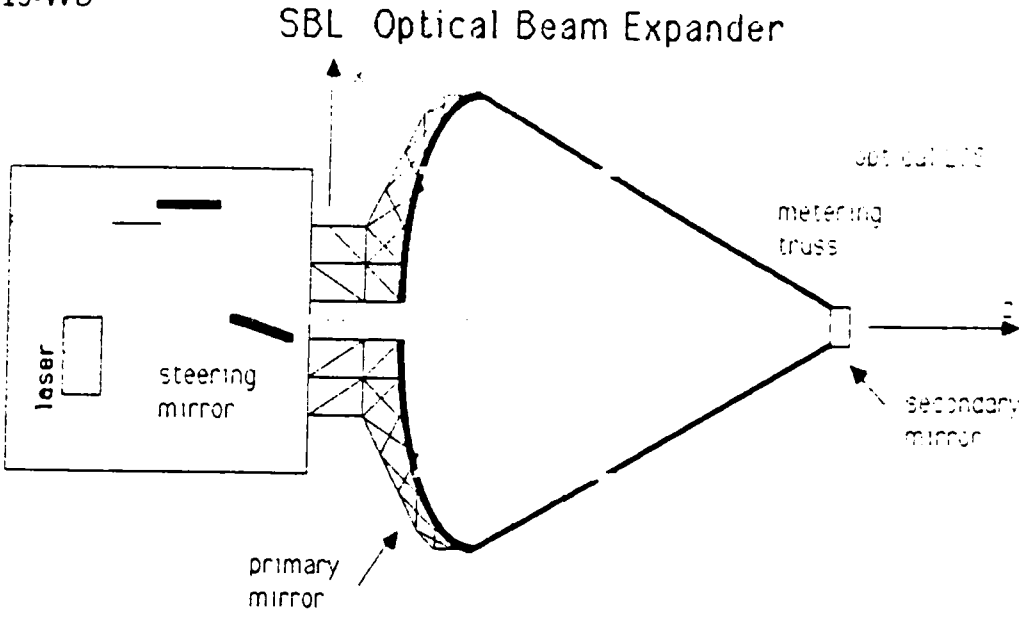

Figure 6.1: Optical Train for Typical Laser Beam Expander

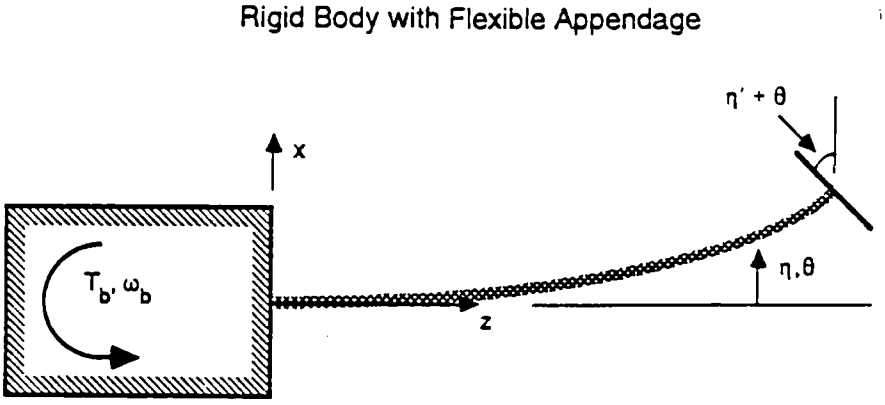

$$I_b\dot{\omega}_b + \int_0^l \{z(\ddot{\eta} + \dot{\omega}_b z + \omega_b^2\eta)\rho A + (\dot{\omega}_b + \ddot{\theta})\rho I\}dz = T_b$$

$$\rho A(\ddot{\eta} + \dot{\omega}_b z + \omega_b^2\eta) + \kappa GA(\eta'' + \theta') = 0$$

$$\rho I(\dot{\omega}_b + \ddot{\theta}) + EI\theta'' - \kappa GA(\eta' - \theta) = 0$$

Geometric Boundary Conditions: $\eta(0,t) = 0$ and $\theta(0,t) = 0$

Natural Boundary Conditions: $\eta'(l,t) = 0$ and $\theta'(l,t) = 0$

Rigid Body LOS = θ_b

Relative LOS = $2\{\eta'(l,t) + \theta(l,t)\}$

Figure 6.2: Planar slewing model for optical beam expander

$$M_s\ddot{u} + N\ddot{\theta} + K_u = 0 \tag{6.4}$$

where

$$J_\theta = M_\omega + \bar{\eta}^T N_\eta \bar{\eta}$$

$$M_s = \begin{bmatrix} N_\eta & 0 \\ 0 & N_\theta \end{bmatrix}, \quad N = \begin{bmatrix} N_{\omega_b \eta} \\ N_{\omega_b \theta} \end{bmatrix}$$

$$K_\theta = 2\omega_b \bar{\eta}^T N_\eta \bar{\eta},$$

$$K_u = \begin{bmatrix} (K_\eta - \omega_b^2 N_\eta) & K_{\eta\theta} \\ K_{\eta\theta}^T & K_\theta \end{bmatrix} \begin{pmatrix} \bar{\eta} \\ \bar{\theta} \end{pmatrix} + \begin{bmatrix} B_\eta & B_{\eta\theta} \\ B_{\eta\theta}^T & B_\theta \end{bmatrix} \begin{pmatrix} \dot{\bar{\eta}} \\ \dot{\bar{\theta}} \end{pmatrix}.$$

The PFL torque is

$$T_b = K_\theta + \hat{M}_{11}^{-1}(\hat{M}_{12} K_u + v) \tag{6.5}$$

where

$$\hat{M} = \begin{bmatrix} \hat{M}_{11} & \hat{M}_{12} \\ \hat{M}_{21} & \hat{M}_{22} \end{bmatrix} = \begin{bmatrix} J_\theta & N^T \\ N & M_s \end{bmatrix}^{-1}.$$

and v is the new, synthetic control input. The nonlinear feedback transformation linearizes the input-output map from $v \mapsto y$ and decouples the u dynamics so that;

$$\ddot{y} = v.$$

The resulting system is stable if and only if the decoupled, zero dynamics are stable. In this case, the zero dynamics are readily obtained from (6.3) by letting $\theta \to 0, \dot{\theta} \to 0, \ddot{\theta} \to 0$;

$$M_s\ddot{u} + K_u = 0,$$

which is the (linear) cantilevered dynamics of the flexible appendage. Clearly, this is (practically) stable as long as sufficient damping (either active or passive) is present in the structure.

Design of time-optimal slewing of the decoupled, linear, θ_b dynamics is now straightforward and practical implementation is discussed next.

Pseudo-Time Optimal Control of Ideal Rigid Body Inertia. Time-optimal slewing of a pure inertia subject to limited acceleration consists of a bang-bang acceleration with constant acceleration up to a switching instant at which time a constant deceleration is applied. Implementation of time-optimal control for a pure inertia involves determination of a switching condition for the ideal, bang-bang acceleration (control). For feedback control we would like to obtain a switching surface in the phase plane $(\theta, \dot{\theta})$. The ideal bang-bang control is discontinuous with respect to this switching surface.

Trajectories in the phase plane of $(\theta, \dot{\theta})$ for constant acceleration can be obtained from the flow of

$$\ddot{\theta} = \alpha_{max}$$

with α_{max} a constant. The required switching condition is defined in terms of a switching surface given by the phase-plane trajectory approaching the origin which satisfies the condition;

$$2\alpha_{max}\theta \pm \dot{\theta}^2 = 0$$

with sign depending on the sign of α_{max}. For $\alpha_{max} > 0$ the required ideal switching surface is given by

$$s(\theta, \dot{\theta}) = 2\alpha_{max}\theta + \dot{\theta}|\dot{\theta}| = 0,$$

and the ideal, time-optimal acceleration is a switching law of the form,

$$\alpha = -\text{sgn}\{2\alpha_{max}\theta + \dot{\theta}|\dot{\theta}|\}.$$

Practical application of the above control is limited by the requirement for instantaneous torque (acceleration) switching and by he tendency for a feedback implementation of the above form to limit cycle in the region near the phase plane origin.

A practical, pseudo-time-optimal control can be implemented using feedback by replacing the requirement for instantaneous switching with a direct limit on acceleration slewing rate. This is achieved by replacing the sgn function with a saturation function of the form,

$$\text{sat}(\epsilon) = \begin{cases} \alpha_{max}, & \epsilon > \alpha_{max} \\ \epsilon, & |\epsilon| \leq \alpha_{max} \\ -\alpha_{max}, & \epsilon < -\alpha_{max} \end{cases}.$$

The pseudo-time-optimal control can then be implemented in the form,

$$\alpha = -\text{sat}\{g_1(f(\omega) + 2\alpha_{max}\theta)\} \tag{6.6}$$

where $\omega = \dot{\theta}$, the nonlinear function $f(\omega)$ is a piecewise continuous approximation to the ideal quadratic switching surface

$$f(\omega) = \begin{cases} \omega^2 + g_2^2/4, & \omega > g_2/2 \\ g_2\omega, & |\omega| \leq g_2/2 \\ -\omega^2 - g_2^2/4, & \omega < -g_2/2 \end{cases}.$$

The constant gain g_1 is chosen to represent slew rate limiting in the torque actuator and g_2 is chosen to provide stable (damped) pointing response.

Given the nonlinear PFL transformation the pseudo-time-optimal control can now be implemented directly for principal body LOS slewing by setting $v = \alpha$ in (6.5) with α given in (6.6).

6.2 Simulation Results for Principal Body LOS Slewing

The finite dimensional simulation model for planar slewing is now used to illustrate the behavior of the combined nonlinear PFL and pseudo-time-optimal control given by (6.5), (6.6) and $v = \alpha$. The FEM model is described in Section 3.4.2 and is based on physical parameters given in Table 6.1 which are loosely taken from the system study [Lea87]. The elastic and shear moduli are chosen to roughly approximate the reported first modal frequency of the metering truss obtained from the structural analysis of the benchmark SBL system [Lea87]. The internal dissipation parameters, ζ_3 (ζ_4) were chosen, somewhat arbitrarily, as small fractions ($\tilde{2}\%$) of the elastic (resp. shear) modulus. The external damping coefficients ζ_1, ζ_2

Parameter	Value	Description
I_b	1.325E+06	principal body moment of inertia
ℓ	15.	length of appendage
ρ	1520.	mass density of appendage
A	0.01298	cross section area of appendage
E	1.6E+07	appendage elasticity modulus
κG	6.4E+06	appendage shear modulus
I	693.11	appendage area moment
ζ_1, ζ_2	0.0	external dissipation coefficient
ζ_3	1661.44	internal dissipation coefficient
ζ_4	0.222E+09	internal dissipation coefficient

Table 6.1: Physical Parameters for Simulation Model (in MKS units)

mode	frequency (r/s)	mode	frequency (r/s)
1	6.8167991	7	64.716684
2	19.996775	8	73.055738
3	20.941475	9	87.662067
4	36.418957	10	91.188281
5	41.217664	11	118.80496
6	54.057492	12	139.11817

Table 6.2: Undamped Frequencies of Cantilevered Appendage Dynamics

are set to zero to simulate space environment. The resulting undamped frequencies of the cantilevered appendage dynamics are given in Table 6.2.

The resulting response in principal body LOS θ_b for $N = 5$ finite elements is shown in Figure 6.3 for a 30 degree slew. The commanded ideal LOS acceleration α obtained from (6.6) with $\theta = \theta_b$, $\omega = \omega_b$ is shown in Figure 6.4. The required linearizing torque T_b obtained from (6.5) is shown in Figure 6.5. Clearly, substantial additional torque capability is needed to implement the exact PFL control and decouple the effect of the flexible appendage on the rigid body attitude. A principal focus of the FY89 project will be to investigate options for approximating the PFL torque so that both torque authority and torque bandwidth can be relaxed. See the appendix on Slew Induced Deformation Shaping.

For optical LOS slewing the resulting relative LOS Δ_{LOS} given in (6.2) will also be of concern. Figure 6.6 displays the response in Δ_{LOS} as obtained in (6.2) for the simple planar slewing model. Clearly, excessive deformation of the secondary mirror orientation will degrade the optical LOS after the completion of the primary body LOS slewing maneuver. In the next section we describe a method for decoupling and PFL for the effective optical LOS in addition to the primary body attitude by introducing additional control capability.

6.3 Optical LOS Slewing using Steering Mirror Compensation for Structural Deformation.

For rapid slewing and precision pointing of space-based optical systems and essential consideration is structural interaction with the optical train alignment and resulting degradation of system performance. With respect to the benchmark model of the laser beam expander we focus on the relative alignment of the primary and secondary mirror due to elastic deformation of the metering truss. Throughout this study we have assumed that the introduction of active structural control on the metering truss is precluded by considerations of optical path occlusion from expanded cross section of the truss members with additional control components. The system study [Lea87] considers various options for truss configurations and strut material but does not consider active control of the truss.

It is easy to show that PFL of the simple model of effective system optical LOS given in (6.1) using the rigid body torque T_b only is not feasible because the system response from T_b to θ_{LOS} is *nonminimum phase*. This is an essential characteristic of distributed parameter models for structural dynamics with one or more spatial dimensions. As is well known for the case of linear models for such systems the response from generalized force control to position output will be minimum phase only if the point of control and observation are spatially colocated. However, in this case additional control degrees of freedom are available using the optical system components. Referring to Figure 6.1 the optical steering mirrors are included to provide fine pointing adjustment of the optical LOS.

Consider a simple model of the effect of relative angular motion of the steering mirror, θ_m, on the system relative LOS (measured in the primary body fixed frame) given by,

$$\Delta_{LOS} = 2\{\eta_z(\ell) + \theta(\ell)\} - 2\theta_m. \tag{6.7}$$

We assume that the steering mirror is mounted on the primary body. Its dynamic interaction

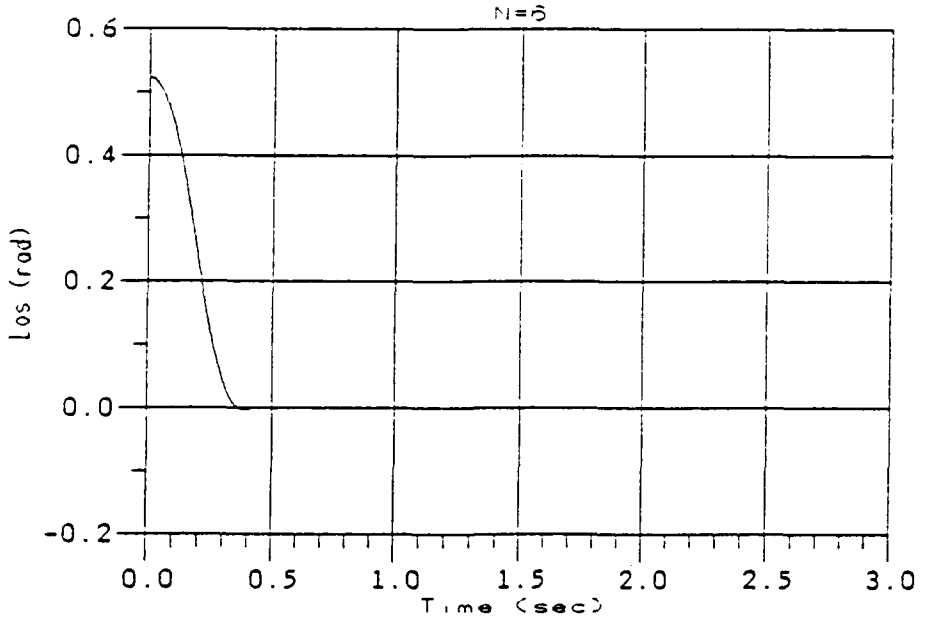

Figure 6.3: Principal Body LOS Slew with PFL Decoupling Control.

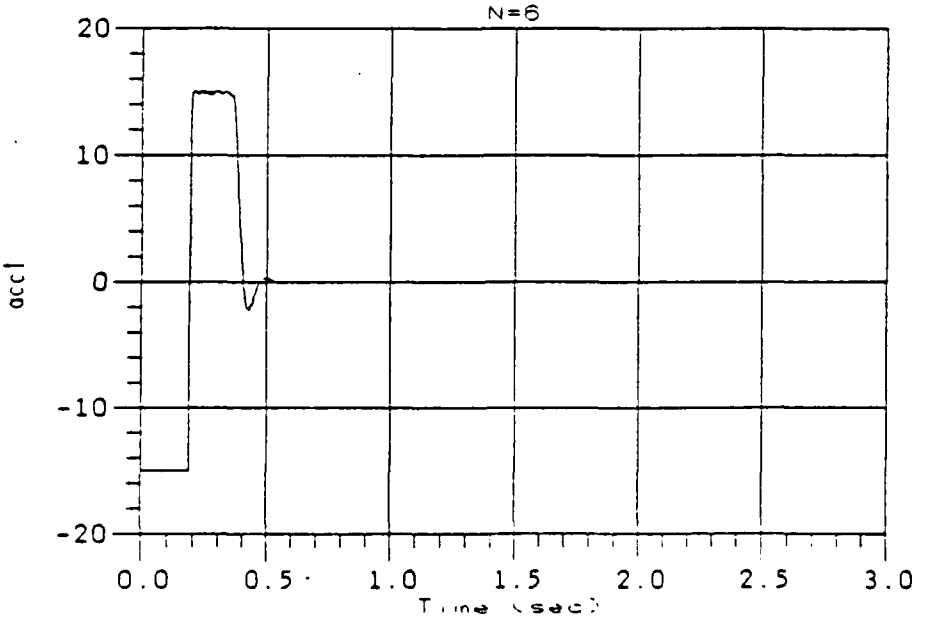

Figure 6.4: Ideal Commanded LOS Acceleration Profile.

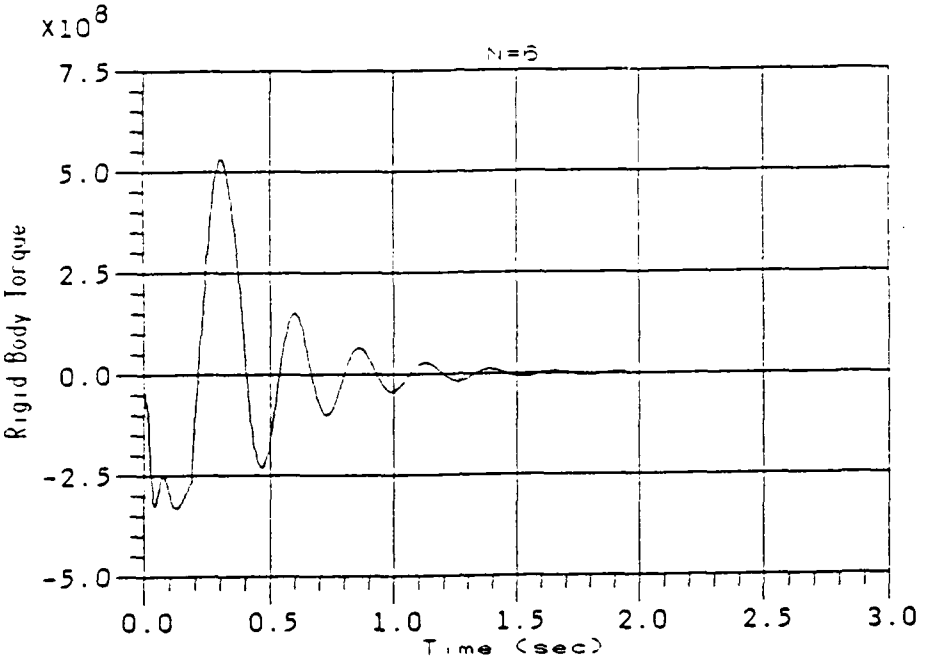

Figure 6.5: PFL/Decoupling Torque T_b for Principal Body LOS Slew

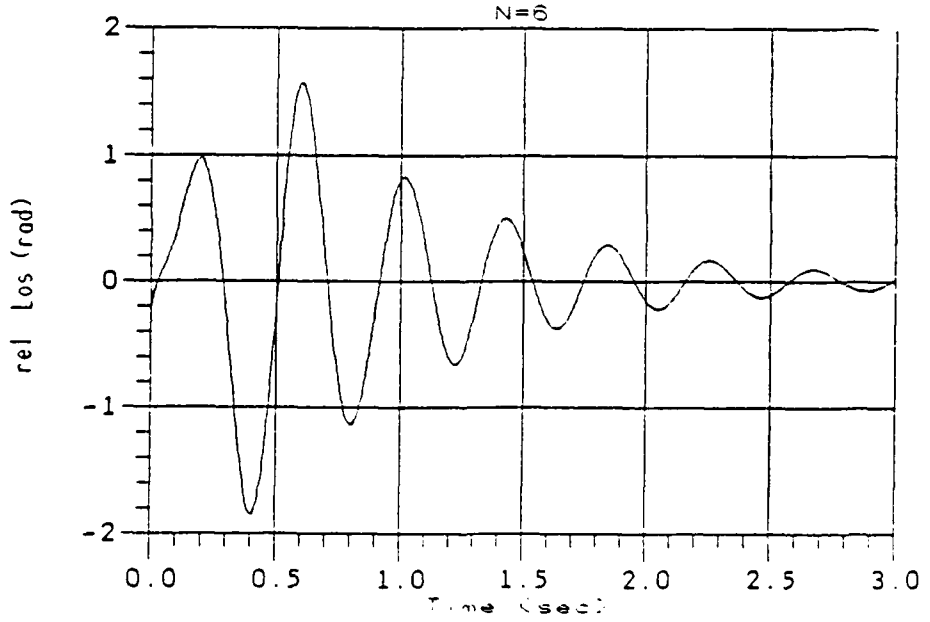

Figure 6.6: Relative Optical LOS Δ_{LOS} for Decoupled Principal Body Slew

with the body is given by the modified equations of motion (for the reduced order model);

$$[M_\omega + \bar{\eta}^T N_\eta \bar{\eta}]\dot{\omega}_b + I_m\dot{\omega}_m + N^T_{\omega_b\eta}\ddot{\bar{\eta}} + N^T_{\omega_b\theta}\ddot{\bar{\theta}} + \omega_b\bar{\eta}^T N_\eta\dot{\bar{\eta}} = T_b, \tag{6.8}$$

$$I_m(\dot{\omega}_b - \dot{\omega}_m) = T_m, \tag{6.9}$$

$$N_\eta\ddot{\bar{\eta}} + \dot{\omega}_b N_{\omega_b\eta} - \omega_b^2 N_\eta\bar{\eta} + K_\eta\bar{\eta} + K_{\eta\theta}\bar{\theta} + B_\eta\dot{\bar{\eta}} + B_{\eta\theta}\dot{\bar{\theta}} = 0, \tag{6.10}$$

$$N_\theta\ddot{\bar{\theta}} + \dot{\omega}_b N_{\omega_b\theta} + K_\theta\bar{\theta} + K^T_{\eta\theta}\bar{\eta} + B_\theta\dot{\bar{\theta}} + B^T_{\eta\theta}\dot{\bar{\eta}} = 0, \tag{6.11}$$

where I_m is the steering mirror inertia and T_m is the control torque applied to the steering mirror in the body frame. We have assumed a frictionless mount.

We now show that the two-input, two-output system from $(T_b, T_m) \mapsto (\theta_b, \theta_m)$ is relative degree 2, minimum phase, and can be linearized by PFL transformation. Furthermore, the resulting PFL response is *decoupled* in the sense that after the introduction of nonlinear feedback the response from the new synthetic inputs $(v_1, v_2) \mapsto (\theta_b, \theta_m)$ is of the form,

$$\begin{aligned} \ddot{\theta}_b &= v_1 \\ \ddot{\theta}_m &= v_2. \end{aligned}$$

To compute the 2-input/2-output PFL torques we identify a transformation of the generalized coordinates;

$$y_1 = \theta_b \tag{6.12}$$

$$y_2 = 2\{\eta_z(\ell) + \theta(\ell)\} - 2\theta_m. \tag{6.13}$$

From the finite element model described in Section 3.4.2 we can see using B-splines that the local slope is obtained as,

$$\eta_z(z,t)|_{z=\ell} \approx \left.\frac{\partial\Phi^T(z)}{\partial z}\bar{\eta}(t)\right|_{z=\ell} = -(\tfrac{N}{\ell})\eta_N(t), \tag{6.14}$$

so that we obtain the relative LOS for the finite element model in the form,

$$\begin{aligned} \Delta_{LOS} &\approx 2\{[0,\ldots,0,-(\tfrac{N}{\ell})]\bar{\eta} + [0,\ldots,0,1]\bar{\theta}\} - 2\theta_m, \\ &= \bar{c}^T_\eta\bar{\eta} + \bar{c}^T_\theta\bar{\theta} - 2\theta_m. \end{aligned} \tag{6.15}$$

From the above we can rewrite the modified system equations of motion in terms of the new generalized coordinates y_1, y_2 and using the FEM LOS approximation as,

$$\begin{aligned} [M_\omega + \bar{\eta}^T N_\eta\bar{\eta}]\ddot{y}_1 - \tfrac{1}{2}I_m\ddot{y}_2 + [N^T_{\omega_b\eta} + I_m\bar{c}^T_\eta]\ddot{\bar{\eta}} + [N^T_{\omega_b\theta} + I_m\bar{c}^T_\theta]\ddot{\bar{\theta}} \\ + 2\dot{y}_1\bar{\eta}^T N_\eta\dot{\bar{\eta}} = T_b, \end{aligned} \tag{6.16}$$

$$I_m\ddot{y}_1 + \tfrac{1}{2}I_m\ddot{y}_2 - I_m\bar{c}^T_\eta\ddot{\bar{\eta}} - I_m\bar{c}^T_\theta\ddot{\bar{\theta}} = T_m, \tag{6.17}$$

$$N_\eta\ddot{\bar{\eta}} + \ddot{y}_1 N_{\omega_b\eta} - \dot{y}_1^2 N_\eta\bar{\eta} + K_\eta\bar{\eta} + K_{\eta\theta}\bar{\theta} + B_\eta\dot{\bar{\eta}} + B_{\eta\theta}\dot{\bar{\theta}} = 0, \tag{6.18}$$

$$N_\theta\ddot{\bar{\theta}} + \ddot{y}_1 N_{\omega_b\theta} + K_\theta\bar{\theta} + K^T_{\eta\theta}\bar{\eta} + B_\theta\dot{\bar{\theta}} + B^T_{\eta\theta}\dot{\bar{\eta}} = 0. \tag{6.19}$$

Then the required decoupling torques T_b, T_m can be obtained directly from the above equations in the form

$$\begin{aligned} T_b &= [N^T_{\omega_b\eta} + I_m\bar{c}^T_\eta]\ddot{\bar{\eta}} + [N^T_{\omega_b\theta} + I_m\bar{c}^T_\theta]\ddot{\bar{\theta}} + 2\dot{y}_1\bar{\eta}^T N_\eta\dot{\bar{\eta}} \\ &\quad + [M_\omega + \bar{\eta}^T N_\eta\bar{\eta}]\alpha_1 - \tfrac{1}{2}I_m\alpha_2, \qquad (6.20) \\ T_m &= -I_m\bar{c}^T_\eta\ddot{\bar{\eta}} - I_m\bar{c}^T_\theta\ddot{\bar{\theta}} + I_m\alpha_1 + \tfrac{1}{2}I_m\alpha_2. \qquad (6.21) \end{aligned}$$

The required slewing controls can now be generated for the decoupled dynamics of the principal body LOS $y_1 = \theta_b$ and relative (body frame) LOS, $y_2 = \Delta_{LOS}$ exactly as before.

Remark. In this form it is clear that the PFL obtains the decoupled, linearized relations by exact cancelation of terms. It is also clear that potential for relatively simple implementation using accelerometers may offer advantages in this case since the PFL control is then insensitive to stiffness and damping properties of the elastic appendage. A goal of the FY89 effort will be to investigate the potential for the use of simplified and reliable PFL implementation using low cost, solid state accelerometers at numerous locations on the structure. We note that conclusive results in this area can be obtained only after a dynamic model of the accelerometer is included in the analysis and control design. The potential for such control implementation is important for several reasons not the least of which is the evolving technology for structural components with embedded solid state sensors and actuators (e.g. using piezoelectrics) [De86].

6.4 Simulation Results for Optical LOS Slewing

The above PFL decoupling control (6.20)-(6.21) was simulated for the ideal case with the addition of the steering mirror dynamics as given in (6.16)-(6.19). The resulting response in the principal body LOS θ_b and the relative (body frame) LOS, Δ_{LOS}, for a 30 degree slew are shown in Figure 6.7. The required linearizing torques T_b and T_m are shown in Figure 6.9-6.10. The ideal commanded acceleration for the rigid body slew α_1 is identical to that obtained for the case of principal body slewing since the slewing controls are decoupled by the introduction of PFL torques. A measure of appendage deformation resulting from the slew can be obtained by examining the response of the steering mirror θ_m (see Figure 6.8) and the deformation at the end of the appendage (at the secondary mirror) η_N, θ_N (see Figure 6.11). In this framework requirements for stiffness and damping of the metering truss can be determined based on structural limits of the secondary mirror deflection and angular limits of the steering mirror without concern for effective dynamic pointing precision.

7 Survey of Methods in Robust Nonlinear Control

7.1 Importance of Robust Control Design for Nonlinear Slewing Control

Recently considerable research effort has been expended in developing new methods for *robust control system design*. The goal of these methods has been to obtain quantifiable limits on the stability and performance of a control system with internal dynamics (of both

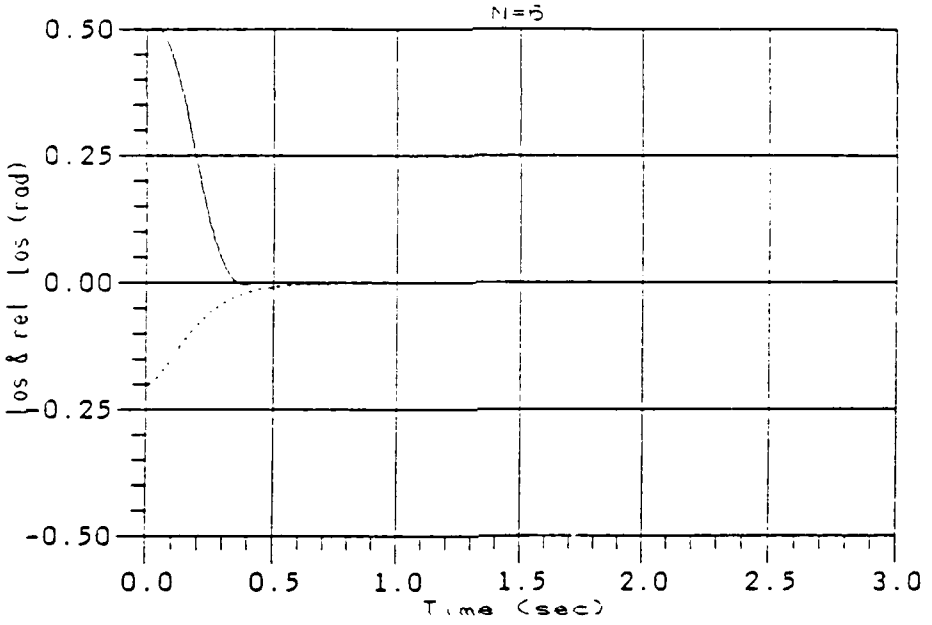

Figure 6.7: Optical System LOS Slew with Steering Mirror Control

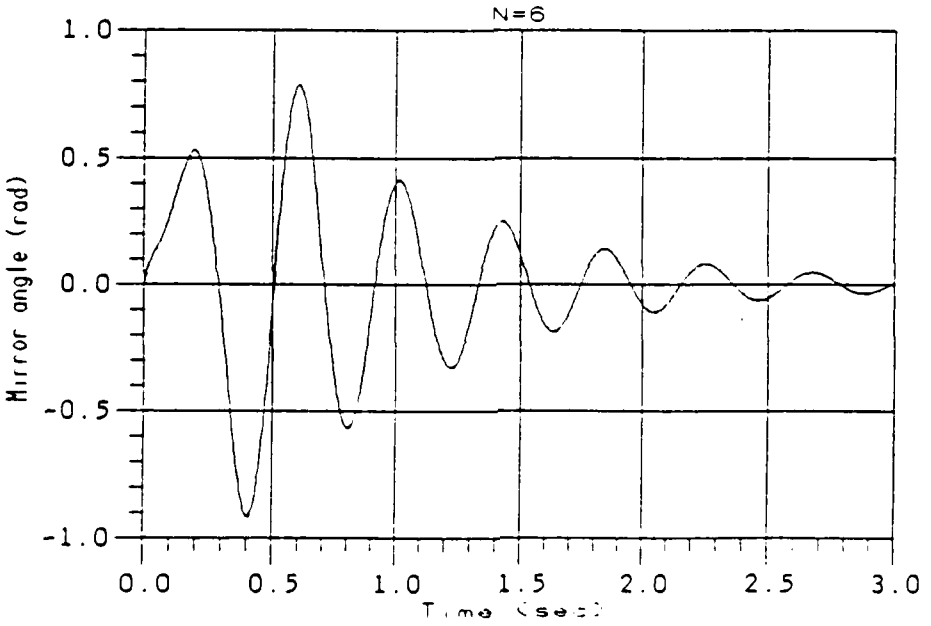

Figure 6.8: Steering Mirror Angular Deflection θ_m

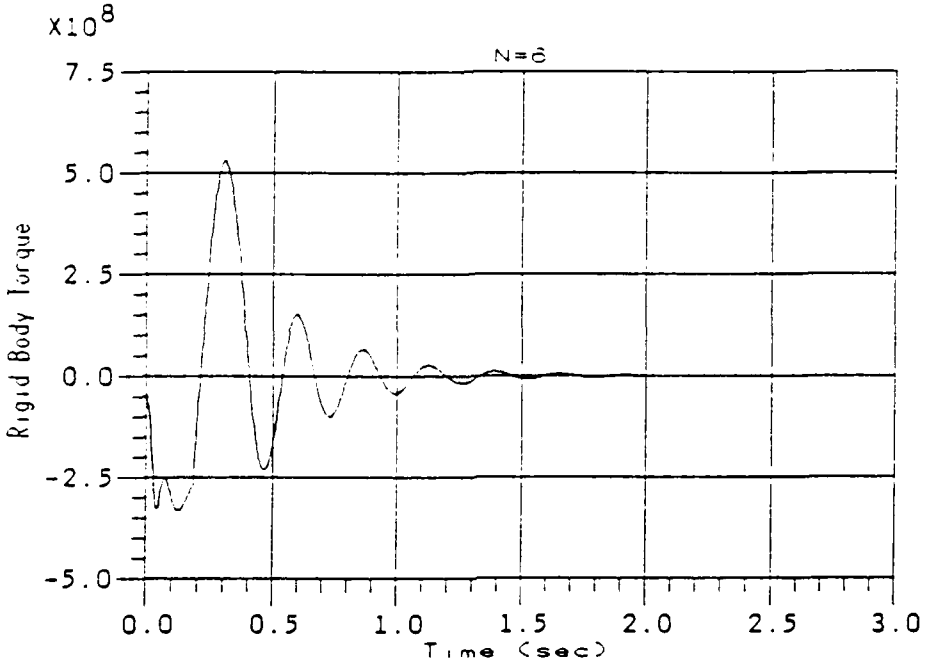

Figure 6.9: Rigid Body Linearizing Torque T_b for Optical LOS Decoupling

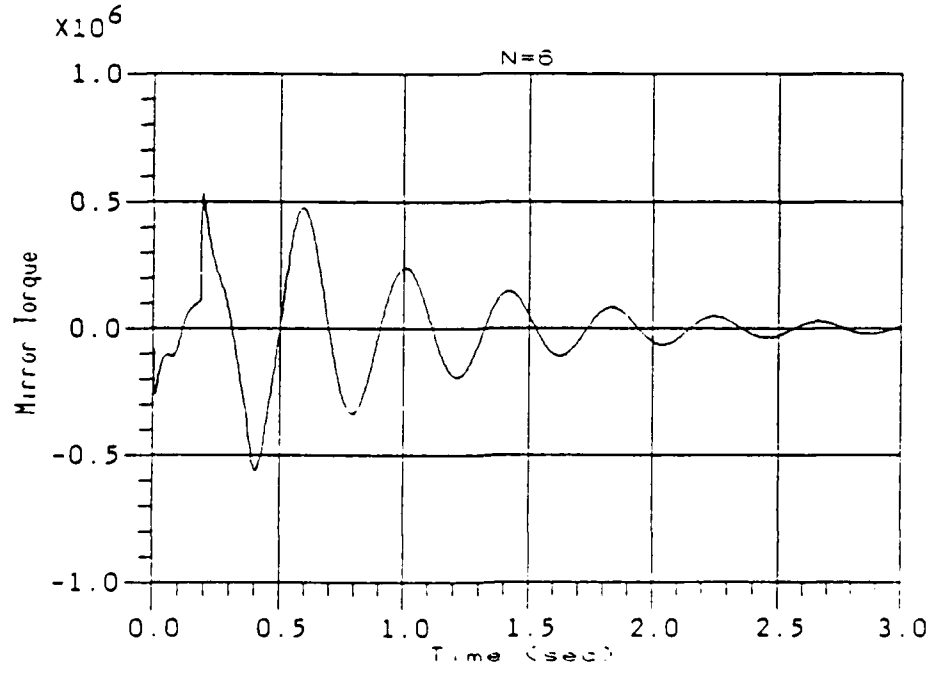

Figure 6.10: Steering Mirror Linearizing Torque T_m

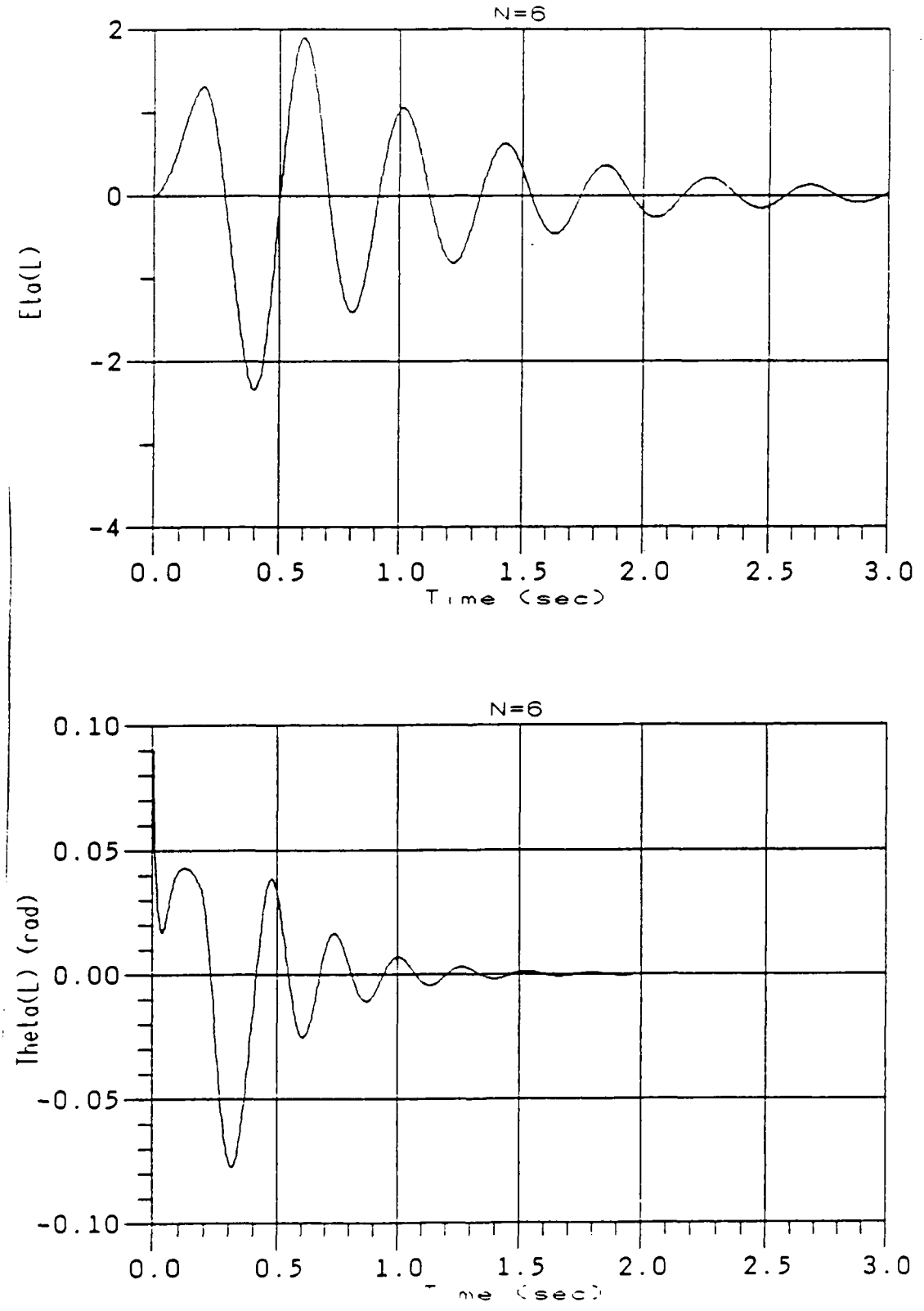

Figure 6.11: Appendage Deformation at Secondary Mirror for 30deg. Slew

the plant and the controller) which may vary in specific, quantifiable ways either due to changes in time or initial model imprecision. The importance of such methods can not be underestimated in practical applications. The primary emphasis in the engineering literature of the past 10 years on the robust control problem is the use of linear plant models and linear control law dynamics.

Early results of Nyquist [Nyq32] and the Bode [Bod45] provided an analytic basis for the fundamental engineering tradeoff between dynamic stability and a scalar loop-gain parameter of a single closed loop feedback control. In the early 1970's the focus of research turned to the robust stability of multiloop feedback control utilizing various extensions of Nyquist's theorems as pioneered by Rosenbrock [Ros74, Ros72]. Recognizing the critical need to predict stability of feedback control with certain nonlinear effects the engineering community developed various ways to bound certain nonlinear effects with linear systems and obtain (albeit somewhat conservative) stability results. A central contribution in this area is the work of Zames [Zam63] which provides the basis for the cornerstone of robust linear control theory known as the *small gain theorem*. Using this theorem results can be obtained for the class of *sector bounded* nonlinearities and have more recently been extended to multiloop control systems by using singular value bounds (i.e., L_2 norm) of the transfer function (matrix) frequency response. An essential feature of such methods for design is that the design engineer must have a model for the overall nonlinear system where the nonlinearities are memoryless and sector bounded and interact with a model of the system (linear) dynamics through a fixed number of feedback loops. Thus these methods support design of linear control systems for plants which may contain certain isolated nonlinear effects. In this study we have considered a more direct and comprehensive approach to nonlinear control system design in which the system nonlinear dynamics are utilized to effectively 'linearize' certain aspects of the system response.

Our main interest in the robust control problem for slewing control of flexible structures stems from:

1. Concern for practical application of advanced nonlinear control system design methods including both EFL and PFL for the class of models considered for slewing of SBL type systems. Such concerns include:
   (a) predicting performance limits with model dynamics based on imprecisely known parameters
   (b) predicting performance limits with reduced order model dynamics,
   (c) predicting performance in the presence of variation of system dynamics due to environmental changes effecting model parameters,
   (d) predicting performance in the presence of variation of system dynamics due to parasitic dynamics unknown at design time.
2. Concern for design of laboratory experiments to demonstrate advanced nonlinear control laws for rapid slewing control of flexible structures. Such concerns include:
   (a) predicting performance with modeling imprecision due to both parasitic dynamics and parametric variation,

(b) assuring stable and reliable operation of experiments including stable "tune up" procedures for testing high performance, high gain control laws.

In this section we will briefly review some available results in robust control system design for nonlinear systems which we believe will be important tools to address the above practical concerns. It is important to emphasize that the crucial issue in robust control of nonlinear slewing of flexible structures will be the incorporation of concerns for the parasitic (high frequency) dynamic uncertainty which is intrinsic in the distributed parameter dynamics of the flexible structure and the nonlinear (and parametric) uncertainty due to the dominance of certain nonlinear effects (such as Coriolis and gyroscopic accelerations) which arise because of the dynamic requirements of rapid slewing.

7.1.1 Classification of Robust Control Results and Assumptions

It is sometimes useful in surveying a literature as diverse as robust control design has become to attempt to classify results according to types of assumptions placed on the system dynamic model. The diversity available reflects an intense area of research where—very roughly put—the goal is to obtain the *least conservative* characterization of conditions for robust stability and performance with the *least restrictive* assumptions on the plant dynamics. Thus we can classify available results according to assumptions on model uncertainty as:

- parametric versus nonparametric (or parsitic),
- structured versus nonstructured.

Structured vs. Nonstructured Uncertainty. We indicate model uncertainty as *structured* if the uncertainty is characterized as being localized in the system dynamics (i.e., it effects a structured portion of the system model only) and *unstructured* otherwise.

Parametric versus nonparametric uncertainties. Parmetric models for dynamic uncertainly include cases where both physical and artifical model parameters are allowed to vary over specific sets. Such plant model variation does not incorporate changes in model order in a natural way. Nonparametric (or parasitic) model uncertainty attempts to characterize model variation which can incorporate changes in the effective dynamic degrees of freedom. We remark that the methods of *singular perturbation analysis* decribed for example in Kokotovic [Kok85] attempt to reconcile these two views of model uncertainty. As such we expect these method to play an important role in robust control of rapid slewing of flexible structures. (See Appendix C for preliminary results on application of these ideas to design of control for a flexible multibody system.)

7.2 Robust Stability of Linear Systems

By way of introduction, motivation, and comparison with available methods for nonlinear systems, we briefly review the general results for robust stabilization of linear systems.

The two common linear multivariable plant models used in literature are:

- State-variable models generally written in the form:

$$\dot{x} = Ax + Bu, \quad y = Cx + Du$$

- Transfer-function matrix models denoted $G(s)$ where $G(s)$ is a $p \times q$ matrix with entries made up of rational functions in the complex Laplace transform variable s.

Each one of these plant models requires its own type of uncertainty model. Some of these uncertainties for state-variable models can be modelled as follows:

Parametric unstructured: Let $Ax \rightarrow (A + \delta A)x$, where δA is constrained only in norm, i.e, $\| \delta A \| \leq a$.

Parametric structured: Two examples of model uncertain assumptions in this category are:

1. $Ax \rightarrow (A + \sum_i q_i A_i)x$, $-1 \leq q_i \leq 1$ where the parametric uncertainty, represented by q_i, is *structured* by virtue of the structure of the A_i.

2. Refering the linear state space model above $(A, B) \rightarrow (A + \delta A(q), B + \delta B(q))$ where q is assumed to belong to a known compact set. We say δA and δB satisfy the *structure matching* conditions if:

$$\delta A = BD, \quad \delta B = BE. \tag{7.1}$$

For robust stability of linear systems it is often more useful to characterize model uncertainty in terms of the frequency response or transfer function model. Uncertainty in G has been characterized as:

Multiplicative unstructured nonparametric; e.g., $G \rightarrow (I + L)G$ or $G(I + L)$ where $\|L(jw)\| < l_m(w)$. Here, $\|L\|$ denotes the norm of the matrix L.

Additive unstructured nonparametric; e.g., $G \rightarrow \delta G$, where $\|\delta G\| < l_a(w)$.

Additive/multiplicative structured nonparametric; same as above but only certain elements of L and δG are variable.

We remark that using transfer function models for uncertainty one can readily characterize parasitic dynamic uncertainty. This is a central reason for the popularity of frequency response methods for control system design. Recently the development of control design methods based on worst case optimization in the Hardy space H^∞ of transfer functions has provided a formal design approach for linear systems based on a well defined optimization criterion which embodies robustness [Zam81].

The vast literature on optimal robust control design is outside the scope of the present study. It significance for EFL and PFL is a subject which we will study in more detail in the next year. For now we confine our comments to its potential for addressing the robust stabilization of the effective linearized system obtained from the nonlinear EFL (or PFL) compensator (cf. [Spo86]).

7.2.1 A State Space Approach for Linear Systems

An important approach to robust control system design was obtained by Barmish, Corless, and Leitmann [BCL83]. They use Lyapunov-function theory to design robustly stable controllers for linear systems. The main advantage of their method is that, as we will see later, it can easily be generalized to nonlinear systems. The authors show that if the plant dynamics are given by:

$$\dot{x} = (A + \Delta A)x + (B + \Delta B)u \tag{7.2}$$

and the *matching conditions*:

$$\Delta A = BD, \quad \Delta B = BE \tag{7.3}$$

hold for the plant uncertainty, with $\| D \| \leq \rho_D$ and $\| E \| < 1$, then the state feedback $u = -2\gamma_0 B^T P x$ will always robustly stabilize System (7.2), provided that the positive scalar γ_0 is chosen sufficiently large. The matrix P in the state-feedback control law is given as a solution of the Lyapunov matrix equation, $A^T P + PA = -H$, where H is any positive definite matrix. The matching conditions (7.2) do impose a special structure on the permissible plant variations. Patel et al [PTS77], and Yedavalli [Yed85] also exploit Lyapunov function theory to obtain conditions on the A matrix in the state-variable plant description for robust stabilization.

7.3 Robust Stabilization of Nonlinear Systems.

Recent developments in feedback design of nonlinear systems fall into two categories. Results which are *geometric* in nature are essentially independent of a coordinate system for the state space and view the system as a collection of vector fields evolving on a manifold which can be embedded in a larger Euclidean space. A second body of results are asymptotic in nature and use Lyapunov and/or singular perturbation techniques.

7.3.1 Geometric methods in nonlinear control.

The inital emphasis in the development of geometrical methods for nonlinear control was to extend the well known linear theory of Wonham [Won74] to linear systems which are affine in the control variable. The methods of EFL and PFL described in this report are examples of this line of development.

Unfortunately, these geometric techniques present some limitations from the engineering point of view. One such limitation is that results of a geometric nature are sometimes difficult to apply in practice because highly accurate models must be available in order to verify that certain exact conditions of the theory are satisfied. Moreover, since the construction of the linearizing feedback involves "cancellation" of certain nonlinearities, it leaves open many questions regarding sensitivity and robustness of the control implementation. One approach which has been pursued by several researchers is to use the available freedom in the linear controller design (once effective linearization has been achieved for a nominal model) to recover stability robustness [MC80, GMS82].

It is interesting to note the interpretation given by Meyer [Mey81] to EFL and its relation to a trajectory-dependent Taylor series expansion of the nonlinear vector fields. Consider a

nonlinear system given by,

$$\dot{x}(t) = f(x) + g(x)u.$$

To obtain EFL control we seek transformation of the state and feedback so that the effective system is in a linear canonical form,

$$\begin{aligned} \dot{y}_1 &= y_2, \\ &\vdots \\ \dot{y}_n &= v, \end{aligned}$$

where the transformation is effected by the maps $T(x,u) \mapsto y$ and $W(y,v) \mapsto u$ which effectively invert the transformation to linearized coordinates. If we consider a Taylor series expansion of the nonlinear system in the neighborhood of a given state trajectory $x(t)$—which we assume is valid pointwise on $x(t)$—we obtain a linearized model of the form

$$\dot{x} = (a_0 + a_1 t) + Ax + Bu,$$

where a_0, a_1, A, B are constant (at least locally). Under these assumptions Meyer suggests that the effective T and W maps can be interpreted as (linear) transformations of the local nonhomogeneous linear model just obtained to the canonical form via

$$y = Tx + c_0 + c_1 t,$$

and

$$u = Wv + Ry + b_0 + b_1 t.$$

The matrices T, W, R depend on the homogeneous part (A, B) of the local linearized model. However, the introduction of nonhomegeous part in the effective linear system is nonstandard and results on robust linear control must be carefully reevaluated in this context.

7.3.2 Asymptotic methods

The second body of results consists of mainly Lyapunov-based techniques to design robustly stable controllers for the nonlinear system. Roughly speaking, a nonlinear system $\dot{x} = f(x)$ is asymptotically stable if there exists a function (Lyapunov function) $V(x)$ which is positive for all non-zero x and which has a time-derivative $\dot{V}(x)$ which is negative for all non-zero x. Obviously, if the inequalities in question are true for all admissible variations in $f(x)$, the Lyapunov stability theory also provides conditions for robust stabilization. An early paper on the application of Lyapunov function to robust stabilizaton is the paper of Gutman and Leitman [GL76]. The monograph of Safonov [Saf80] also contains an extensive discussion of the application of Lyapunov functions to robust stabilization.

In contrast to geometric methods, asymptotic methods do not rely on transforming the system into a more convenient canonical form; rather, they consider uncertainty as a class of bounded perturbations to the state model. The methods often employ effective high-gain feedback to combat uncertainty and exogenous disturbances. Among such methods are the so-called *Variable Strucure Control (VSC)* methods which were discussed in the previous

report [BBK88] and the controller structures proposed by Corless and Leitmann [CL81] which generalizes the design for linear systems described previously. The Corless-Leitmann robust controller guarantees a form of stabilty called *uniform ultimate boundedness* of the state to an arbitrarily small neighborhood of the origin; and might be termed *practical stability*. The type of uncertainty models they consider contain mainly parametric structured uncertainties satisfying a generalized version of the matching conditions (7.2). The need for these matching conditions represents one of the main restrictions of robust control methodologies, for both the linear and nonlinear case. In the next year we will examine the application of these assumptions for the class of nonlinear models described in this report and investigate the meaning of the matching conditions for slewing of flexible structures.

7.3.3 Parametric structured uncertainties

Geometric methods. The main geometric results in the literature on the robust stabilization of nonlinear systems with structured uncertainties involve two assumptions which may restrict application. The first is that the results are restricted to the class of feedback linearizable systems; i.e., systems which are exactly linearizable (using EFL) or minimum-phase systems (using PFL). The second restriction is that the uncertainties which account for the difference between the true plant and the simplified given model, are assumed to satisfy the *structure matching conditions*. The basic design paradigm is that once the linearizing change of coordinates and feedback is applied to the uncertain nonlinear model, a perturbed *linear* model is obtained. The key point is that the uncertainties on the linear model will retain the same nice structure of the uncertainties (via matching conditions) on the nonlinear model. The available freedom in the linear system design phase can then be used (as suggested by Meyer [GMS82] and) as discussed in the previous sections. Spong [Spo86] and Kravaris [Kra87] follow this same approach and use a similar type of controller. Kravaris's result is less restrictive since he assumes only that the system is minimum phase and applies PFL rather than EFL. (As we have suggested throughout this study PFL is an essential practical feature of the control problem for rapid slewing of flexible structures.)

For simplicity of presentation we describe Spong's approach. The true plant is assumed to be of the form:

$$\begin{aligned} \dot{x} &= f(x) + \Sigma_{i=1}^{m} g_i(x) u_i(t) \\ &= f(x) + G(x)u \end{aligned} \tag{7.4}$$

with the usual smoothness assumptions on $f, g_1, \ldots, g_m$ on R^n and $f(0) = 0$.

Assumption 1: There exists a diffeomorphism $T(x)$ on R^n and nonlinear smooth functions $\alpha(x), \beta(x)$ of appropriate dimensions, with $\beta(x)$ invertible, such that with the change of coordinates $z = T(x)$ and nonlinear feedback $u = \alpha(x) + \beta(x)v$, the plant (3) becomes:

$$\dot{z} = Az + Bv \tag{7.5}$$

with (A, B) in Brunovsky canonical form. The design model is:

$$\dot{x} = \hat{f}(x) + \hat{G}(x)u \tag{7.6}$$

where $\hat{f}, \hat{G}$ are nominal versions of f, G respectively.

Assumption 2 : Let

$$\begin{aligned} \Delta f(x) &= f(x) - \hat{f}(x) \\ \Delta G(x) &= G(x) - \hat{G}(x) \end{aligned}$$

denote the mismatch between the plant and the model. We assume there exist smooth functions $D(x), E(x)$ on R^n such that the following matching conditions are satisfied:

$$\begin{aligned} \Delta f(x) &= \hat{G}(x)D(x), \\ \Delta G(x) &= \hat{G}(x)E(x). \end{aligned}$$

Assumption 2 combined with Assumption 1 implies that the model (7.5) is also feedback linearizable with the same change of coordinates $T(x)$ used for the original plant and a nonlinear feedback $u = \hat{\alpha}(x) + \hat{\beta}(x)v$ to the same canonical linear system (7.5). An example that satisfies these constraints can be found in mechanics. Two rigid robot manipulators are in the same orbit under the action of feedback, that is they can both be linearized using the same change of coordinates $z = T(x)$ and different feedbacks provided that they have the same number of joints and powered and unpowered joints of the manipulators coincide.

If we apply the linearizing change of coordinates $z = T(x)$ and the nonlinear feedback $u = \hat{\alpha}(x) + \hat{\beta}(x)v$ to the true plant (7.5), we obtain a perturbed linear system with structured uncertainties:

$$\dot{z} = Az + B\{v + \eta(z, v)\} \tag{7.7}$$

where

$$\begin{aligned} \eta(z, v) &= \hat{\beta}(x)^{-1}\{D(x) + E(x)(\hat{\alpha}(x) + \hat{\beta}(x)v)|_{x=T^{-1}(z)}\}, \\ &= \phi(z) + \psi(z)v. \end{aligned}$$

The following additional assumptions are made on the nonlinearity $\eta(z, v)$;

Assumption 3: There exists a positive constant $\alpha < 1$ such that for $z \in R^n$:

$$\| \psi(z) \| \leq \alpha$$

.

Assumption 4: There exist positive constants a and b such that for $z \in R^n$:

$$\| \phi(z) \| \leq a + b \| z \|$$

.

Design of the v-controller. Several robust controllers can now be introduced:

(i) The first controller proposed is a linear dynamic compensator $v(s) = C(s)z(s)$. The multi-loop version of the small gain theorem [DV75] shows that the control signal $v(t)$ and the "uncertainty" η are bounded in L_∞ provided $C(s)$ is designed in such a way as to satisfy the modelling assumptions (3) and (4) and the stability condition provided by the small gain theorem. To design such a compensator $C(s)$, the stable factorization approach which was developed during recent years by various researchers and given a exposition in [Vid85], is used.

(ii) The second approach for design focuses on *practical stability*. One designs a control law for v that guarantees the uniform ultimate boundedness of the state $z(t)$ to an arbitrarily small neighborhood of the origin. Two state feedback schemes can be designed using this approach to guarantee stability of the uncertain linear system (7.6) within the modelling assumptions (7.5) and (7.5). The first one is a saturating nonlinear controller and the other one is a high gain linear controller. The design methodology is based on the second method of Lyapunov.

The controller v is taken as $v = Kz + \Delta v$ where K is chosen so that $A + BK$ is Hurwitz. The uncertain linear system (7.6) becomes then:

$$\dot{z} = (A + BK)z + B\{\Delta v + \eta(z, \Delta v)\} \tag{7.8}$$

One way to design Δv is (following the work of Leitmann [Lei81]) to choose Δv as a saturating nonlinear quantity:

$$\Delta v = \begin{cases} -\rho(z,t)\frac{B^T P z}{\| B^T P z \|}; \text{ if } \| B^T P z \| > \epsilon \\ \frac{-\rho(z,t)}{\epsilon} B^T P z; \text{ if } \| B^T P z \| < \epsilon \end{cases}, \tag{7.9}$$

for some (given) $\epsilon > 0$, ρ satisfying,

$$\| \eta \| \leq \rho(z,t), \tag{7.10}$$

$$\| \Delta v \| \leq \rho(z,t), \tag{7.11}$$

and P, the unique positive definite solution to the Lyapunov equation;

$$(A + BK)^T P + P(A + BK) + Q = 0.$$

The idea is that the function $V(z) = z^T P z$ (which is a Lyapunov function for the linear system $(A + BK, B)$) is a Lyapunov function for the nonlinear system (7.7) provided that η satisfies (7.9). The uniform ultimate boundedness set can then be made arbitrarily small by decreasing ϵ. For $\epsilon = 0$, the system is asymptotically stable and the control law (8) is discontinuous.

Another way to design Δv follows from the work of Thorp, Barmish [TB81] and others on robust linear control. Here we take Δv as a strictly linear, but high gain control law;

$$\Delta v(t) = -\gamma B^T P z,$$

where $\gamma > 0$ is sufficiently large so that the state $z(t)$ is uniformly ultimately bounded. The calculation of γ and the ultimate boundedness set can be found in [TB81].

Lyapunov-based methods: As mentioned earlier, most of the results that use Lyapunov-based techniques to design robustly stable controllers for nonlinear systems use either explicitely or implicitely high gain feedback to combat uncertainties. One of the interesting results on robust stabilization of nonlinear systems with parametric structured uncertainties is the controller proposed by Corless and Leitmann (as a generalization of their earlier linear control methods). The stability concept used is termed "practical stability" and differs slightly from the traditional Lyapunov stability. Normally Lyapunov arguements are used in design to guarantee uniform asymptotic stability of an equilibrium state. However, in practice one is often content with uniform ultimate boundedness to some set in finite time. The uncertain dynamical system is assumed to be described by the state equation,

$$\dot{x} = f(x(t),t) + \Delta f(x(t),t) + [B(x(t),t) + \Delta B(x(t),t)]u(t)$$

where $x(t) \in R^n$ is the state, $u(t) \in R^m$ is the control, and $f(x,t), \Delta f(x,t), B(x,t)$ and $\Delta B(x,t)$ are matrices of appropriate dimensions which depend on the structure of the system. Additional conditions may be imposed on how Δf and ΔB structurally enter the state equations.

Assumption 1: Δf and ΔB satisfy the structure matching conditions; i.e., there are mappings

$$h(.) : R^n \times R \rightarrow R^m \text{ and } E(.) : R^n \times R \rightarrow R^{m \times m}$$

such that

$$\begin{aligned} \Delta f(x,t) &= B(x,t)h(x,t) \\ \Delta B(x,t) &= B(x,t)E(x,t) \end{aligned} \tag{7.12}$$

for all $x \in R^n$ and $t \in R$.

Because of this assumption, all uncertain elements can be "lumped" and the system is written,

$$\dot{x}(t) = f(x(t),t) + B(x(t),t)u(t) + B(x(t),t)e(x(t),t). \tag{7.13}$$

The "nominal" system, that is, the system without uncertainty, is described by

$$\dot{x} = f(x(t),t) + B(x(t),t)u(t).$$

Based only on the knowledge of the maximum possible value (which may depend on x and t) of the norm $\| e(x,t) \|$, the aim is to find a feedback control $u(.) : R^n \times R \rightarrow R^m$ such that given (x_0, t_0), a corresponding response $x(.) : [t_0, \infty) \rightarrow R^n$ exists, and every such response enters a neighborhood of $x = 0$ in finite time and remains within it thereafter. This is *uniform ultimate boundedness*. The following additional conditions are also assumed:

Assumption 2: The known functions f, B as well as the unknown function e are continuous functions, and $f(0,t) = 0$ for all $t \in R$.

Assumption 3: The norm of the uncertain element is bounded by a known function; that is, for all $(x,t) \in R^n \times R$

$$\| e(x,t) \| \leq \rho(x,t)$$

where the known function ρ is a continuous function.

Assumption 4: Given a compact set $E \subset R^n$ and a compact interval $[a,b] \subset R$, there exist continuous functions $m_i(.) : [a,b] \rightarrow R$, $i = 1,2$, such that for all $(x,t) \in E \times [a,b]$

$$\begin{aligned} \| f(x,t) \| &\leq m_1(t), \\ \| B(x,t) \| \rho(x,t) &\leq m_2(t). \end{aligned}$$

Assumption 5: The origin, $x = 0$ is uniformly asymptotically stable for the uncontrolled nominal system $\dot{x} = f(x(t),t)$. In particular, there are a C^1 function (Lyapunov function) $V(.) : R^n \times R \rightarrow R_+$ and continuous, strictly increasing functions $\gamma_i(.) : R_+ \rightarrow R_+$, $i = 1,2,3$ which satisfy

$$\begin{aligned} \gamma_i(0) &= 0, \quad i = 1,2,3 \\ \lim_{r \rightarrow \infty} \gamma_i(r) &= \infty, \quad i = 1,2 \end{aligned}$$

such that for all $(x,t) \in R^n \times R$

$$\gamma_1(\| x \|) \leq V(x,t) \leq \gamma_2(\| x \|)$$

$$\frac{\partial V(x,t)}{\partial t} + \nabla_x^T V(x,t) f(x,t) \leq -\gamma_3(\| x \|).$$

In [CL81], a class of state feedback controls is proposed. A member of this class, $u(.) : R^n \times R \rightarrow R^m$, is a continuous function such that, for given $\epsilon > 0$,

$$u(x,t) = -\frac{\mu(x,t)}{\| \mu(x,t) \|} \rho(x,t), \quad \text{if} \quad \| \mu(x,t) \| > \epsilon, \tag{7.14}$$

$$\| u(x,t) \| \leq \rho(x,t), \quad \text{if} \quad \| \mu(x,t) \| \leq \epsilon, \tag{7.15}$$

where

$$\mu(x,t) = B^T(x,t) \nabla_x V(x,t) \rho(x,t).$$

A particular example of such a control is

$$u(x,t) = \begin{cases} -\frac{\mu(x,t)}{\| \mu(x,t) \|} \rho(x,t) & \text{if } \| \mu(x,t) \| > \epsilon \\ -\frac{\mu(x,t)}{\epsilon} \rho(x,t) & \text{if } \| \mu(x,t) \| \leq \epsilon \end{cases}$$

It is shown in [CL81] that a control of the type (7.14)-(7.15) guarantees ultimate boundedness of all possible system responses within an arbitrarily small neighborhood of the zero state (by letting $\epsilon \rightarrow 0$). Furthermore, the set of ultimate boundedness as well as an upper bound on the time interval required to reach it are given explicitely in terms of the functions γ_i

defined above. More specifically, it is shown that a solution $x(.) : [t_0, t_1] \rightarrow R^n, x(t_0) = x_0$, of the closed loop system:

$$\dot{x}(t) = f(x(t), t) + B(x(t), t)[u(x(t), t) + e(x(t), t)]$$

with $u(x(t), t)$ satisfying (7.14)–(7.15), exists and satisfies

$$\| x_0 \| \leq r \Rightarrow \| x(t) \| \leq d(r), \quad \forall t \in [t_0, t_1]$$

where

$$d(r) = \begin{cases} (\gamma_1^{-1} \circ \gamma_2)(R) & \text{if } r \leq R \\ (\gamma_1^{-1} \circ \gamma_2)(r) & \text{if } r > R \end{cases}$$

and

$$R = \gamma_3^{-1}(2\epsilon).$$

Furthermore, the solution has a continuation over $[t_0, \infty)$ and for $\| x_0 \| \leq r$ and given $\bar{d} > (\gamma_1^{-1} \circ \gamma_2)(R)$

$$\| x(t) \| \leq \bar{d}, \quad \forall t \geq t_0 + T(\bar{d}, r)$$

where

$$T(\bar{d}, r) = \begin{cases} 0 & \text{if } r \leq \bar{R} \\ \frac{\gamma_2(r) - \gamma_1(\bar{R})}{\gamma_3(\bar{R}) - 2\epsilon} & \text{if } r > \bar{R} \end{cases}$$

and

$$\bar{R} = (\gamma_2^{-1} \circ \gamma_1)(\bar{d}).$$

7.3.4 Nonparametric nonstructured uncertainties:

In the case of unstructured but "not too large" nonlinear model/plant mismatch, Kravaris [Kra87] follows exactly the same principle as described previously; i.e., use feedback to make the system linear then put a robust linear controller around it to stabilize the overall system. The interesting point in this procedure is the fact that Kravaris evaluates the unstructured uncertainty in such a way that it is possible to apply frequency-domain results from linear robust control literature. More precisely, and since only partial linearization is used, the approach taken is the following:

(i) Make the input/output response of the system linear by appropriate input-output linearizing state feedback.

(ii) Evaluate the uncertainty as a multiplicative band of the resulting input-output system.

(iii) Design an external robust linear regulator on the basis of linear theory.

Step (i): Input/Output linearizing state feedback: Consider the nonlinear system:

$$\begin{aligned} \dot{x} &= f(x) + g(x)u \\ y &= h(x) \end{aligned} \tag{7.16}$$

where $x \in R^n, u \in R, y \in R$. The problem of finding a static state feedback of the form $u = \psi(x, v)$ such that the $v \mapsto y$ input/output is linear and of minimal order was posed and resolved in [Isi85]. The results are:

The minimal order of the $v \mapsto y$ system is the *relative degree* of (7.16), i.e., the smallest integer r satisfyng:

$$\langle dh, ad_f^{r-1} g \rangle \neq 0.$$

The input/output linearizing state feedback is given by:

$$u = \frac{v - \Sigma_{k=0}^{r} \beta_k L_f^k(h)}{(-1)^{r-1} \beta_r \langle dh, ad_f^{r-1}(g) \rangle} \tag{7.17}$$

where β_k are arbitrarily selected numbers. The corresponding closed-loop response is given by:

$$\Sigma_{k=0}^{r} \beta_k \frac{d^k y}{dt^k} = v.$$

Assumption 1: Assume that the nonlinear system (7.16) is minimum phase, that is the $(n - r)$ unobservable or zero dynamics are stable.

Step (ii): Structure of the uncertainty: The way Kravaris evaluates the uncertainty is by assuming that the plant/model mismatch can be expressed as a Volterra operator applied to the model. That is, if we consider the family Π of nonlinear systems $y = \widehat{M}(u)$ (not necessarily of the same order), then:

1. For all plants $\widehat{M}$ in Π, there exists a Volterra operator of the form:

   $$\Lambda_m(.) = l_m(t - \tau).(\tau) d\tau$$

   such that:

   $$\widehat{M}(u) - M(u) = \Lambda_m M(u), \quad \forall u$$

   where $M(u)$ represents the input/output map of the model (7.16).

2. An upper bound $l(w)$ of l_m is available such that

   $$\bar{l}_m(i\omega) < l(\omega), \quad \forall \omega$$

   where the overbar denotes the Laplace transform.

Step (iii): Robust linear control design for linearized dynamics: Once again, results from the robust linear control literature are used. Since Kravaris is using frequency domain bounds on the uncertainty, he applies standard linear system results for robust control [DS81]. For the family of plants Π, if we take the nonlinear state feedback (7.17), and the external feedback controller:

$$\bar{v}(s) = C(s)[\bar{y}_{sp}(s) - \bar{y}(s)]$$

and we assume that the closed-loop system corresponding to the model M is stable, then the closed loop system will be stable for all plants in Π if:

$$\frac{C(i\omega)}{\Sigma_{k=0}^{r} \beta_k (i\omega)^k + C(i\omega)} < \frac{1}{l(\omega)}.$$

7.3.5 Parasitic/Unmodelled dynamics:

In [TKM88] Kokotovic and Marino attempt to unify geometric and asymptotic methodologies. While geometric conditions such as conditions for feedback linearization are restrictive but exact, asymptotic time-scale results are less restrictive but approximate. A geometric characterization of asymptotic time-scale properties is the existence of an invariant manifold in which the system is described by a reduced order model (Marino and Kokotovic [MK88]). One possibile way to relax the feedback linearization conditions can be obtained by requiring that they be satisfied only for a *reduced order model*. This idea has been suggested by Kokotovic [Kok85] and developed for a flexible robotic manipulator in Spong et al [SKK87]. It is shown that the nonlinear controller preserves the regulation property in a prescribed stability region in the presence of unmodelled dynamics. The size of the region can be estimated.

In most applications, the design model is of lower order than the plant because of some unmodelled dynamics present in the plant. Following [TKM88] we assume the singularly perturbed model of the plant can be obtained in the form,

$$\dot{x} = f_1(x) + F_1(x)z + G_1(x)u, \quad x \in R^n, u \in R^m, \tag{7.18}$$

$$\mu\dot{z} = f_2(x) + F_2(x)z + G_2(x)u, \quad z \in R^r, \tag{7.19}$$

where the functions $f_1, f_2, F_1, F_2, G_1, G_2$ are bounded and differentiable with respect to x for all $x \in B_x$ (a 'ball' in R^n), $(x, z) = 0$ is an equilibrium point, and $\mu > 0$ is the singular perturbation parameter. z is the state of the unmodelled dynamics.

Assumption 1: The unmodelled dynamics z are asymptotically stable for all fixed values of $x \in B_x$, that is, there exists a constant $\sigma > 0$ such that:

$$\mathrm{Re}\lambda\{F_2(x)\} \leq -\sigma < 0.$$

Remark: We note that the stability assumption of the unmodeled or *residual* dynamics is a natural one for structural control since we will utlitmately rely on the natural damping of the structure to stabilize its (possibly very) high frequency dynamics.

The assumption $\mu \ll 1$ implies that the unmodelled dynamics are "fast" relative to the dynamics of x. A reduced order model can be obtained by taking $\mu \to 0$ which obtains the model,

$$\dot{x} = f(x) + G(x)u \tag{7.20}$$

where f and G are defined by:

$$f(x) = f_1(x) - F_1(x)F_2^{-1}(x)f_2(x),$$

$$G(x) = G_1(x) - F_1(x)F_2^{-1}(x)G_2(x).$$

Assumption 2: $\forall x \in B_x$, the reduced order model (7.20) is feedback linearizable, that is, there exists a state diffeomorphism $\bar{x} = \Phi(x)$ and a state feedback control $u = \alpha(x)$ such that, given an $n \times n$ Hurwitz matrix A, the identity:

$$\frac{\partial \Phi(x)}{\partial x}[f(x) + G(x)\alpha(x)] = A\Phi(x)$$

holds for all $x \in B_x$. If Φ and α are applied to the full order system (7.18)-(7.19), and the new fast variable $\eta = z - h(x)$ is introduced where $h(x)$ is the so-called "manifold function"

$$h(x) = -F_2^{-1}(x)[f_2(x) + G_2(x)\alpha(x)],$$

then the full order system becomes,

$$\dot{x} = \Phi_x^{-1} A\Phi(x) + F_1(x)\eta, \tag{7.21}$$

$$\mu\dot{\eta} = F_2(x)\eta - \mu\dot{h}. \tag{7.22}$$

Stability analysis: Let P_s and $P_f(x)$ be defined as the symmetric positive definite solutions of,

$$P_s A + A^T P_s = -I_n,$$

$$P_f(x)F_2(x) + F_2^T(x)P_f(x) = -I_r.$$

Then the Lyapunov function to be employed is,

$$V(x,\eta) = c_1\Phi^T(x)P_s\Phi(x) + c_2\eta^T P_f(x)\eta. \tag{7.23}$$

This function is a weighted sum of a slow part characterizing the stability properties in the manifold $\eta = 0$, and a fast part characterzing the off-manifold behavior.

If the bounds c_1^*, c_2^* and c_3^* are evaluated over $x \in B_x$ as,

$$2 \parallel P_f(x) \parallel k_1^* \leq c_1^*,$$

$$2 \parallel P_s\Phi_x(x)F_1(x) \parallel \leq c_2^*,$$

$$2 \parallel P_f(x) \parallel k_2^* + \parallel \dot{P}_f(x) \parallel \leq c_3^*,$$

where the constants k_1^* and k_2^* are determined from the requirement that for all $x \in B_x$;

$$\parallel h_x(x)\Phi_x^{-1}(x)A \parallel \leq k_1^*,$$

$$\parallel h_x(x)F_1(x) \parallel \leq k_2^*,$$

then using the Lyapunov function (7.23), the following stability result is obtained:

Result: The equilibrium $x = 0, \eta = 0$ of the feedback system (7.18)-(7.19) is asymptotically stable for all:

$$\mu \in (0, \frac{1}{c_1^* c_2^* + c_3^*}) \tag{7.24}$$

and an estimate of its region of attraction is:

$$S_D = \{x, \eta : \ V(x, \eta) \leq c^*\}$$

where $c^*$is the largest constant such that the set $\{x : V(x, 0) \leq c^*\}$ belongs to B_x. This result describes a robustness property with respect to dynamic uncertainty. It states that the stability properties of the reduced order design are preserved, at least in S_D, for unmodelled dynamics scaled by any μ in the interval (7.24).

8 Conclusions and Directions for FY89 Effort

We have demonstrated using a combination of simulation and analysis the potential benefits of nonlinear control system design for rapid slewing and precision pointing using the ideas of PFL. In the next year we will proceed to design several laboratory experiments to further demonstrate feasibility and to test options for implementation which provide robust operation with imprecise modeling of the elastic structure.

References

[Aga84] A. S. Agarwala. *Modeling and Simulation of Hyperbolic Distributed Systems Arising in Process Dynamics.* PhD thesis, Drexel Univ., June 1984.

[AM78] R. Abraham and J. E. Marsden. *Foundations of Mechanics.* Benjamin/Cummings, Reading, MA, 1978.

[Arn78] V.I. Arnold. *Mathematical Methods of Classical Mechanics.* Springer-Verlag, New York, 1978.

[BBK88] W. H. Bennett, G. L. Blankenship, and H. G. Kwatny. *Nonlinear Dynamics and Control of Flexible Structures.* Technical Report SEI-TR-88-01, SEI, March 1988. Res. Progress Rept. to AFOSR/SDIO.

[BCL83] B. R. Barmish, M. Corless, and G. Leitmann. A new class of stabilizing controllers for uncertain dynamical systems. *SIAM J. Cntl. Optim.*, 21:246–255, 1983.

[BI84] C.I. Byrnes and A. Isidori. A frequency domain philosophy for nonlinear systems, with application to stabilization and adaptive control. In *Proc. IEEE CDC*, Las Vegas, NV, 1984.

[BI85] C. I. Byrnes and A. Isidori. Global feedback stabilization of nonlinear systems. In *Proc. 24th IEEE CDC*, pages 1031–1037, Dec. 1985.

[BK89] W.H. Bennett and H.G. Kwatny. Continuum modeling of flexible structures with application to vibration control. *AIAA J.*, January 1989. to appear.

[BL87] J. Baillieul and M. Levi. Rotational elastic dynamics. *Physica 27D*, 27:43–62, 1987.

[Bod45] H. W. Bode. *Network Analysis and Feedback Amplifier Design.* Van Nostrand, 1945.

[Bro78] R.W. Brockett. Feedback invariants for nonlinear systems. In *Proc. 6th IFAC World Congress*, pages 1115–1120, Helsinki, 1978.

[CKEFKP68] S. H. Crandall, D. C. Karnopp, Jr. E. F. Kurtz, and D. C. Pridmore-Brown. *Dynamics of Mechanical and Electromechanical Systems.* McGraw-Hill Book Co., New York, 1968.

[CL81] M. J. Corless and G. Leitmann. Continuous state feedback guaranteeing uniform ultimate boundedness for uncertain dynamic systems. *IEEE Trans. Auto. Cntrl.*, AC-26:1139–1144, 1981.

[De86] A. Das and et al. Spacecraft dyanmics and control program at AFRPL. In *NASA/DOD CSI*, November 1986.

[DS81] J. C. Doyle and G. Stein. Multivariable feedback design: concepts for a classical/modern synthesis. *IEEE Trans on Auto. Cntrl.*, AC-26(1):4–16, 1981.

[DV75] C.A. Desoer and M. Vidyasagar. *Feedback Systems: Input-Output Properties.* Academic Press, Inc., New York, 1975.

[Dwy84] T. A. W. Dwyer. Exact nonlinear control of large angle rotational maneuvers. *IEEE Trans. on Auto. Control*, AC-29(9):769–774, 1984.

[FH87] R. B. Fernandez and J. K. Hedrick. Control of multivariable nonlinear systems by the sliding mode method. *Int. J. Control*, 46(3):1019–1040, 1987.

[Gea88] S. Ginter and et al. *Slew Actuator System Requirements Study.* Technical Report AFAL-TR-88-034, June 1988.

[GL76] S. Gutman and G. Leitman. Stabilizing control for linear systems with bounded parameter and input uncertainty. In *Proc. 7th IFIP Conf. on Optimization Techniques*, page 729, Springer-Verlag, 1976.

[GMS82] R. Hunt G. Meyer and R. Su. Design of a helicopter autopilot by means of linearizing transformations. In *Advances in Guidance and Control Systems*, pages 15–1–11, Lisbon, 1982.

[Gol82] H. Goldstein. *Classical Mechanics.* Addison-Wesley, Reading, MA, 1982.

[Hir79] R. M. Hirschorn. Invertibility of nonlinear control systems. *SIAM J. Optim. and Control*, 17(2):289–297, 1979.

[HSM83] R. Hunt, R. Su, and G. Meyer. Global transformation of nonlinear systems. *IEEE Trans. Automatic Control*, AC-28:24–31, 1983.

[Isi85] A. Isidori. *Nonlinear Control Systems: An Introduction.* Springer-Verlag, 1985.

[KC87] C. Kravaris and C-B Chung. Nonlinear state feedback synthesis by global input/output linearization. *AIChE Journal*, 33(4):592–603, April 1987.

[Kok85] P.V. Kokotovic. Recent trends in feedback design: an overview. *Automatica*, 21:225–236, 1985.

[Kra87] C. Kravaris. On the internal stability and robust design of globally linearizing control systems. In *Proc. ACC*, pages 270–279, 1987.

[Kre73] A. J. Krener. On the equivalence of control systems and linearization of nonlinear systems. *SIAM J. Cont. and Optim.*, 11:670, 1973.

[Lea87] M. Lock and et al. *Structural Dynamic Response of a Space Based Laser System.* Technical Report AD-B109 212, February 1987.

[Lei81] G. Leitmann. On the efficacy of nonlinear control in uncertain linear systems. *J. Dyn. Syst. Meas. Contr.*, 102, 1981.

[Lio71] J.L. Lions. *Optimal Control of Systems Governed by Partial Differential Equations.* Springer-Verlag, New York, 1971.

[MC80] G. Meyer and L. Cicolani. Applications of nonlinear system inverses to automatic flight control design–systems concepts and flight evaluations. In P. Kent, editor, *Theory and Applications of Optimal Control in Aerospace Systems*, pages 10–1–29, 1980.

[Mei67] L. Meirovich. *Analytical Methods in Vibrations.* McMillan, New York, 1967.

[Mey81] G. Meyer. The design of exact nonlinear model followers. In *Proc. JACC*, 1981. paper FA-3A.

[MK88] R. Marino and P. V. Kokotovic. A geometric approach to nonlinear singularly perturbed contol systems. *Automatica*, 24:31–42, 1988.

[Nyq32] H. Nyquist. Regeneration theory. *Bell Syst. Tech. J*, 11:126–147, 1932.

[Pos88] T.A. Posbergh. *Modeling and Control of Mixed and Flexible Structures.* PhD thesis, University of MD, 1988.

[Pre75] P. M. Prenter. *Splines and Variational Analysis.* Wiley-Interscience, New York, 1975.

[PTS77] R. V. Patel, M. Toda, and B. Sridhar. Robustness of linear quadratic state feedback designs in the presence of system uncertainty. *IEEE Trans. Auto. Cntrl.*, AC-22:945–949, 1977.

[RM57] R. D. Richtmeyer and K.W. Morton. *Difference Methods for Initial-Value Problems.* Wiler: Interscience, New York, 1957.

[Ros72] H. H. Rosenbrock. The stability of multivariable systems. *IEEE J. Auto. Cntrl.*, AC-17:105–107, 1972.

[Ros74] H. H. Rosenbrock. *Computer-Aided Control System Design.* Academic Press, Inc., 1974.

[Saf80] M. G. Safonov. *Stability and Robustness of Multivariable Feedback systems.* MIT Press, 1980.

[SF73] G. Strang and G. J. Fix. *An Analysis of the Finite Element Method.* Prentice-Hall, Englewood Cliffs, NJ, 1973.

[SKK87] M. W. Spong, K. Khoransani, and P. V. Kokotovic. An integral manifold approach to the feedback control of flexible joints robots. *IEEE J. Robotics Automation*, RA-3:291–300, 198

[Spo86] M. W. Spong. Robust stabilization for lass of nonlinear systems. In C. I. Byrnes and A. Lindquist, editors, *Theory and Applications of Nonlinear Control Systems*, North-Holland, 1986.

[Sta79] I. Stakgold. *Green's Functions and Boundary Value Problems.* John Wiley and Sons Inc., NY, 1979.

[TB81] J.S. Thorp and B. R. Barmish. On guaranteed stability of uncertain linear systems via linear control. *J. Opt. Theory and Appl.*, 35:559–579, 1981.

[TKM88] D. G. Taylor, P. V. Kokotovic, and R. Marino. Adaptive regulation of nonlinear systems with unmodelled dynamics. preprint, 1988.

[Vid85] M. Vidyasagar. *Control System Synthesis: A Factorization Approach.* MIT Press, 1985.

[Won74] W. M. Wonham. *Linear Multivariable Control: A Geometric Approach.* Springer-Verlag, 1974.

[Yed85] R. K. Yedavalli. Perturbation bounds for robust stability in linear state space models. *Int. J. Cntrl.*, 42:1507–1517, 1985.

[Zam63] G. Zames. Functional analysis applied to nonlinear feedback systems. *IEEE Trans. on Circuit Theory*, 392–404, 1963.

[Zam81] G. Zames. Feedback and optimal sensitivity: model reference transformations, multiplicative seminorms, and approximate inverses. *IEEE Trans. Auto. Control*, AC-26:301–320, 1981.

A A Lemma for Lagrangian Modeling

In this appendix we provide some useful identities for performing the calculations indicated above.

Consider a spatial coordinate frame, denoted the 'body' frame rotating relative to a second reference frame, denoted the 'inertial' frame, with angular velocity ω in body coordinates. If the relative angular position is characterized by parameters $\xi \in \Re^3$, say Euler parameters, then $\omega = \Gamma(\xi)\dot{\xi}$, and we have the following.

Lemma 1 Consider a function $K(\omega)$, where $\omega = \Sigma(\xi)\dot{\xi}$. Then

$$\left[\frac{d}{dt}\frac{\partial K}{\partial \dot{\xi}} - \frac{\partial K}{\partial \xi}\right]^T = \Sigma^T(\xi)\left[\frac{da}{dt} + \omega \times a\right] \tag{A.1}$$

where

$$a = \left(\frac{\partial K}{\partial \omega}\right)^T. \tag{A.2}$$

□

Proof: Direct computation yields

$$\begin{aligned}\frac{\partial K}{\partial \dot{\xi}} &= \left(\frac{\partial K}{\partial \omega}\right)\Sigma(\xi) \\ \frac{\partial K}{\partial \xi} &= \left(\frac{\partial K}{\partial \omega}\right)\frac{\partial}{\partial \xi}(\Sigma(\xi)\dot{\xi})\end{aligned}$$

and

$$\frac{d}{dt}\frac{\partial K}{\partial \dot{\xi}} - \frac{\partial K}{\partial \xi} = \left[\frac{d}{dt}\left(\frac{\partial K}{\partial \omega}\right)\right] + \left(\frac{\partial K}{\partial \omega}\right)\left[\dot{\Sigma}(\xi) - \frac{\partial}{\partial \xi}(\Sigma(\xi)\dot{\xi})\right].$$

We need only show that

$$\dot{\Sigma}(\xi) - \frac{\partial}{\partial \xi}(\Sigma(\xi)\dot{\xi}) = -\Omega\Sigma(\xi).$$

Let σ_i denote the i^{th} column of Σ. Then the above matrix equation can be interpreted as three vector equations

$$\left(\frac{\partial}{\partial \xi}\sigma_i(\xi)\right)\dot{\xi} = \dot{\sigma}_i + \omega \times \sigma_i, \quad \text{for } i = 1, 2, 3$$

The validity of these equations follows from the observation that each σ_i is a vector denoting the coordinates of a point P in the body reference frame. The quantity on the left is the velocity of the point P in the inertial frame, whereas $\dot{\sigma}_i$ denotes the velocity of P in the body frame.

□

B Supporting Computations for B-spline model of planar slewing with uniform Beam appendage

In this appendix we summarize the computation by explicit integration of the required tridiagonal matrix parameters obtained from the B-spline finite element model for planar slewing of a rigid body with attached appendage consisting of a uniform beam. See Section 4.4.1 for details of the model development.

By definition, the $N \times N$ matrix $\tilde{N}$ given in (4.69) has elements given in terms of linear B-splines as

$$[\tilde{N}]_{ij} = \int_0^\ell B_{i-1}^1(z) B_{j-1}^i(z)\, dz$$

for $i, j = 1, \ldots, N$. Given the "hat" shaped, linear B-spline,

$$B_i^1(z) := (\tfrac{N}{\ell})[z - i(\tfrac{\ell}{N})] B_i^0(z) + (\tfrac{N}{\ell})[(i+2)\frac{\ell}{N} - z] B_{i+1}^0(z)$$

where the zero order B-spline is chosen with continuity from the left; i.e.,

$$B_i^0(z) := \begin{cases} 1, & \text{if } x_i \le x < x_{i+1} \\ 0, & \text{else} \end{cases} . \tag{B.1}$$

Then we have three nonzero cases to consider.

Case 1: $i = j = N$. Then

$$[\tilde{N}]_{ij} = \int_{z_{N-1}}^{z_N} (\tfrac{N}{\ell})^2 (z_N - z)\, dz = \frac{1}{3}\,\frac{\ell}{N}.$$

Case 2: $i = j \pm 1$. (Refer to Figure 2.1.) Here we obtain a simple form for the integral by transformation of the variable and limits of integration;

$$\begin{aligned} [\tilde{N}]_{ij} &= \int_0^\ell B_{i-1}^1(z) B_{j-1}^1(z)\, dz \\ &= \int_{z_{j-1}}^{z_j} (\tfrac{N}{\ell})^2 (z - z_{j-1})(z_j - z)\, dz \\ &= (\tfrac{N}{\ell})^2 \int_0^{\frac{\ell}{N}} x(\tfrac{\ell}{N} - x)\, dx = \frac{1}{6}\,\frac{\ell}{N} \end{aligned}$$

Case 3: $i = j < N$.

$$\begin{aligned} [\tilde{N}]_{ij} &= \int_0^\ell B_{i-1}^1(z) B_{j-1}^1(z)\, dz \\ &= \int_{z_{j-2}}^{z_{j-1}} (\tfrac{N}{\ell})^2 (z - z_{j-2})^2\, dz + \int_{z_{j-1}}^{z_j} (\tfrac{N}{\ell})^2 (z_j - z)^2\, dz \\ &= \int_0^{\frac{\ell}{N}} (\tfrac{N}{\ell})^2 x^2 dx + \int_0^{\frac{\ell}{N}} (\tfrac{N}{\ell})^2 (\tfrac{\ell}{N} - x)^2\, dx \\ &= \frac{2}{3}\,\frac{\ell}{N}. \end{aligned}$$

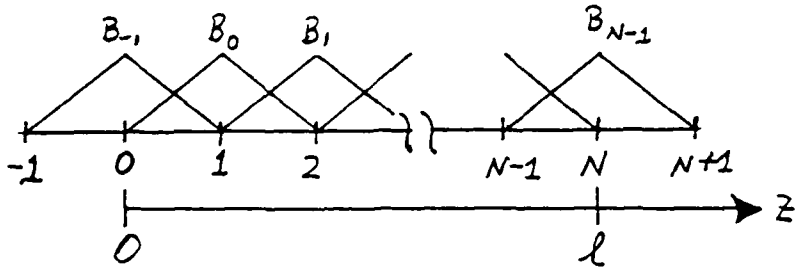

Figure 2.1: Linear B-spline functions on z domain.

For the $N \times N$ tridiagonal matrix $\tilde{N}'$ with elements

$$[\tilde{N}']_{ij} = \int_0^\ell \frac{\partial}{\partial z} B^1_{i-1}(z) \frac{\partial}{\partial z} B^1_{j-1}(z)\, dz$$

for $i, j = 1, \ldots, N$ we obtain three nonzero cases.

Case 1: $i = j < N$.

$$[\tilde{N}']_{ij} = \int_0^{\frac{\ell}{N}} (\tfrac{N}{\ell})^2\, dz + \int_0^{\frac{\ell}{N}} (\tfrac{N}{\ell})^2\, dz = 2(\tfrac{N}{\ell}).$$

Case 2: $i = j = N$.

$$[\tilde{N}']_{ij} = \int_0^{\frac{\ell}{N}} (\tfrac{N}{\ell})^2\, dz = \frac{N}{\ell}.$$

Case 3: $i = j \pm 1$. For $i = j + 1$ we obtain,

$$\begin{aligned} [\tilde{N}']_{ij} &= \int_{z_{i+1}}^{z_{i+2}} -(\tfrac{N}{\ell})^2\, dz \\ &= -(\tfrac{N}{\ell}). \end{aligned}$$

Similarly, for $i = j - 1$.

The $N \times N$ matrix $\tilde{K}'$ has elements

$$[\tilde{K}']_{ij} = \int_0^\ell \frac{\partial}{\partial z} B^1_{i-1}(z) B^1_{j-1}(z)\, dz$$

which has two nonzero cases of interest.

Case 1: $i = j$.

$$[\tilde{K}']_{ij} = \int_{z_i}^{z_{i+1}} (\tfrac{N}{\ell})^2 (z - z_i)\, dz + \int_{z_{i+1}}^{z_{i+2}} -(\tfrac{N}{\ell})^2 (z_{i+2} - z)\, dz = 0$$

Case 2: $i = j + 1$.

$$\begin{aligned} [\tilde{K}']_{ij} &= \int_{z_i}^{z_{i+1}} (\tfrac{N}{\ell})^2 (z_{i+2} - z)\, dz \\ &= (\tfrac{N}{\ell})^2 \int_0^{\frac{\ell}{N}} (\tfrac{\ell}{N} - x) dx \\ &= \frac{1}{2} \end{aligned}$$

Case 3: $i = j - 1$.

$$[\tilde{K}']_{ij} = -(\tfrac{N}{\ell})^2 \int_0^{\frac{\ell}{N}} (\tfrac{\ell}{N} - x)dx = -\frac{1}{2}.$$

Under the assumptions of the planar slewing model, the $1 \times N$ coupling coefficient matrix $N^T_{\omega_h \eta}$ has elements

$$[N^T_{\omega_h \eta}]_i = \rho A \int_0^{\ell} z B_i^1(z)\, dz,$$

for $i = 1, \ldots, N$. There are two cases of interest.

Case 1: $i < N$.

$$\int_0^{\ell} z B_i^1(z) dz = \int_{z_i}^{z_{i+1}} (\tfrac{N}{\ell}) z[z - i(\tfrac{\ell}{N})] dz + \int_{z_{i+1}}^{z_{i+2}} (\tfrac{N}{\ell}) z[(i+2)(\tfrac{\ell}{N}) - z]\, dz.$$

Changing limits of integration by the transformation $x = z - z_i$ in the first integral gives

$$\begin{aligned} \int_{z_i}^{z_{i+1}} (\tfrac{N}{\ell}) z[z - i(\tfrac{\ell}{N})] dz &= (\tfrac{N}{\ell}) \int_0^{\frac{\ell}{N}} (x + i\tfrac{\ell}{N}) x\, dx \\ &= (\tfrac{\ell}{N})^2 (\frac{1}{3} + i\frac{1}{2}). \end{aligned}$$

Changing variables (and limits) of integration in the second integral yields

$$\begin{aligned} \int_{z_{i+1}}^{z_{i+2}} (\tfrac{N}{\ell}) z[(i+2)(\tfrac{\ell}{N}) - z]\, dz &= (\tfrac{N}{\ell}) \int_0^{\frac{\ell}{N}} (x + (i+1)\tfrac{\ell}{N})(\tfrac{\ell}{N} - x) dx \\ &= (\tfrac{\ell}{N})^2 [\frac{1}{6} + \frac{i+1}{2}]. \end{aligned}$$

From which we can obtain

$$\int_0^{\ell} z B_i^1(z) dz = (\tfrac{\ell}{N})^2 (1 + i).$$

Case 2: $i = N$.

$$\begin{aligned} \int_0^{\ell} z B_i^1(z)\, dz &= \int_{z_{N-1}}^{z_N} (\tfrac{N}{\ell}) z[z - z_{N-1}]\, dz \\ &= \int_0^{\frac{\ell}{N}} (\tfrac{N}{\ell})(x + (N-1)\tfrac{\ell}{N}) x\, dx \\ &= (\tfrac{\ell}{N})^2 [\frac{N}{2} - \frac{1}{6}]. \end{aligned}$$

C A Study of Slew Induced Deformation Shaping

Proc. ASME Winter Annual Meeting (Chicago, IL Nov. 1988)

NONLINEAR MODELING AND ESTIMATON OF SLEW INDUCED STRUCTURAL DEFORMATIONS

Thomas A. W. Dwyer, III

and

Fakhreddine Karray

ABSTRACT

A model of the nonlinear dynamics of a deformable maneuvering multi body system is described, whereby elastic deformations are modeled by restoring forces and dissipative forces at point mass appendages. This model is brought into bilinear form. Estimation of deformations occasioned by rapid slewing maneuvers is carried out by a filter based on a globally equivalent linear model of the bilinear dynamics, and is shown to be an improvement over the extended Kalman filter. To further alleviate the computational burden, the estimated deformation state is propagated between observations by a low dimensional operator spline interpolator of bilinear system Volterra series, which is easily implemented.

INTRODUCTION

This paper proposes a new nonlinear, nonparametric method for off line modeling and on line estimation of the deformation of a flexible structure, undergoing rapid rotational maneuvers.

In these circumstances, the structural stiffness and damping coefficients depend on the angular acceleration ω_2 the angular rate ω and the square of the angular rate ω^2. In the single axis case, the excitation of the structure is represented by the vector $u^T = (\omega, \omega^2, 2\omega)$, to which the structural dynamics responds as a "bilinear" (i.e., parametrically excited) system. A similar technique for multiaxial rotations yields a bilinear model with respect to matrix valued excitations.

Two methods of estimation and modeling are combined to achieve deformation state determination:

a. A method based on a feedback linearized procedure which gives an estimate of the deformation state by means of a filter constructed from the equivalent linear dynamics, which is faster than the extended Kalman filter.
b. The modeling of the deformation state of the structure by means of Volterra series interpolators.

MODEL OF A DEFORMABLE STRUCTURE AND EQUATIONS OF MOTION

For purposes of illustration of the principles involved, our structure will consist of a primary mirror, attached to a spacecraft, and a secondary mirror attached to the primary in the shape of a Cassegrain telescope by means of idealized massless links. The primary mirror structure will also be regarded as attached to the spacecraft by means of a massless link. Equivalently the same model can be thought to represent a laser beam expander, as in figure 1.

The simplified telescope part of the structure can itself be modeled as a system of two masses attached together by a single "equivalent" link with "equivalent" stiffness and damping coefficients, so that the same restoring forces at the secondary are obtained as if with more than one link. The modeling is summarized in the appendix, and figure 2 illustrates the geometry.

Expressed in the body fixed coordinate system $O(b^1, b^2, b^3)$, the coupled vibrational, translational and rotational equations of such a structure become:

Vibrational:

$$M_o\{\ddot{y}+2\Omega\dot{y}+[\dot{\Omega}+\Omega^2]y+[\dot{\Omega}+\Omega^2]\rho+La_o\}+C\dot{y}+Ky=f$$

Translational:

$$ma_o+L^TM_o\{\ddot{y}+2\Omega\dot{y}+[\dot{\Omega}+\Omega^2]y\}=L^Tf+f^o$$

Rotational:

$$\{J_o+J_1(\rho,y)+\tfrac{1}{2}J_1(y,y)\}\omega +$$

$$\tilde{\omega}\{J_o+J_1(\rho,y)+\tfrac{1}{2}J_1(y,y)\}\omega +$$

$$\Gamma(\rho+y)^TM_o\ddot{y}+R_1(\omega,\rho+y)\dot{y}-\tilde{a}_oL^TM_oy+C_R\omega+K_r\int^t\omega(\alpha)d\alpha=$$

$$\tau+\Gamma(\rho+y)^Tf$$

y denotes the (2nx1)(for planar motion or (3nx1) for out of plane motion) matrix of deflection coordinates of the centers of n appendages from their undeformed positions, n=2 in the case when the secondary mirror and the spacecraft platform are regarded as appendages of the primary. τ is the torque about the

(also used in defining $R = \mathrm{diag}[r_j]$ for K_2), are chosen so that

$$\Sigma_i r_i |B_i|^2 \leq 2a/N$$

where N = dim x and "a" bounds the eigenvalues of A, i.e. $|\exp At|^2 < N\exp(-2at)$, for square integrable inputs (lower bounds on the weights are also needed when the inputs are not so, but are bounded: (Dwyer, 1986)).

The advantages of such modeling are:

- *The model dimension is equal to the number of test inputs.
- *Modeling error is distributed throughout the chosen input signal class (i.e. by frequency or amplitude), rather than depending on nearness to a single reference trajectory.
- *The interpolated signal (response) can be proven to converge asymptotically to the true system response for any (unknown) excitation in the chosen signal class.

In this technique of modeling, we can record the real data $y^{(1)}, \ldots, y^{(m)}$ by exciting the real system with (constant or nonconstant) test inputs to construct the interpolator. The test inputs can be chosen to better approximate the expected excitations of the system. Thus, we can deduce that the real system time responses are used for model matching, rather than responses synthesized from the mathematical model.

The problem with this technique, however, lies in the fact that we should have storage of curves in order to compute the c_i's. This number is equal to mxN x I^N, where m is the number of test inputs, N is the dimension of the state to be modeled and I is the number of possible initial values of each component. This difficulty does not allow the system to run in real time: e.g., for the case of n point masses linked by massless but elastic connections one has N = 2n in the planar motion case.

ON-LINE ESTIMATION

In this section we try to profit from the last two techniques and create a more effective one by making use of the transition matrix spline of the bilinear system of our model:

$$\hat{n}(t) = \hat{\Phi}(t, t_k)\hat{n}(t, t_k).$$

In fact the transition matrix spline $\hat{\Phi}$ interpolates the transition matrices Φ corresponding to the bilinear system model excited by constant or piecewise constant test inputs $u^{(i)}$. This permits the construction of the response of the real time system in piecewise closed form, thereby replacing response curve storage by an analytic transition matrix generator, rather than the construction of the coefficient interpolator c_i's from the output test signal $y^i(y^1, y^2, \ldots, y^m)$.

One gets $c_i = \{c^{pq}\}$ from $y_i = \{\Phi^{pq}\}$ where Φ^{pq} is the (p, q) entry in the transition matrix with $u^{(i)}$ constants:

$$\Phi_i = \exp\{(A + \Sigma_j B_j u^{(j)}\}$$

The interpolated transition matrix is then used to update between observations the structural state estimates obtained from a filter based on a globally feedback-linearized transformation (seen in section 3.1) of the bilinear structural model. This last technique has the following features:

- * $\hat{\Phi}$ is open loop, with $\hat{n}$ made to match the real system at discrete intervals by re-initializing:

$$\begin{matrix}\hat{n}(t_1) \\ \vdots \\ \hat{n}(t_k)\end{matrix} = \hat{\Phi}(t, t_k) \begin{matrix}\hat{n}(t_1) \\ \vdots \\ \hat{n}(t_k)\end{matrix}$$

In contrast, the direct modeling of the I/O operator

$$\hat{n} = \Sigma_i c_i \exp \int^t u^T R u^{-1} dt$$

continuously tracks the true system time response $n^1(t)$, but in this case $c_i(t)$ cannot be generated analytically and must be computed off-line.

*The presence of an additive, even if not actively suppressed, input does not give rise to a steady state tracking error observed in the earlier literature when additive as well as multiplicative inputs are present, as is the case for rapidly slewing structures. Indeed, a convolution correction based on Φ can be added.

*The number of curves to be generated is only m x N^2 instead of m x N x I^N, (where again N = 2N for the example of a structure composed of point masses connected by elastic appendages and in plane motion).

*The possibly high dimensional recursive filter can run at a slower sampling rate, consistent with on board CPU capabilities.

Interpolation Example

An interpolator was designed for the same two bodies beam expander model previously described. The interpolator was optimized for input vectors $u^T = (u_1, u_2, u_3)$ of the form (constant, o, o), (o, constant, o) and (o, o, constant), chosen with a negative constant during the first half of a 10 second nominal minimum time rotation, and positive during the second half, with the deformation state re-initialized at mid maneuver (5 seconds) from the feedback-linearized filter described previously. The constants were selected for boundedness of the interpolator according to (Dwyer, 1986) in effect upper bounds on the expected ω, ω^2 and 2ω respectively. The interpolator response is given in figures 6 and 7.

DISCUSSION: APPLICATION TO CONTROL

The computed torque which will orient the system in the required maneuver will be sensitive to model accuracy. This can be alleviated by variable structure control at the cost of chattering. A technique developed by Slotine (1984) suggests that if we know the error between the unknown computed torque and the actual computed torque, then we can find an optimal interpolation of the variable structure corrections on each side of the ideal sliding surface that effects compromises with the accuracy of the system model used for torque computation and the control bandwidth, to track in an optimum way the required trajectory. This error can actually be derived from the on-line modeling of the state deformation. In fact, an upper bound exists between the unknown true structural transition matrix Φ and the operator spline interpolator $\hat{\Phi}$ (Dwyer 1986). And because the computed torque is related to those functions through the equations of motion, then we can assume that an optimal computed torque correction compatible with the robustness of the model can be found. This will be reported elsewhere.

REFERENCES

1. J. L. Junkins and J. D. Turner, "Optimal Spacecraft Rotational Maneuvers," Elsevier, 1986.

2. M. S. Fadali, S. Gardner and T. A. W. Dwyer, III, "Nonlinear Decoupling and Control of Manipulators with Sensor and Actuator Noise," Proc. 2nd IASTED Internat. Conf. on Applied Control and Identification (Los Angeles, CA, Dec. 10-12, 1986), Acta Press, Calgary, 1987.

3. T. A. W. Dwyer, III, "Operator Spline Methods in the Design of Nonlinear Equalizers," Proc. IEEE ISCAS (San Jose, CA, May 5-7, 1986), v. 2, pp. 701-703.

4. T. A. W. Dwyer, III, "optimal Interpolation and Smoothing of Bilinear Systems," Proc. ACC (Seattle, WA, June 18-20, 1986), v. 1, pp. 394-397.

5. R. J. P. de Figueiredo and T. A. W. Dwyer, III, "A Best Approximation Framework and Implementation for Simulation of Large-Scale Nonlinear Systems," IEEE Trans. on Circuits and Systems, v. CAS-27, No. 11 (Nov. 1980), pp. 1005-1014.

6. J. J. E. Slotine, "Sliding Controller Design for Non-linear Systems," Int. J. of control, v. 40, No. 2 (1984), pp. 421-434.

ACKNOWLEDGMENTS

This research was supported by SDIO/IST and managed by AFOSR under contract F49620-87-C-0103. Support for the second author also came from NASA Grant NAG-1-613.

APPENDIX

Notation of Symbols Met in the Text and Graphics:

$\vec{\rho}^i$ Position of i-th appendage if undeformed.

$O(\vec{b}^1, \vec{b}^2, \vec{b}^3)$: Body fixed reference system

c: True center of mass

$N(\vec{n}^1, \vec{n}^2, \vec{n}^3)$: Inertial reference system.

$\vec{c}$: The vector from body fixed coordinate to the instantaneous center of mass:

$$\vec{c} = \mu^o \vec{\rho}^o + \sum \mu^j (\vec{x}^j + \vec{\rho}^j).$$

if O is the undeformed system's center of mass, then:

$$\vec{c} = \sum \mu^j \vec{x}^j.$$

where:

$$\mu^j = \frac{m^j}{m^o + \sum_j m^j}$$

μ^j is called the mass ratio of the j-th appendage, and μ^o is called the mass ratio of the main body. $\vec{f}^i$ is the net external force applied to the (center of mass of) the i-th appendage,

$$\text{let } y = \begin{matrix} x_2^1 \\ \vdots \end{matrix} = \text{col}(x^i), \quad x^i = (x_1^i, x_2^i, x_3^i)^T$$

$$\rho = \begin{matrix} \rho^1 \\ \rho^2 \\ \vdots \end{matrix} = \text{col}(\rho), \quad \rho^i = (\rho_1^i, \rho_2^i, \rho_3^i)^T$$

$$\omega = \begin{matrix} \omega^1 \\ \omega^2 \\ \omega^3 \end{matrix}$$

where:

$$\vec{x}^j = x_1^j \vec{b}^1 + x^j \vec{b}^2 + x_3^j \vec{b}^3$$

$$\vec{\rho}^j = \rho_1^j \vec{b}^1 + \rho^j \vec{b}^2 + \rho_3^j \vec{b}^3$$

$$\vec{\omega} = \omega_1 \vec{b}^1 + \omega_2 \vec{b}^2 + \omega_3 \vec{b}^3$$

$\vec{\omega}$ is the angular velocity vector of the body fixed coordinate frame

$O(\vec{b}^1, \vec{b}^2, \vec{b}^3)$.

$\bar{I} = \text{diag}([I])$ and $L = \text{col}([I], [I], \ldots)$ where $[I]$ denotes the 3 x 3 identity matrix.

$$\Omega = \text{diag}(\bar{\omega}) = \omega \text{ where } \bar{\omega} = \begin{matrix} 0 & -\omega_3 & \omega_2 \\ \omega_3 & 0 & -\omega_1 \\ -\omega_2 & \omega_1 & 0 \end{matrix}$$

$M_o = \text{diag}(m^i[I])$ & $N = \frac{1}{m^o} M_o L = \text{col}(\mu^i[I])$

$K = \text{diag}(k^i[I])$ and $C = \text{diag}(c^i[I])$.

$\Gamma^T(\rho) = [\tilde{\rho}1 | \tilde{\rho}2 | \ldots]$, $\tilde{\rho}j$ defined as $\tilde{\omega}$

$J_o = J_{hub} + \Gamma^T(\rho) M_o \Gamma(\rho)$

$J_1(\rho, y) = \Gamma^T(\rho) M_o \Gamma(y) + \Gamma^T(y) M_o \Gamma(\rho)$

$R_1(\omega, \rho) = [m^1(\bar{x}^1\bar{\omega} + \bar{\omega}\bar{x}^1 + \widetilde{\bar{x}^1\omega}) | \ldots]$

For planar motion, every third rows and columns are omitted. One then has $\vec{\omega} = \dot{\theta}\vec{k}$, and if $J = \text{diag}([\begin{matrix} 0 & -1 \\ 1 & 0 \end{matrix}])$, then the 3n x 3n matrix Ω is replaced throughout by the 2n x 2n matrix $\dot{\theta}J$, Ω^2 by $\dot{\theta}^2 J^2 = -\dot{\theta}^2 \bar{I}$ (where $\bar{I}$ is now the 2n x 2n

identity) and $\ddot{a}$ by $\delta\ddot{J}$. Finally, M in the equation of planar motion is

$M = [\bar{I} - NL^T]M_o$, where M_o, $\bar{I}$, N, L are redefined to be (2n x 2n).

Figure 1

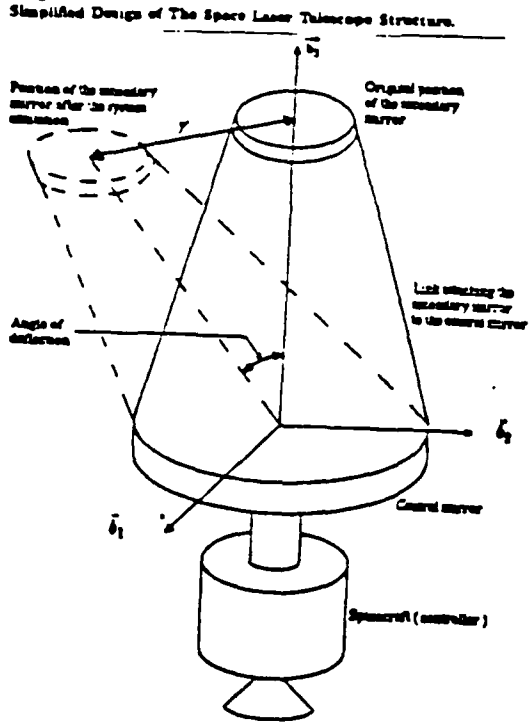

Simplified Design of The Space Laser Telescope Structure.

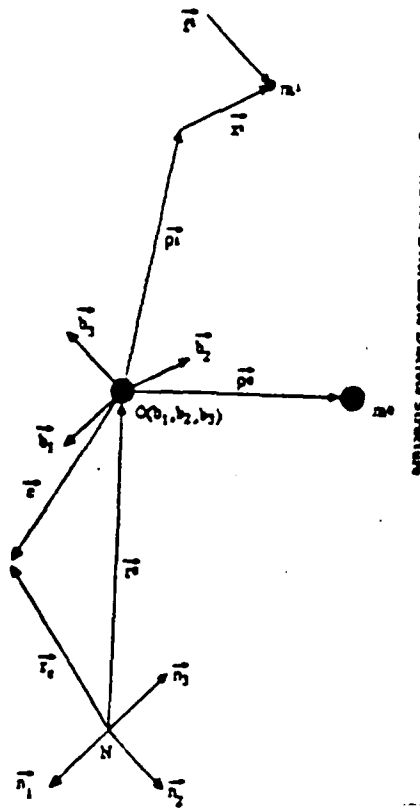

Figure 2
Vectorial Configuration of a Deformable Discrete Structure

Figure 3
Extended Kalman Filter Method

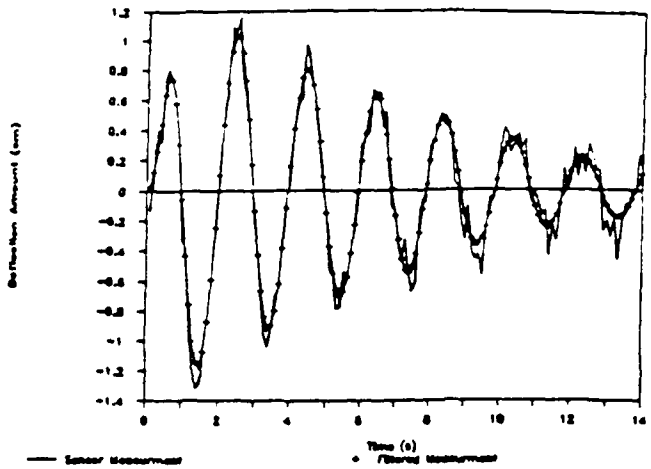

Figure 4
FeedbackLinearized Procedure

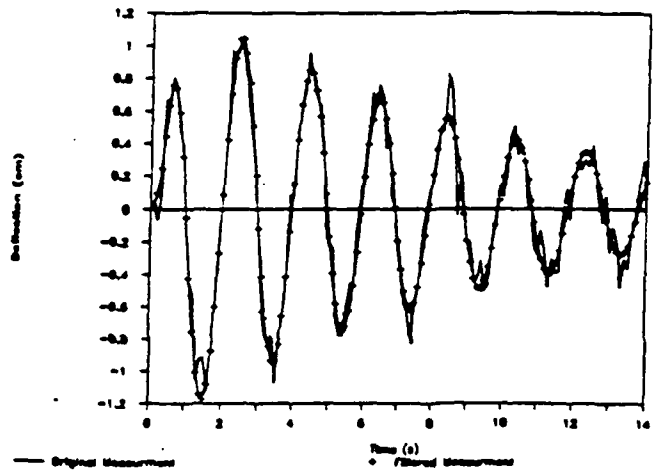

Figure 5
Error Comparison Graphic

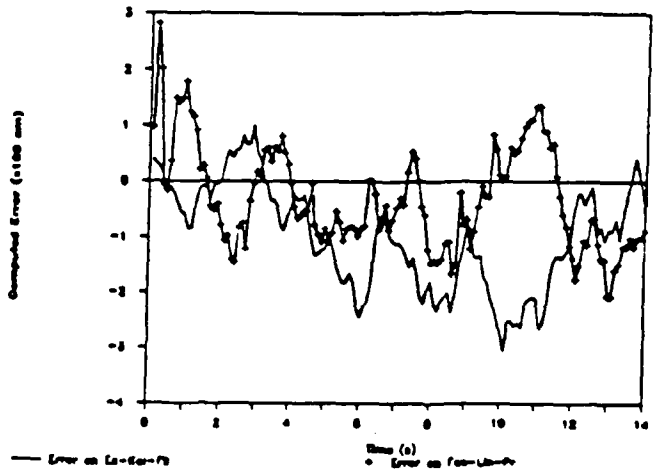

page number 10

Figure 6
Deflection Computed By Interpolation

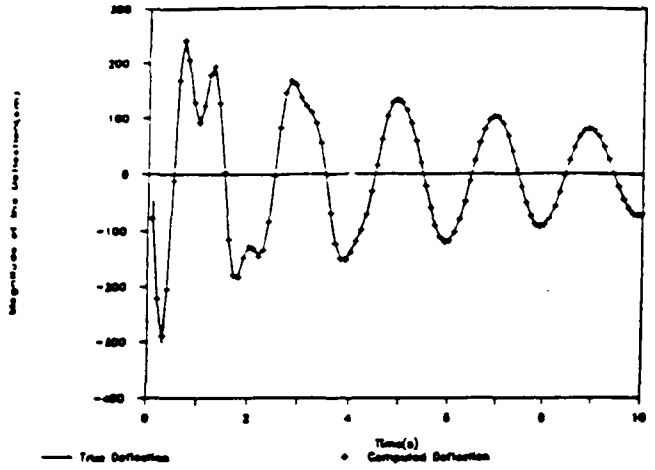

Figure 7
Computed Error of the Interpolator

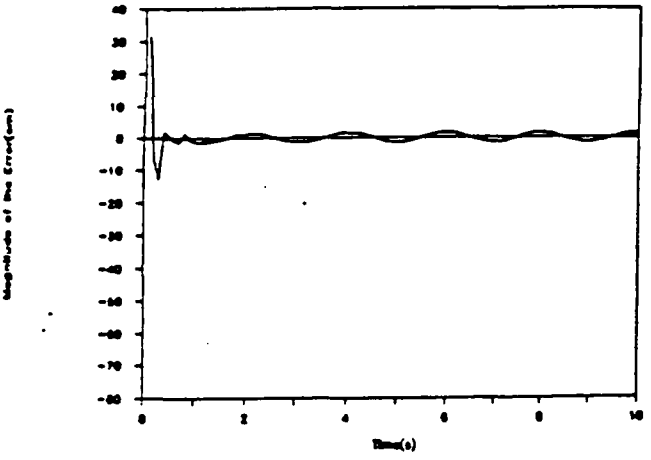

Proc. 27th IEEE Conf. on Decision and Control (Austin, TX Dec, 9-11, 1988)

SLEW-INDUCED DEFORMATION SHAPING[1]

T.A.W. Dwyer, III
Department of Aeronautical and Astronautical Engineering
University of Illinois
Urbana, IL 61801

Abstract

Computed torques for pointing and tracking require compensation for slew-induced structural, forebody/aftbody, or optical train alignment deformations, hereafter called deformations. Thus even if only line-of-sight variables are to be commanded, yet full state feedback is needed. The solution proposed here is to decouple by feedforward of the line-of-sight slew dynamics into the deformation control loop. It is also shown in this paper how arbitrarily few actuators are needed for such deformation shaping, at the cost of higher differentiability of the reference line-of-sight dynamics. The low rates, single axis case is developed here in detail, and its extendability to high rates and multiple axes by global feedback linearization is outlined.

Introduction

In recent work on the control of robots with elastic joints, the state of the coupled rigid and elastic dynamics is forced to evolve in a "slow" integral manifold, so that the elastic distortion to the computed torque becomes a transient, i.e., the "transversal" (off-manifold) dynamics. That approach is followed here in treating the problem of slewing with deformable bodies, to show how a family of control-dependent slow manifolds can be constructed, on each of which the slew-induced deformations are expressible in terms of (higher derivatives of) the slewing angle. This relieves the bandwidth requirements of the primary slew actuator, but generally requires that slew-generated "deformation shaping" forces or moments also be applied, such as through available structural actuators. In the absence of sufficient natural damping, it is shown how a "fast" correction can also be applied, involving an on-line synthesis of the "transversal" part of the deformation. This requires higher control bandwidth than if only the slow control were used, but only from the deformation shaping actuators, not from the slew actuator. The role of "prior" or "posterior" global feedback linearization for the extension of the method to the multiaxial or high rates situation is then outlined, as well as the interpretation of the slow manifolds as sliding surfaces for robust variable structure control implementation.

Deformable Rotational Dynamics

The model for a rotating body to be used here is given by Eqns. (1), (2).

$$J\ddot{\theta} + c\dot{\theta} + k\theta + \underline{n}^T\ddot{\underline{y}} = \tau + \underline{e}^T\underline{f} \tag{1}$$

$$M\ddot{\underline{y}} + C\dot{\underline{y}} + K\underline{y} + \underline{d}\ddot{\theta} = E\underline{f} \tag{2}$$

where rotation about an axis through the undeformed center of mass, measured by the angle θ in radians is presumed, entailing deformations represented by an nx1 column matrix $\underline{y}(t)$ of generalized coordinates. A torque τ about the same axis with respect to which the attitude angle θ is measured entails matching rotation-deformation coupling coefficients, $\underline{n} = \underline{d}$. Deformation shaping forces or moments are encoded by the mx1 matrix $\underline{f}$ of generalized forces. To fix ideas, the central hub with symmetrically placed and antisymmetrically deforming cantilevered appendages developed in [1] can be considered, wherein the coefficient matrices as well as deformations are expressed in terms of assumed mode shapes.

More general models, involving either coupling nonlinearities arising from gyroscopic effects or full spatially distributed deformation dynamics or both, are found in [2], [3], [4], [5], but then time-varying dynamics or unbounded operator coefficients arise, for which the present method is still under development.

Slew-Induced Deformations

The standard "proportional plus derivative" control law given by Eqn. (3) requires feedforward of measured structural acceleration to the pointing and tracking torque control,

$$\tau = \hat{J}\ddot{\theta}^* + \hat{c}\dot{\theta}^* + \hat{k}\theta^* + \hat{\underline{n}}^T\ddot{\underline{y}} - a_1(\dot{\theta} - \dot{\theta}^*) - a_0(\theta - \theta^*) \tag{3}$$

where hats denote estimates and θ^* is the commanded angular trajectory. With a good model and good sensors the closed loop dynamics is then approximated by Eqn. (4),

$$J\Delta\ddot{\theta} + (c + a_1)\Delta\dot{\theta} + (k + a_0)\Delta\theta = \underline{0} \tag{4}$$

where $\Delta\theta := \theta - \theta^*$ and no structural controls 'per se' are applied: $\underline{f} = \underline{0}$.

Besides the (everywhere present) question of model accuracy, the need for high bandwidth slew torque actuators and for full order structural sensing arises.

Exact Slow Manifolds

Following [6] - [8] in part, it is shown here how deformation-induced line of sight disturbances can be reduced to transients: Eqns. (1), (2) are first put into singular perturbation form: Let $\bar{K}$ be a normalized stiffness matrix, so that one has K expressed in terms of $\bar{K}$ and a perturbation parameter $\varepsilon > 0$:

$$\bar{K} = \varepsilon K \tag{5}$$

[1] Research supported in part by SDIO and managed by AFOSR (AFSC) under contract F49620-87-C-0103, and by NASA Grant NAG-1-613.

Without loss of generality one may set $M = I$ = identity and $K = \omega_1^2 \,\mathrm{diag}\,(1, \omega_2^2/\omega_1^2, \ldots)$ with $\omega_1 < \omega_2 < \ldots$, then set $\varepsilon = \omega_1^{-2}$, so that $\bar{K} = \mathrm{diag}\,(1, (\omega_2/\omega_1)^2, \ldots)$. Whatever the physical interpretation, one may seek polynomial controls in the parameter ε,

$$\tau = \tau_o + \varepsilon\tau_1 + \ldots + \varepsilon^p \tau_p \tag{6}$$

$$\underline{f} = \underline{f}_o + \varepsilon\underline{f}_1 + \ldots + \varepsilon^p \underline{f}_p \tag{7}$$

such that the deformations can be expressed as perturbations from the rigid body limit as $\varepsilon \to 0$, i.e.,

$$\underline{y} = \varepsilon\underline{z} + \underline{y}' \tag{8}$$

with the normalized deformation $\underline{z}$ (which has units of force) also a polynomial in ε,

$$\underline{z} = \underline{z}_o + \varepsilon\underline{z}_1 + \ldots + \varepsilon^{p-1}\,\underline{z}_{p-1} \tag{9}$$

and $\underline{y}'(t) \to \underline{0}$ as $t \to \infty$. Indeed, insertion of Eqns. (5) and (8) into Eqns. (1) and (2) brings the latter to singular perturbation form,

$$J\ddot{\theta} + c\dot{\theta} + k\theta + \varepsilon\,\underline{n}^T\ddot{\underline{z}} = \tau + \underline{e}^T\underline{f} + \nu \tag{10}$$

$$\varepsilon(M\ddot{\underline{z}} + C\dot{\underline{z}}) + \bar{K}\underline{z} + \underline{d}\,\ddot{\theta} = E\underline{f} \tag{11}$$

where the disturbance ν is given by Eqn. (12),

$$\nu = -\,\underline{n}^T\ddot{\underline{y}}' \tag{12}$$

and $\underline{y}'$ is governed by

$$M\ddot{\underline{y}}' + C\dot{\underline{y}}' + K\underline{y}' = \underline{0} \tag{13}$$

If $\varepsilon = 0$ then $\underline{z} = \underline{z}_o$ lies in the "rigid body manifold",

$$\underline{z}_o = \bar{K}^{-1}\left(E'\underline{f} - \underline{d}'\tau + \underline{c}'\,\dot{\theta} + \underline{k}'\theta\right) = h_o(\theta, \dot{\theta}, \tau, \underline{f}) \tag{14}$$

where

$E' = E - \underline{d}J^{-1}\underline{n}^T$, $\underline{d}' = J^{-1}\underline{d}$, $\underline{c}' = \underline{d}J^{-1}c$ and $\underline{k}' = \underline{d}\,J^{-1}k$. Then by Tychonov's theorem of singular perturbations [6], for (in general small enough) $\varepsilon > 0$ there is also a neighboring "slow manifold",

$$\underline{z} = \underline{z}_o + \varepsilon\underline{z}_1 + \ldots = h_\varepsilon(\theta, \dot{\theta}, \underline{f}, \tau, \dot{\underline{f}}, \dot{\tau}, \ldots) \tag{15}$$

where if $\underline{z}(t_o) = h_\varepsilon$ (at t_o) then $\underline{z}(t) = h_\varepsilon$ (at t) for all $t \geq t_o$.

In particular, slow manifolds corresponding to polynomial controls in ε can be found that yield polynomial representations in ε (in which case ε need not be "small"): indeed, the insertion of the expansions (6), (7) and (9) into Eqns. (10) and (11), followed by collection of equal powers of ε, yield the following recursive formulas,

$$J\ddot{\theta} + c\dot{\theta} + k\theta = \tau_o + \underline{e}^T\underline{f}_o + \nu \tag{16}$$

$$\bar{K}\,\underline{z}_o + \underline{d}\,\ddot{\theta} = E\,\underline{f}_o \tag{17}$$

$$\underline{n}^T\ddot{\underline{z}}_j = \tau_{j+1} + \underline{e}^T\underline{f}_{j+1} \tag{18}$$

$$M\ddot{\underline{z}}_j + C\dot{\underline{z}}_j + \bar{K}\,\underline{z}_{j+1} = E\,\underline{f}_{j+1} \tag{19}$$

for $j = 0, \ldots, p-2$, and

$$\underline{n}^T\ddot{\underline{z}}_{p-1} = \tau_p + \underline{e}^T\underline{f}_p \tag{20}$$

$$M\ddot{\underline{z}}_{p-1} + C\dot{\underline{z}}_{p-1} = E\,\underline{f}_p \tag{21}$$

where $\underline{z}_p = \underline{0}$ is presumed, so that if one sets $\tau_j = 0$ and $\underline{f}_j = \underline{0}$ for $j \geq p + 1$ then also $\underline{z}_j = \underline{0}$ for $j \geq p$. Thus, the postulated polynomial solution given by Eqn. (9) is verified. In particular, no convergence considerations arise and no truncation is needed (hence, the term "exact slow manifolds"). This is possible if and only if Eqns. (16) - (21) can be solved for $\tau_j, \underline{f}_j$, $j = 0, \ldots, p$, as discussed next.

Deformation Suppression

The simplest choice of slow manifold is $\underline{z} = \underline{0}$, which exists if and only if it is possible to solve Eqn. (22) below for τ_o and $\underline{f}_o$,

$$\phi_o(s)\theta = \varepsilon_o\begin{pmatrix}\tau_o\\ \underline{f}_o\end{pmatrix} + \begin{pmatrix}\nu\\ \underline{0}\end{pmatrix} \tag{22}$$

where

$$\phi_o(s) = \begin{pmatrix} Js^2 + cs + k \\ \underline{d}s^2 \end{pmatrix} \tag{23}$$

and

$$\varepsilon_o = \begin{bmatrix} 1 & \underline{e}^T \\ \underline{0} & E \end{bmatrix} \tag{24}$$

obtained by setting $\underline{z}_o = \underline{0}$ in Eqns. (16) and (17), and then Laplace-transforming (the same symbols $\theta, \tau, \underline{f}, \underline{z}, \underline{y}$ will be used both in the time and frequency domains).

Noting that $\dim \varepsilon_o = (1+n) \times (1+m)$ (where $n = \dim \underline{y}$ and $m = \dim \underline{f}$), it is seen that ε_o is square if and only if $m = n$ ("independent modal space control"). Then ε_o is invertible if and only if E is invertible; indeed then Eqns. (16), (17) yield

$$\boxed{(J - \underline{e}^T E^{-1}\underline{d})\ddot{\theta} + c\dot{\theta} + k\theta = \tau_o + \nu} \tag{25}$$

$$\boxed{E^{-1}\,\underline{d}\,\ddot{\theta} = \underline{f}_o} \tag{26}$$

Letting $\Delta\theta := \theta - \theta^*$, the tracking problem is then reduced to a regulator problem based on the reduced slow dynamics given by Eqn. (25), that is, to the choice of a stabilizing regulator $H_o(s)$ for the block

diagram in Figure 1:

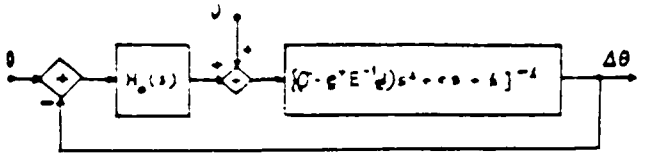

Figure 1

The slew torque is then given by Eqn. (27):

$$\tau = \tau_o + (J - \underline{e}^T E^{-1} \underline{d}) s^2 \theta - H_o(s) \Delta\theta \qquad (27)$$

For Eqn. (25) to be a valid slew dynamics model, it is also necessary to apply a deformation suppressing control $\underline{f}$, which is found from Eqn. (26) by insertion therein of the closed loop pointing angle θ found by inversion of Eqn. (25):

$$\underline{f} = \underline{f}_o = E^{-1} \underline{d} s^2 \{(J - \underline{e}^T E^{-1} \underline{d}) s^2 + cs + k\}^{-1} \tau_o = E^{-1} \underline{d} s^2 \theta$$

$$- E^{-1} \underline{d} s^2 \{(J - \underline{e}^T E^{-1} \underline{d}) s^2 + cs + k\}^{-1} H_o(s) \Delta\theta \qquad (28)$$

In particular, if a proportional and derivative regulator $H_o(s) = a_1 s + a_o$ is selected, the closed loop pointing error dynamics becomes as shown in Eqn. (29):

$$(J - \underline{e}^T E^{-1} \underline{d}) \Delta\ddot{\theta} + (c + a_1) \Delta\dot{\theta} + (k + a_o) \Delta\theta = \nu \qquad (29)$$

In contrast with Eqn. (4), the driving term $\nu = -\underline{n}^T \underline{\ddot{y}}$ is a transient as expected, and yet, unlike Eqn. (3), no high frequency correction term is needed in the slew control law of Eqn. (27). The need for structural sensors and high bandwidth actuators in the implementation of the control law given by Eqn. (3) is now replaced by the need for full order structural control. This is alleviated next.

First Order Deformation Shaping

If c_o in Eqn. (22) is not invertible, the system cannot be "rigidfied", but the coupling term $\underline{n}^T \underline{\ddot{y}}$ can still be replaced by the fast transient plus higher derivative terms in the pointing variable θ. The simplest choice of such a slow manifold is $\underline{z} = \underline{z}_o$, which exists if and only if it is possible to solve Eqn. (30) below for $\tau_o, \tau_1, \underline{f}_o$ and $\underline{f}_1$.

$$\underline{\phi}_1(s)\, \theta = c_1(s) (\tau_o, \underline{f}_o^T, \varepsilon\tau_1, \varepsilon \underline{f}_1^T)^T + (\nu, 0, \underline{0}^T)^T \qquad (30)$$

where

$$\underline{\phi}_1^T(s) = (\varepsilon s^2 + cs + k, -\underline{n}^T K^{-1} \underline{d} s^4,$$

$$- [(Ms + C) K^{-1} \underline{d} s^3]^T) \qquad (31)$$

and

$$c_1(s) = \begin{bmatrix} 1 & \underline{e}^T & \cdots & 1 & \underline{0}^T \\ 0 & -\underline{n}^T K^{-1} E s^2 & & 0 & \underline{e}^T \\ \underline{0} & -[Ms + C] K^{-1} E s & & \underline{0} & E \end{bmatrix} \qquad (32)$$

Equations (30), (31), (32) are obtained by solving Eqn. (17) for $\underline{z}_o$, to yield

$$\underline{z}_o = \bar{K}^{-1} \{E \underline{f}_o - \underline{d} s^2 \theta\} \qquad (33)$$

in the frequency domain, then inserting Eqn. (33) into Eqns. (16), (20) and (21) with p=1 (hence $\underline{z}_1 = 0$).

Noting that dim $c_1(s) = (2+n) \times (2+2m)$, it is seen that $c_1(s)$ is square if and only if $m=n/2$. In this case, if $c_1(s)$ is generically invertible one may set

$$c_1^{-1}(s) \phi_1(s) = : (Y_o^\tau(s), \underline{Y}_o^f(s)^T, Y_1^\tau(s), \underline{Y}_1^f(s)^T)^T \qquad (34)$$

(which is independent of ε), and then define the slow transfer functions for $\tau = \tau_o + \varepsilon\tau_1$ and $\underline{f} = \underline{f}_o + \varepsilon \underline{f}_1$ as follows:

$$Y^\tau(s) := Y_o^\tau(s) + Y_1^\tau(s) \qquad (35)$$

$$\underline{Y}^f(s) := \underline{Y}_o^f(s) + \underline{Y}_1^f(s) \qquad (36)$$

Equation (30) then yields

$$\boxed{Y^\tau(s)\theta = \tau + \nu_1} \qquad (37)$$

$$\boxed{\underline{Y}^f(s)\theta = \underline{f}} \qquad (38)$$

where the transient disturbance ν_1 is given in terms of ν of Eqns. (12) and (13):

$$\nu_1 = (1 | \underline{0}^T | \underline{0}^T)\, c_1(s)^{-1} (\nu, 0, \underline{0}^T)^T \qquad (39)$$

No transient appears in Eqn. (38) because, instead of directly inverting all of $c_1(s)$, it is possible to solve separately for τ_o in terms of $\underline{f}_o$ (and θ) from Eqn. (16) and for τ_1 in terms of $\underline{f}_o$ and $\underline{f}_1$ from Eqn. (20), while $(\underline{f}_o, \varepsilon \underline{f}_1)$ are obtainable only from Eqn. (21) with $\underline{z}_o$ from Eqn. (17), neither of which contain ν.

The tracking problem is now reduced to a regulator problem based on the reduced slew dynamics given by Eqn. (3), that is, to the choice of a stabilizing regulator $H_1(s)$ for the block diagram of Figure 2:

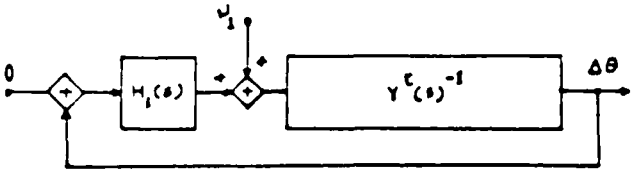

Figure 2

The low bandwidth slew torque control is then given by Eqn. (40):

$$\tau = \tau_o + \varepsilon\tau_1 = Y^T(s)^{-1}\theta^* - H_1(s)\Delta\theta \qquad (40)$$

For Eqn. (37) to be a valid slew dynamics model, it is again necessary to apply a deformation shaping control $\underline{f}$, which is now found from Eqn. (38) by insertion therein of the closed loop pointing angle θ found by inversion of Eqn. (37):

$$\underline{f} = \underline{f}_o + \varepsilon\underline{f}_1 = \underline{Y}^f(s)Y^T(s)^{-1}\tau = \underline{Y}^f(s)\theta^*$$

$$- \underline{Y}^f(s)Y^T(s)^{-1}H_1(s)\Delta\theta \qquad (41)$$

The closed loop pointing error dynamics now becomes as shown in Eqn. (42):

$$\{Y^T(s) + H_1(s)\}\,\Delta\theta = v_1 \qquad (42)$$

It turns out that each scalar component $Y_i^f(s)$ of $\underline{Y}^f(s)$ has the same number of poles and the same number of zeros as $Y^T(s)$. In particular, the poles of $Y^T(s)$ and of each $Y_i^f(s)$ are given by $\det \varepsilon_1(s)$.

Thus, only the compensation $H_1(s)$ determines the number of derivatives of the pointing error $\Delta\theta$ that are needed to generate $\underline{f}$ from Eqn. (41), as well as τ from Eqn. (40). This is an exact generalization of the "independent modal space control" case given by Eqns. (27) and (28). In particular, the high frequency disturbance to the slew dynamics is again reduced to a transient (now v_1), and no high frequency correction is needed for the pointing control torque τ.

P - Th Order Deformation Shaping

More generally, a slow manifold with the representation of Eqn. (9) as a (p-1)-th order polynomial in ε exists if and only if Eqn. (43) below can be solved for τ_j, $\underline{f}_j$, $j = 0, \ldots, p$,

$$\underline{\phi}_p(s)\theta = \varepsilon_p(s)(\tau_o, \underline{f}_o^T, \ldots, \varepsilon^p\tau_p, \varepsilon^p\underline{f}_p^T)^T$$

$$+ (v, 0, \ldots, \underline{0}^T)^T \qquad (43)$$

where $\underline{\phi}_p(s)$ and $\varepsilon_p(s)$ are found by successive elimination of $\underline{z}_p, \ldots, \underline{z}_{p-1}$ in Eqns. (16) - (21). Now $\underline{\phi}_p(s)$ is $(p+1+n)$ - dimensional and $\dim \varepsilon_p(s) = (p+1+n) \times ((p+1) \times (1+m))$. It follows that $\varepsilon_p(s)$ is square if and only if the following relation holds true of $n = \dim \underline{y}$, $m = \dim \underline{f}$ and p :

$$p = \frac{n - m}{m} \qquad (44)$$

2p derivatives of θ then determine the slow part $\varepsilon\underline{z}$ of $\underline{y}$.

For an invertible $\varepsilon_p(s)$ one again sets

$$\varepsilon_p(s)^{-1}\underline{\phi}_p(s) = [Y_o^T(s), \underline{Y}_o^f(s)^T, \ldots, Y_p^T(s), \underline{Y}_p^f(s)^T]^T \qquad (45)$$

to construct the slow transfer functions for

$$\tau = \sum_{j=0}^{p} \varepsilon^j\tau_j \quad \text{and for} \quad \underline{f} = \sum_{j=0}^{p} \varepsilon^j\underline{f}_j .$$

$$\boxed{Y^T(s)\theta = \tau + v_p} \qquad (46)$$

$$\boxed{\underline{Y}^f(s)\theta = \underline{f}} \qquad (47)$$

where

$$Y^T(s) = \sum_{j=0}^{p} Y_j^T(s) \qquad (48)$$

$$\underline{Y}^f(s) = \sum_{j=0}^{p} \underline{Y}_j^f(s) \qquad (49)$$

and the transient v_p is again found from v of Eqns. (12) and (13):

$$v_p = (1, \underline{0}^T, \ldots, 1, \underline{0}^T)\varepsilon_p(s)^{-1}(v, 0, \ldots, 0, \underline{0}^T)^T \qquad (50)$$

Again no transient appears in Eqn. (47) for $\underline{f}$, only in Eqn. (46) for τ. This is because, instead of directly inverting $\varepsilon_p(s)$, it is also possible to proceed as follows:

(a) Solve recursively for $\underline{z}_p$ in terms of $\underline{f}_j$ for $j=0,\ldots,p$ (and 2p derivatives of θ) from Eqns. (17) and (19), which do not contain v;

(b) Insert $\underline{z}_p$ in terms of $\underline{f}_j$'s into Eqn. (21), which is decomposable into n equations in $(p+1)$ m unknowns (the m components of $\underline{f}_j$ for $j=0,\ldots,p$, where here $n = (p+1)\,m$ according to Eqn. (44), again not containing v;

(c) Solve recursively for τ_o in terms of $\underline{f}_o$ from Eqn. (16) (through which v appears), then for τ_{j+1} in terms of $\underline{f}_{j+1}$ and $\underline{f}_j, \ldots, \underline{f}_o$ (through $\underline{z}_j$) from Eqn. (18).

It is from (b) that Eqn. (47) arises, independently of v, and from (c) that Eqn. (46) arises.

Again the tracking problem is reduced to the design of a stabilizing regulator $H_p(s)$ replacing $H_1(s)$ in the block diagram of Figure 2, where the high frequency transient v_p replaces v_1, with Eqn. (48) now giving the transfer function $Y^T(s)^{-1}$ instead of Eqn. (35).

The consequent low bandwidth slew torque τ is then given by the counterpart of Eqn. (40), and the shaping control $\underline{f}$ by the counterpart of Eqn. (41), with $H_1(s)$ replaced by $H_p(s)$ and with $Y^T(s)^{-1}$ and $\underline{Y}^f(s)$ found from Eqns. (48) and (49).

Fast Control

If there is insufficient or non-existent "a priori" damping C in the deformation dynamics for adequate time scale separation, the shaping control can be augmented by a "fast" term $\underline{f}'$, as advocated in the singular perturbation literature, e.g., [6] and references therein. That is, Eqn. (41) for $\underline{f}$ (or its $H_o(s)$ counterpart) can be replaced by Eqns. (51)

and (52) below, with no change to Eqn. (40) for τ (or to its $H_p(s)$ counterpart),

$$\underline{f} = \underline{Y}^f(s)\, Y^T(s)^{-1}\tau - \underline{f}' \tag{51}$$

$$\underline{f}' = A_1(\dot{\hat{\underline{y}}} - \varepsilon\,\dot{\underline{z}}) + A_0(\hat{\underline{y}} - \varepsilon\,\underline{z}) \tag{52}$$

where $\hat{\underline{y}}$ and $\dot{\hat{\underline{y}}}$ now must be obtained from deformation sensors, but $\varepsilon\underline{z}$, $\varepsilon\dot{\underline{z}}$ from Eqn. (9), hence in terms of the $\underline{f}_j$'s, i.e., of $\underline{Y}_j^f(s)Y^T(s)^{-1}\tau$ for $j=0,\ldots,p$.

Since the "fast" off-manifold term $\underline{y}'$ in Eqn. (8) is modeled by $\underline{y} - \varepsilon\underline{z}$, it follows that $\underline{f}'$ is nothing but proportional plus derivative control of the fast dynamics. In particular, $\underline{f}' \to \underline{0}$ as required in [6]: indeed, the fast dynamics of Eqn. (13) is now replaced by that of Eqn. (53),

$$M\ddot{\underline{y}}' + [C + A_1]\dot{\underline{y}}' + [K + A_0]\underline{y}' = \underline{0} \tag{53}$$

hence $\underline{y}' \to \underline{0}$ by designer-selected choice of the gains A_1 and A_0.

In the above approach, no change is needed in the slow dynamics and corresponding control laws, where the original K and C are retained, provided v is replaced by $v - \underline{e}'\underline{f}'$ ($\to 0$) wherever appearing. An alternative is to design the fast control first, i.e., omit $\varepsilon\underline{z}$, $\varepsilon\dot{\underline{z}}$ from Eqn. (52), with consequently greater simplicity in the implementation of $\underline{f}'$. But then C must be replaced by $C + A_1$ and K by $K + A_0$ in all the slow control algorithms.

Example

Let n=2 and m=1, hence p=1, so that $\underline{z} = \underline{z}_0$ for appropriate choices of $\tau = \tau_0 + \varepsilon\tau_1$ and of $\underline{f} = \underline{f}_0 + \varepsilon\underline{f}_1$. Let also $E = e_1\ e_2)^T$, $\underline{e} = e$, $\underline{d} = (d_1, d_2)^T$, $\underline{n} = \underline{d}$, $M = I$, $C = \mathrm{diag}\,(c_1, c_2)$ and $K = \mathrm{diag}\,(k_1, k_2)$. One then finds

$$\underline{\phi}_1(s) = [\phi_{11}(s),\ \phi_{12}(s),\ \phi_{13}(s),\ \phi_{14}(s)^T \tag{54}$$

where

$$\phi_{11}(s) = Js^2 + cs + k \tag{55}$$

$$\phi_{12}(s) = (d_1^2/k_1 - d_2^2/k_2)s^4 \tag{56}$$

$$\phi_{13}(s) = (s + c_1)(d_1/k_1)s^3 \tag{57}$$

$$\phi_{14}(s) = (s + c_2)\,(d_2/k_2)s^3 \tag{58}$$

and

$$\varepsilon_1(s) = [\underline{\varepsilon}_{11}(s), \underline{\varepsilon}_{12}(s), \underline{\varepsilon}_{13}(s), \underline{\varepsilon}_{14}(s)] \tag{59}$$

where

$$\underline{\varepsilon}_{11}(s)^T = (1,0,0,0) \tag{60}$$

$$\underline{\varepsilon}_{12}(s)^T = (e, [d_1(e_1/k_1) + d_2(e_2/k_2)]s^2\ ,$$

$$(s + c_1)(e_1/k_1)s, (s + c_2)(e_2/k_2)s) \tag{61}$$

$$\underline{\varepsilon}_{13}(s)^T = (0,-1,0,0) \tag{62}$$

$$\underline{\varepsilon}_{14}(s)^T = (0,-e,-e_1,-e_2) \tag{63}$$

so that

$$\det \varepsilon_1(s) = e_1e_2[(s + c_1)/k_1$$

$$- (s + c_2)/k_2]s = : \delta_2(s) \tag{64}$$

Inversion of $\varepsilon_1(s)$ yields the following forms of Eqns. (35) and (36),

$$Y^T(s) = \frac{p_6^T(s)}{\delta_2(s)} \tag{65}$$

$$Y^f(s) = \frac{p_6^f(s)}{\delta_2(s)} \tag{66}$$

where the denominator is the quadratic polynomial given by Eqn. (64), while the numerators are 6-th degree polynomials.

In the idealized case of a perfect slew actuator, i.e., c=0 and k=0 in Eqn. (1), as well as no structural damping, i.e., C=0 in Eqn. (2), so that $c_1 = c_2 = 0$, the numerator and denominator of $Y^T(s)$ and $Y^f(s)$ take the forms below,

$$p_6^T = s^4(a_2s^2 + a_0)/k_1k_2 \tag{67}$$

$$p_6^f(s) = s^4(b_2s^2 + b_0)/k_1k_2 \tag{68}$$

$$\delta_2(s) = s^2c_0/k_1k_2 \tag{69}$$

where

$$a_0 = e_1e_2(k_2 - k_1) + e_1d_2k_1 - e_2d_1k_2 \tag{70}$$

$$a_2 = e_1e_2(d_1^2 - d_2^2) + d_1d_2(e_2^2 - e_1^2)$$

$$+ d_2e_1 - d_1e_2 \tag{71}$$

$$b_0 = e_2d_1k_2 - e_1d_2k_1 \tag{72}$$

$$b_2 = d_1e_2 - d_2e_1 \tag{73}$$

$$c_0 = e_1e_2(k_2 - k_1) \tag{74}$$

It follows that the transfer function to be regulated in the block diagram of Figure 2 becomes the "type 2" system shown in Eqn. (75),

$$Y^T(s)^{-1} = \frac{c_0}{s^2(a_2s^2 + a_0)} \tag{75}$$

which can be stabilized by a "damped PID" controller of the form given in Eqn. (76):

$$H_1(s) = K(s^2 + p_1 s + p_0)/(s + q) \qquad (76)$$

In particular, by matching coefficients of the closed loop transfer function with those of $(s + \lambda)^5$, the filter parameters can be chosen to be $q = 5\lambda$, $K = 10\lambda^3 a_2 - a_0 q$, $p_1 = 5\lambda^4/c_0 K$ and $p_0 = 1/c_0 K$, provided one selects $\lambda = \sqrt{a_0/10a_2}$ as the "slow time constant" (whenever a_0 and a_2 have the same sign). More generally, any control design method, be it LQR, H^∞ or co-prime factorization, can be used.

The "slow" part of the shaping control is then given by Eqn. (41), where the feedback part consists of the compensation $H_1(s)$ selected as above for use in Eqn. (40), cascaded with the two stage lead-lag filter given below:

$$Y^f(s)Y^\tau(s)^{-1} = (b_2 s^2 + b_0)/(a_2 s^2 + a_0) \qquad (77)$$

In the absence of damping as presumed here, a "fast" correction' to f must be added, in accordance to Eqn. (52), where A_0 and A_1 are freely chosen to impose time scale separation. The required "slow" term $c\underline{z}$ in f' is found from Eqn. (33), yielding the expression below in terms of the independently designed slow slewing torque τ :

$$\underline{y} - \underline{y}' = c\underline{z}_o = K^{-1}\{E\underline{Y}_o^f(s) - \underline{d}s^2\}Y^\tau(s)^{-1}\tau$$

$$= \left\{\begin{pmatrix} e_1/k_1 \\ e_2/k_2 \end{pmatrix} \frac{b_2 s^2 + b_0}{a_2 s^2 + a_0} - \begin{pmatrix} d_1^2/k_1 \\ d_2^2/k_2 \end{pmatrix} \frac{c_0}{(a_2 s^2 + a_0)s^2}\right\}\tau \qquad (78)$$

Extensions to Robust, Multiaxial and High Slew Rate Control

It is possible to extend the design methodology proposed herein to multiple slew axes as well as to high slew rates, in which case stiffness and damping coefficients in Eqn. (2) acquire angular rate and angular acceleration - dependent terms, while the rotational dynamics of Eqn. (1) acquire "vector product" terms: cf. [4], [5]. In this situation, the reduced order slewing dynamics obtained by inversion of Eqns. (16) - (21) become nonlinear. It is then possible to first globally feedback-linearize the nonlinear counterparts of Eqns. (1) and (2) with respect to pointing variables, such as in [9], [10] and elsewhere. Alternatively, it may be possible to first invert the nonlinear counterparts of the recursive Eqns. (16) - (21), to obtain nonlinear versions of the decoupled Eqns. (46) and (47) for the slow dynamics, and then seek to globally feedback-linearize Eqn. (46) (Eqn. (47)'s counterpart can be directly used to generate the shaping control f from τ without linearization).

Finally, the question of sensitivity to modeling errors may yield to variable structure control implementation: the presence only of the shaping control f in Eqn. (2) can be exploited to design an "interpolated switching control" following [11], with the selected slow manifolds regarded as the switching surfaces. The pointing control τ can then be designed for the reduced order dynamics on the switching surface, by the "hierarchical" method. These extensions will be discussed elsewhere.

References

[1] J. L. Junkins and J. D. Turner, Optimal Control of Spacecraft Rotational Maneuvers, Elsevier, 1986.

[2] E. Barbieri and U. Ozguner, "Unconstrained and Constrained Mode Expansions for a Flexible Slewing Link," Proc. American Control Conf. (Atlanta, GA, June 15-17, 1988) pp. 83-88.

[3] J. Baillieul and M. Levi, "Rotational Elastic Dynamics," Physica D, Vol. 27 (1987), pp. 43-62.

[4] T.A.W. Dwyer, III and F. Karray, "Nonlinear Modeling and Estimation of Slew-Induced Deformations," Proc. 1988 ASME Winter Annual Meeting (Chicago, IL, Nov. 27 - Dec. 2, 1988).

[5] W. H. Bennett, H. G. Kwatny and G. L. Blankenship, "Nonlinear Dynamics and Control Issues for Space-Based Directed Energy Weapons," Proc. 27th IEEE Conf. on Decision and Control (Austin, TX, December 12-14, 1988).

[6] M. W. Spong, K. Khorasani and P. V. Kokotovic, "An Integral Manifold Approach for the Feedback Control of Flexible Joint Robots," IEEE J. of Robotics and Automation, Vol. RA-3, No. 4 (August 1987), pp. 291-300.

[7] T.A.W. Dwyer, III, "Tracking and Pointing Maneuvers with Slew-Excited Deformation Shaping," AIAA Paper 87-2599, Proc. AIAA Guidance, Navigation and Control Conf. (Monterey, CA, August 17-19, 1987) Vol. 2, pp. 1503-1511.

[8] T.A.W. Dwyer, III, "Automatically Reconfigurable Control for Rapid Retargeting of Flexible Pointing Systems," SPIE Proceedings, Vol. 851, Space Station Automation III (1987), pp. 75-82.

[9] T.A.W. Dwyer, III, H. Sira-Ramirez, S. Monaco and S. Stornelli, "Variable Structure Control of Globally Feedback-Decoupled Deformable Vehicle Maneuvers," Proc. 26th IEEE Conf. on Decision and Control (Los Angeles, CA, December 9-11, 1987), pp. 1281-1287.

[10] A. Iyer and S. N. Singh, "Variable Structure Control of Decoupleable Systems and Attitude Control of Spacecraft in Presence of Uncertainty," Proc. American Control Conf. (Atlanta, GA, June 15-17, 1988), pp. 2238-2243.

[11] J. J. Slotine, "Sliding Controller Design for Nonlinear Systems," Internat. J. of Control, Vol. 40 (1984), pp. 421-434.

$$\dot{e}(t) = \begin{bmatrix} [0] & [I] \\ [0] & [0] \end{bmatrix} - K \begin{bmatrix} [I] & [0] \\ [0] & [I] \end{bmatrix} x(t) +$$

$$\begin{bmatrix} [0] & & [0] \\ [I]\, u' + P(t, t_o)R'(t)^{-1} & & [0] \end{bmatrix} \begin{bmatrix} & h_1^{-1} & \\ & & F_1 h_2^{-1}(.) \end{bmatrix} y(t).$$

For the case of slew-induced structural deformation estimation we find $F_1 = I$ and F_2 = lower half of B(X) defined before. In particular, we find $R_1 = R_1$, so that, in contrast to the extended Kalman filter, only the P-independent forcing term of the Riccati equation given by Q' has to be updated, all other coefficients being now constants. By using this procedure a 25% increase in speed, with 25% increase in accuracy has been found in preliminary simulations. Even so, we still need to process a very high data rate of sensor measurements, which is not easy to implement, especially in space structures, causing time delays in estimation.

Estimation Example

A simplified model of a beam expander was represented by a primary mirror mass elastically linked to a secondary mirror mass. Restoring forces and dissipative forces proportional to relative secondary mirror motion were modeled at the secondary. A piecewise constant angular acceleration was commanded, representing the acceleration-deceleration profile of a minimum time retargeting maneuver. Presumed angular accelerometer and gyro noise covariances were transformed into equivalent process noise for the feedback-linearized filter, with the additional simplification of neglecting a squared noise term corresponding to the second entry $u_2 = \omega^2$ of the equivalent input u. Presumed strain gauge sensor noises were taken from the literature. The relative performance of the extended Kalman filter and the feedback-linearized filter are seen by inspection of figures 3, 4 and 5.

OFF LINE MODELING

In this subsection we use the newly developed method of Bilinear System Optimal Interpolation. This technique applies to dynamical systems which behave in "normal" bilinear form, (by active suppression of the constant bias additive term b:

$$\dot{X} = AX + B(X)u$$

$$y = c^T X$$

which means also:
*The (I/O) behavior is highly nonlinear.
*The system is high dimensional if arising from Carleman linearization.
*There is no clean ARMA model for system identification.
Then, by using optimal interpolation we get:
*Closed form, circuit-implementable bilinear approximations.
*(I/O) based system identification.
*The dimension of the new system is equal to the number of test signals.

Now rather than tolerate the time delay found in the previous techniques of estimation, we use instead the method of operator spline interpolation to find the deflection amount between observations. The input output (I/O) operator V.

V: u→y

from the excitation vector u to an output vector y (such as u introduced before) is imbedded in a Hilbert space of (I/O) operators of candidate bilinear systems, equipped with a reproducing kernel:

$$K_t(u, v) = \exp \int_{t_o}^{t} u^T(s) R^{-1} v(s) ds$$

where the weight matrix R is determined by bounds on the structural frequencies. An interpolator of the form

$$V_t(u) = \sum_i c_i(t) K_t(u, u^i)$$

is constructed, tuned so that the structural responses to preselected test inputs u^i are recorded, and optimally interpolating at system level the responses to other excitations in the signal class. The optimization is formulated as a minimization of the maximum distance between the interpolating operator and any candidate operator that matches the experimental input-output signal pairs. If the system data are not accurate, a weighted minimization that does not require exact matching of system responses can also be used.

This minimization is carried out in a Hilbert space of input-output operators equipped with a weighted "Fock space" scalar product which is the Hilbert sum of the causal L^2 scalar products of the Volterra series of the operators in question. A different procedure to calculate the coefficients c_i must then be used. The general method is discussed in the papers of Dwyer (1986, 1986b) and de Figueiredo and Dwyer (1980).

The Hilbert space structure for m inputs (here m = 3) is defined as follows: let

$i_1, \ldots, i_n \in \{1, \ldots, m\}$ and let

$$h_{n, i_1, \ldots, i_n}^{(t, t_1, \ldots, t_n)} = c^T \exp\{(t - t_1)A\} B_{i_1} \ldots$$

$$\ldots \exp\{(t_{n-1} - t_n)A\}\, B_{i_n} \exp(t_n A)\} x(0)$$

where $B = [B_1 | B_2 | \ldots]$

These are the Volterra kernels for $u_{i_1}(t_1) \ldots u_{i_n}(t_n)$. Then

$$\langle V_t, V_t \rangle = \sum_n \sum_{i_1} \ldots \sum_{i_n} r_{i_1} \ldots r_{i_n} \int_o^t \int_o^{t_1} \ldots \int_o^{t_n}$$

$$h_{n, i_1, \ldots i_n} h_{n, i_1 \ldots i_n}\, dt_n \ldots dt_1$$

which yields the reproducing property

$$\langle V_t, K_t(u, .) \rangle = V_t(u)$$

The Volterra series for a bilinear system will yield a bounded norm $\langle V_t, V_t \rangle$ provided the weights r_j

page [illegible]

undeformed system center of mass.

f is the (2nx1)(say, 4x1 here) matrix of body coordinates of external forces acting on the centers of mass of the n appendages.

f_0 is the external force acting at the center of the body fixed coordinate system. All other notations used are appended.

We can easily notice that all three equations are interrelated. If we take now only the vibrational equation of motion, and set the rotation around a single axis, $\omega=\dot{\theta}k$, and if the translational acceleration term a_0 is substituted from the translational equation, then we have:

$$M\ddot{y}+(C+2\dot{\theta}JM)\dot{y}+(K+(\ddot{\theta}+J\dot{\theta}^2)JM)y+(\ddot{\theta}+\dot{\theta}^2J)Jn=f'+N(L^Tf+f^0)$$

where now $n = M_0 s$, M is redefined to account for contributions due to translation and every third row or column is omitted in all matrices. If we set v to be a new variable such that $v=My+n$, $\bar{C}=CM^{-1}$, $\bar{K}=KM^{-1}$ and $u'=(\omega,\omega^2,\dot{\omega})$, then the rotational equation of motion becomes:

$$\ddot{v}+(\bar{C}+u_3J)\dot{v}+(\bar{K}+u_1J+u_2J^2)v=f+\bar{K}n$$

This transformed equation can also be written in bilinear form, which will be used frequently in the following sections:

$$\dot{X}=AX+B(X)u+b$$

Where:

$$A=\begin{bmatrix} 0 & I \\ -\bar{K} & -\bar{C} \end{bmatrix}$$

$$B(X) = \begin{bmatrix} [0] & [0] \\ JX_1 & J^2X_1 \end{bmatrix} \quad [0] \quad JX_2$$

and

$$b = \begin{bmatrix} [0] \\ f'+Kn \end{bmatrix}$$

X_1 and X_2 are the vector components of the general state vector $X = (v', \dot{v}')'$.

This simplified model, insofar as the links are regarded as mass-less, exhibits all the coupling effects between slewing motion and vibrational motion. A distributed model under the assumption of symmetry about the mass center also yields product terms between $\dot{\theta}^2$ and structural deformations, and can be found in Chapter 9 of the book by Junkins and Turner (1986). That model of a symmetric four appendage spacecraft can also be used to illustrate the procedures being developed in this study, if desired.

ESTIMATION AND MODELING OF THE DEFORMATION STATE

Estimation of the State by Means of observers:

Extended Kalman filter formulation:

In general, when we deal with a nonlinear system of which the state variables cannot all be observed (corrupted with noise), then the most commonly used method of filtering or smoothing is the extended Kalman filter formulation. Let the dynamical system be modeled as:

$$\dot{x} = f(x) + G(x)u^* + G(x)\xi.$$

$$y = h(x + v).$$

where u^* is the deterministic (mean) part of the input, ξ is zero mean input noise, and h is defined in our case as:

$$h_1(\cdot) = M^{-1}(\cdot - n).$$

$$h_2(\cdot) = M^{-1}(\cdot).$$

let $R_i\delta(t-\tau) = E[v_i^T(t)v_i(\tau)]$ be the covariance matrix of the sensors for v_i and let $Q\delta(t-\tau) = E[\xi^T(t)\xi(\tau)]$ be the covariance matrix of the actuator. The propagation error matrix is defined by P, which satisfies the following differential equation:

$$\dot{P} = P\left[\frac{\partial f}{\partial x}\right]^T + \left[\frac{\partial f}{\partial x}\right]P + G(\hat{x})QG(\hat{x})^T - P\left[\frac{\partial h}{\partial x}\right]^T R^{-1}\left[\frac{\partial h}{\partial x}\right]P$$

and $\hat{x}$ can be expressed as observed,

$$\dot{\hat{x}} = f(\hat{x}) + G(\hat{x})u^* + K(y-h(\hat{x})).$$

$$y = h(x)$$

where K is the extended Kalman gain of the observer and is defined as:

$$K = P\left[\frac{\partial h}{\partial x}\right]^T R^{-1}$$

A newly developed procedure (Fadali, Gardner and Dwyer, 1986) based on a change of variables in preliminary studies gave us a better time of computation and therefore a more reliable set of observed data. This procedure is outlined next.

Feedback Linearized Procedure:

The idea is to change the state configuration of our original system which has the particular form below:

$$\dot{x}_1 = F_1(x_1)x_2$$

$$y_1 = h_1(x_1 + v_1)$$

$$y_2 = h_2(x_2 + v_2)$$

by using the change of

variables $x_1' = x_1$, $x_2' = F_1(x_1)x_2$,

$u' = \dot{x}_1 = F_2(x)u^* + f_2(x)$ and

$y_1' = h_1^{-1}(y_1)$, $y_2' = h_2^{-1}(y_2)$ we get

$$\dot{x}_1' = \dot{x}_2'$$

$$\dot{x}_2' = u'^* + \xi'$$

Where $\xi' = F_1F_2\xi$ and $v_i' = F_1v_i$, so that the covariance of ξ' is approximated by

$$Q' = F_1(\hat{x}_1)F_2(\hat{x})QF_2(\hat{x})^TF_1(\hat{x}_1)^T$$

while that for v_i' is approximated by

$$R_i' = F_1(\hat{x}_1)R_iF_1(\hat{x})^TF_1(\hat{x}_1)^T$$

Then the new error covariance matrix propagation is derived from the following differential equation:

$$\dot{P} = \begin{bmatrix} [0] & [I] \\ [0] & [0] \end{bmatrix} P + P \begin{bmatrix} [0] & [0] \\ [I] & [0] \end{bmatrix} + \begin{bmatrix} [0] \\ [I] \end{bmatrix} Q'\begin{bmatrix} [0] & [I] \end{bmatrix} -$$

$$P \begin{bmatrix} [I] \\ [0] \end{bmatrix} R'^{-1} \begin{bmatrix} [I] & [0] \end{bmatrix} P$$

the observed deformation state is propagated as follows:

A STUDY OF SLEW INDUCED DEFORMATION SHAPING

BY

JOHN RAYMOND HOYLE JR.

B.S. , University of Illinois, 1987

THESIS

Submitted in partial fullfillment of the requirements
for the degree of Master of Science in
Aeronautical and Astronautical Engineering
in the Graduate College of the
University of Illinois at Urbana-Champaign, 1988

Urbana, Illinois

ACKNOWLEDGEMENT

This work has been partly supported through Techno-Sciences, Inc. by SDIO under contract F49620-87-C-0103, and managed by AFOSR (AFSC).

ABSTRACT

Computed torques for pointing and tracking require compensation for slew-induced structural, forebody/aftbody, or optical train alignment deformations. Thus even if only line-of-sight variables are to be commanded yet full state feedback is needed, with consequent high bandwidth control requirements. The solution investigated here is to decouple the unwanted deformation state by feedforward of the line-of-sight slew dynamics into the deformation controlforces or moments, for an apparatus consisting of a mirror mounted on an optical bench, that is itself mounted on a rotating table. Adjustable elastic interfaces are used to model slew-induced deformations as angular differences between mirror mounting, optical bench and rate table. Low bandwidth control with fewer actuators than degrees of freedom is shown to be possible, by correcting the computed torques so as to force the interstage angular differences (standing for slew-induced deformations) to evolve in a "slow integral manifold wherein they are modeled as functions of the mirror pointing angle. Simultaneous mirror pointing and independent rate table pointing is also shown to be possible, which represents the situation of pointing an instrument elastically mounted on a maneuvering platform. Comparisons with PID and LQR methods are also made.

TAWD

TABLE OF CONTENTS

I. Introduction

Spacecraft flexible modes have often challenged automatic control system designers. For example, unmodelled antenna deformations caused Explorer to eventually tumble out of control. Often, the solution used for such problems was to make the structure sufficiently rigid and/or the control slow enough that the flexible modes would not be excited by the controls [Ref. 1]. However, this option may not be available in the future for some spacecraft, given the current interest in the use of larger, lightweight space structures with correspondingly lower natural frequencies. The presence of flexible modes that are excited by the controls thus poses a problem.

The solutions to this problem may be split into two classes. In the first class, there are controls available to be dedicated to each of the flexible modes. In the second, more likely case, some of the modes do not have a dedicated controller. This paper applies a method called deformation shaping to a particular problem of this latter case. This method was adapted by Dr. T. Dwyer, as an extension of singular perturbation techniques, such as by Kokotovic [Ref. 2], initially used in control of robots with flexible joints by Spong [Ref. 3]. The method modifies slew induced deformations to produce, in some sense, better dynamics.

A variety of options are available for the first class of solutions. If the flexible mode-pointing control interactions are ignored, a simple PID control of the modes may be attempted, but the results are often unsatisfactory. A somewhat more sophisticated solution is the use of a Linear Quadratic Regulator (LQR) design. Another

possible solution is to rigidify the structure with some application of the controls. After an initial transient, the structure will then be effectively rigid and have no flexible mode-pointing control interactions. This would be ideal, but the type and/or number of actuators rarely allow this control. This class of solutions will be used as a basis of comparison for solutions in the second class, for which all controllers are not available.

The second class of solutions is less well developed. The problem of noncolocated sensors and actuators greatly complicates matters. PID control does not work, and rigidifying control does not as well. It is possible to formulate an LQR problem, but there are some drawbacks to this. Many other solutions are currently proposed, but none are accepted by everyone yet. A solution for a problem in which all controllers are not available will be done using the method of deformation shaping. This will then be compared to control solutions for the same problem in which all controllers are available.

In addition, there are additional considerations particular to this problem. This problem arises from a laboratory model to test precision pointing control methods. Thus, several constraints and additions peculiar to this setup and use are imposed. These include desired performance, actuator and sensor dynamics, and equipment limitations.

The problem posed is first formulated and detailed. Next, the basic theory involved is discussed. The necessary equations are derived, and the control form is specified. Then the control is

designed. The effects of various control design choices are explored, as well as the response of the system to various inputs. Parameter sensitivity and noise effects are briefly discussed, and the control solution is compared to various other solution types. The results are summarized, as well as possible topics for future examination.

II. The Problem

2.1 Problem Formulation

It is desired to make the end of a flexible instrument follow a commanded trajectory as quickly and accurately as possible. The most likely real world counterpart is rapid retargeting slew command. Another possible mission is tracking, but this presents some difficulties. Two scenarios are examined. In the first scenario, only the instrument deformations are shaped or suppressed, and the vehicle trajectory can be commanded separately from the instrument trajectory. For the second scenario, the entire vehicle and instrument system has its deformations shaped by the control.

Controls for the first scenario are derived, applied, and their performance analyzed. This is then done for the second scenario. Both scenarios then have their performance compared to various other more common methods.

2.2 Laboratory Model

The laboratory model was configured to represent single axis dynamics of a multibody spacecraft. The system does not strictly resemble the dynamics of any spacecraft, but can be used to make a meaningful comparison between control methods.

The laboratory model consists of three main bodies as shown in figure 1. The pointing mirror represents the end of a flexible instrument. The optical bench represents the base of the flexible instrument. The rate table may be considered the rest of the vehicle,

such as propulsion package, or a connection to the rest of the spacecraft.

The rate table and the optical bench are isolated from one another by an air bearing, with springs mounted between them to provide an elastic link. Physical considerations limit the total angle difference between the rate table and the optical bench to about five degrees. Two Kimco linear actuators mounted between the two bodies act as a torque actuator. Another actuator, available for control and/or disturbance injection, is the rate table itself.

The optical bench and pointing mirror are also elastically linked through springs, and an Aerotek DC motor connects the two bodies, providing another actuator.

The model's springs were chosen to give the vehicle "typical" *spacecraft natural frequencies.*[Ref. 4] A low frequency mode at .4 Hz simulates very flexible components such as solar panels. Another mode at 1.5 Hz represents some other structural flexibility.

The laboratory model thus imposes several constraints which are not present in the real system, but must be satisfied in the lab. The most important effects come from the angular difference constraints and necessary component simplification.

2.3 The Mathematical Model

The mathematical model is an idealization of the laboratory model, and thus only approximates the laboratory mode. It is depicted in figure 2. The sensors are assumed to be perfect, and the actuators are assumed to follow standard dynamics with certain

parameters, as detailed below. Each body is assumed to be rigid, connected by elastic links. The links are assumed linear, and time degradation of any component is not considered.

The actuators have several constraints imposed on them as shown in figure 3. There are physical limitations in maximum torque available,

Figure 1

Laboratory Model

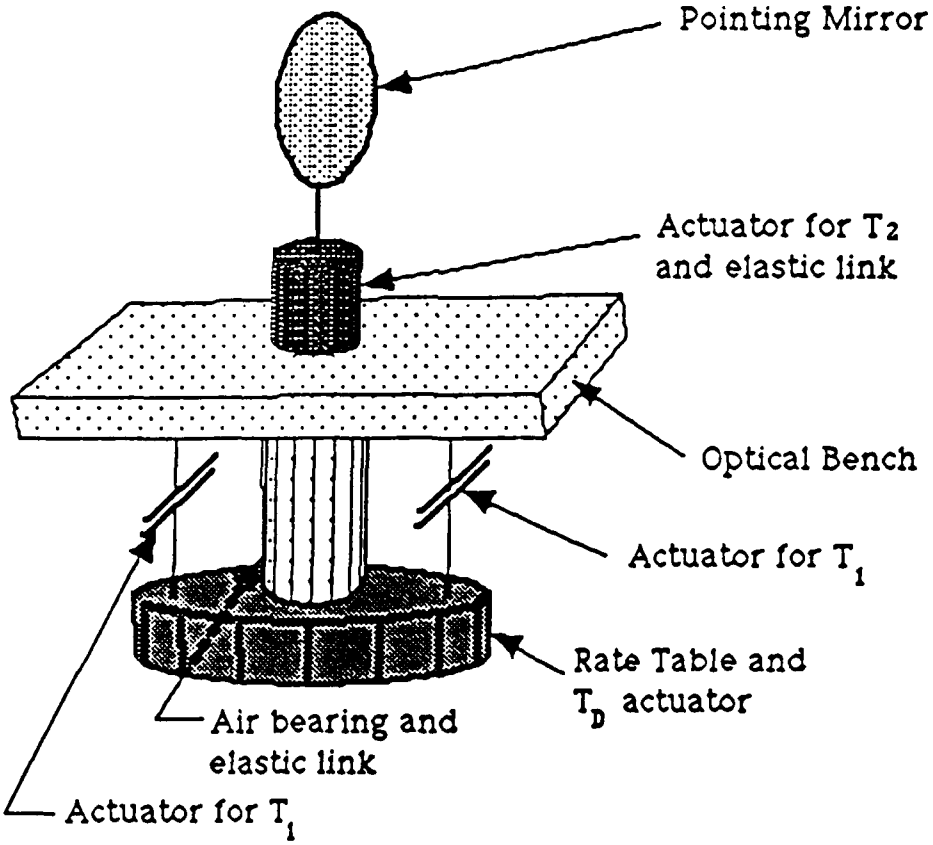

Figure 2

Mathematical Model

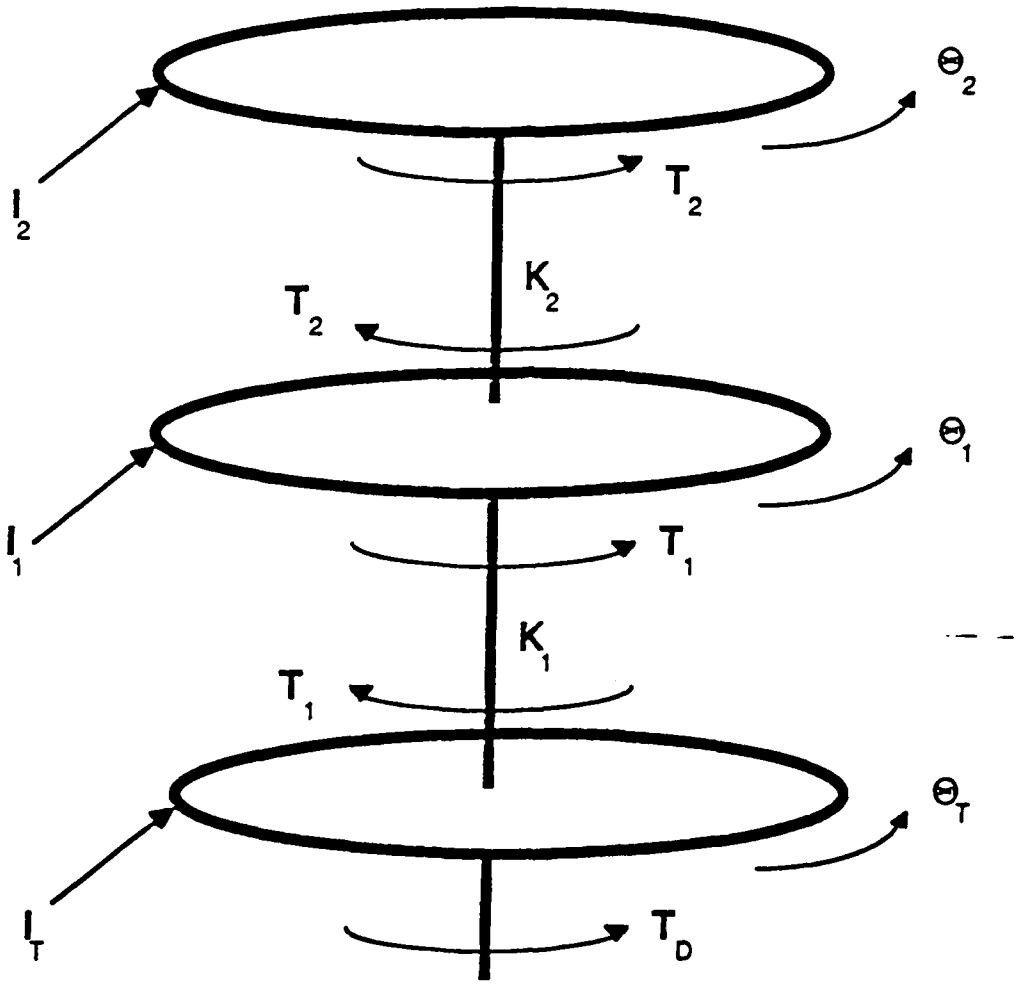

Figure 3

Actuator Constraints

Category	T_D		T_1		T_2	
	Problem Constraint	Physical Constraint	Problem Constraint	Physical Constraint	Problem Constraint	Physical Constraint
Bandwidth	1.5 Hz	38 Hz	30 Hz	48 Hz	8.5 Hz	32 Hz
Maximum Torque	none	27 Nm	none	10.85 Nm	0 Nm	3.26 Nm
Stroke	none	none	none	5 degrees	none	45 degrees

bandwidth, and stroke. The problem constraints on maximum torque and bandwidth are more stringent than the physical limitations, so the physical limitations have little effect. The stroke, however, is a major physical constraint, and is the most significant laboratory model constraint. The motor between the pointing mirror and optical bench has a range of forty-five degrees. Since the maneuvers simulated will be less than or equal to twenty degrees, this constraint has little effect as long as there is little overshoot. Due to the linear, instead of rotational, nature of the Kimco actuators providing T_1, there is a maximum permitted angular difference of about five degrees between the rate table and optical bench. This greatly limits the allowable controls.

The control torques are assumed to be produced by standard PM DC motors, in linear or rotational form. These motors also have controllers so that they produce constant torque output for a constant input signal. Otherwise, the steady state output would be constant rotational or linear speed, and zero torque. The resulting transfer functions for the compensated actuators are

$$\frac{T_{D_{ACTUAL}}(s)}{T_{D_{COMMANDED}}(s)} = \frac{100\pi^2}{s^2+20\pi s+100\pi^2} \qquad [1]$$

$$\frac{T_{1\,ACTUAL}(s)}{T_{1\,COMMANDED}(s)} = \frac{29576}{s^2+219.3s+29576} \qquad [2]$$

$$\frac{T_{2\,ACTUAL}(s)}{T_{2\,COMMANDED}(s)} = \frac{7000}{s^2+166.67s+5991.4} \qquad [3]$$

The details of how these were obtained are in Appendix A. These actuators have only been compensated to produce a constant output torque given a constant input. This compensation does not implement any control scheme on the model.

2.4 Equations of Motion

The equations of motion of this system are

$$I_2\ddot{\theta}_2 + k_2(\theta_2-\theta_1) = T_2 \qquad [4]$$

$$I_1\ddot{\theta}_1 + k_2(\theta_1-\theta_2) + k_1(\theta_1-\theta_T) = T_1 - T_2 \qquad [5]$$

$$I_T\ddot{\theta}_T + k_1(\theta_T-\theta_1) = T_D - T_1 \qquad [6]$$

where

θ_T = angle of rate table with respect to fixed point

θ_1 = angle of optical bench with respect to fixed point

θ_2 = angle of pointing mirror with respect to fixed point

I_T = moment of inertia of rate table about vertical axis= .417 Nmsec^2

I_1=moment of inertia of optical bench about vertical axis

= 1.627 Nmsec^2

I_2= moment of inertia of pointing mirror about vertical axis

= .863 Nmsec^2

k_1 = spring constant for link between rate table and optical bench= 2.27 Nm/rad

k_2 = spring constant for link between optical bench and pointing mirror= 49.8 Nm/rad

T_D = disturbance torque due vehicle maneuvering torque

T_1 = control torque 1

T_2 = control torque 2

These equations can be expressed in matrix form too, but that is used only for Scenario B (below).

The system, actuators, and controllers are connected as in the matrix block diagram shown in figure 4.

Figure 4

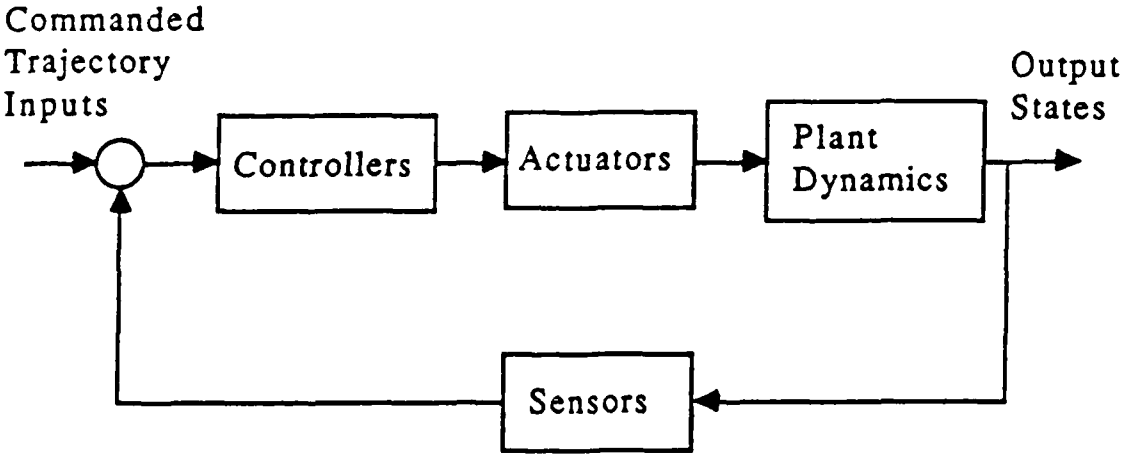

III. Theory

3.1 Introduction to Theory

The equations of motion can be transformed into the singular perturbation equations of motion. They are called this because some of the variables represent parasitic perturbations of the pointing dynamics. There are different possible sets of these singular perturbation variables. However, there are two best choices.for this problem, depending on what dynamics or responses are desired and what controls are available. Two scenarios (i.e. choices of perturbation variables) are considered. The first one consists of the case where only the instrument (i.e. between the mirror and optical bench) deformation is considered a perturbation variable. The second scenario is the case when both instrument and vehicle mounting (i.e. between the optical bench and rate table) deformations are considered perturbation variables. The first scenario allows the instrument to slew and point in a given manner while the vehicle may be moving in some other manner. The second scenario can be interpreted as making the instrument slew and point when the vehicle orientation does not matter.

3.2 Scenario A Perturbation Equations of Motion

This scenario is simpler algebraically since there is only one perturbation variable. It is considered first since the derivation is easier to follow and less cumbersome.

For the first scenario the deformation variable choice used is

$$z = k_2(\theta_1 - \theta_2) \qquad [7]$$

with the definitions:

$$\phi = (\theta_2 - \theta_T) \qquad [8]$$

$$\varepsilon = 1/k_2 \qquad [9]$$

The singular perturbation equations of motion are then

$$I_2\ddot{\theta}_2 - z = T_2 \qquad [10]$$

$$\varepsilon\ddot{z} + \left(\frac{1}{I_1} + \frac{1}{I_2}\right)z + \varepsilon\frac{k_1}{I_1}z + \frac{k_1}{I_1}\phi = \frac{T_1}{I_1} - \left(\frac{1}{I_1} + \frac{1}{I_2}\right)T_2 \qquad [11]$$

$$I_T\ddot{\Theta}_T = T_D - T_1 + k_1\phi + \varepsilon k_1 z \qquad [12]$$

The variable z is proportional to the deformation between top and bottom of the instrument and the variable ϕ is the coupling term between the instrument dynamics [10],[11] and the vehicle dynamics [12].

3.3 The Integral Manifold

The integral manifold approach and its applications are more rigorously discussed in [Ref 5,6]. This is a brief overview of useful ideas.

The integral (or slow) manifold is a certain lower dimensional manifold of the system dynamics which relates the system states and depends upon the controls and the singular perturbation. For some appropriate choice of controls, if the manifold is reached then the

system will remain on the manifold. The appropriate controls can be found by solving a PDE for the manifold.

The perturbation variable can be thought of as the sum of two terms; a term on the manifold, and a fast remainder term.

$$z = z_{IM} + z_f \qquad [13]$$

The faster the remainder term decays to zero the better, since then the integral manifold determines the dynamics. In general, the fast term often decays due to damping in the system. However, for this problem the damping must be added. This is done by a fast control that is detailed below.

3.4 Time Scale Separation

In this problem two different processes are occurring. First, the dynamics are quickly decaying to the integral manifold dynamics. Meanwhile, the manifold dynamics are "slowly" reaching the desired dynamics, as explained below. This leads to a separation of variables based on their time scale. In the fast time scale, the "slow" variables are changing so slowly that they are approximately constant and have little noticeable effect if the "fast" dynamics are fast enough. At most, the fast dynamics will see a constant disturbance. Looking at the slow time scale, if the "fast" variables decay fast enough, the most effect they have on the "slow" variables is a short, transient disturbance input. When considering the variables in the two time scales to be essentially independent, equation [13] can be used to rewrite [10], [11], and [12] as

$$\varepsilon[\ddot{z}_f + \left(\frac{k_1}{I_1} + \left(\frac{1}{I_1} + \frac{1}{I_2}\right)\frac{1}{\varepsilon}\right)z_f] = \Delta + \frac{T_{1_{fast}}}{I_1} \qquad [14]$$

$$I_2\ddot{\theta} - z_{IM} = T_{2_{slow}}\ (+z_f) \qquad [15]$$

$$\varepsilon\ddot{z}_{IM} + \left(\frac{\varepsilon k_1 + 1}{I_1} + \frac{1}{I_2}\right)z_{IM} + k_1\phi = \frac{T_{1_{slow}}}{I_1} - \left(\frac{1}{I_1} + \frac{1}{I_2}\right)T_{2_{slow}} \qquad [16]$$

$$\ddot{\theta}_T - \frac{k_1\phi}{I_T} - \frac{\varepsilon k_1}{I_T}z_{IM} = \frac{T_D}{T_T} - \frac{T_{1_{slow}}}{I_T} + \frac{\varepsilon k_1 z_f}{I_T} \qquad [17]$$

where Δ = a small disturbance input, $T_D = T_{Dslow}$, $T_2 = T_{2slow}$, and

$$T_1 = T_{1slow} + T_{1fast} \qquad [18]$$

since T_1 is assumed to be the only control with high enough bandwidth to have a fast control term. The z_f terms in [15] and [17] are transient disturbance terms which affect the slow dynamics and their impact must be minimized by the slow control. In addition, [14] gives the dynamics of the fast variable. This equation is used to design the fast control T_{1fast} to drive z_f to zero as quickly as possible.

3.5 Fast Control

It is desirable to use feedback to generate a T_{1fast} to drive z_f to zero. There is a choice, however, of whether to feed back only the fast part of z (z_f) or all of z. Since a high pass filter would probably be needed to measure only z_f, all of z will be used as feedback. Therefore, fast and slow terms will arise from this feedback. Only

the fast terms will affect the fast dynamics, as discussed above. The slow terms will affect the slow or manifold dynamics. This control is called the fast control even though it affects the slow dynamics, because it is the only control that is used for control of the fast dynamics. The sensor dynamics of this feedback are neglected.

There are many possible choices for the control form but a proportional-derivative (PD) feedback controller will be used because it is the simplest that can do what is required. The control is of the form

$$T_1 = \tilde{T}_1 - \varepsilon(a_1\dot{z} + a_0 z) \qquad [19]$$

so that

$$T_{1_{fast}} = -\varepsilon(a_1\dot{z}_f + a_0 z_f) \qquad [20]$$

$$T_{1_{slow}} = \tilde{T}_1 - \varepsilon(a_1\dot{z}_{IM} + a_0 z_{IM}) \qquad [21]$$

where T_1 tilda is used for slow control. Then using [20] the compensated fast dynamics are

$$\varepsilon\left[\ddot{z}_f + \frac{a_1\dot{z}_f}{I_1} + \left(\frac{a_0 + k_1}{I_1} + \frac{1}{\varepsilon}\left(\frac{1}{I_1} + \frac{1}{I_2}\right)\right) z_f\right] = \Delta \qquad [22]$$

where Δ is a small disturbance input

The gains a_1 and a_0 may now be chosen for the desired fast dynamics. For example, the fast controller is chosen to make the z_f dynamics behave as a system with damping ratio z= .7071 and damped natural frequency σ as below, where $u_f = \Delta/\varepsilon$.

$$\ddot{z}_f + 2\sigma\dot{z}_f + 2\sigma^2 z_f = u_f \qquad [23]$$

This occurs when the gains are chosen as

$$a_1 = 2\sigma I_1 \qquad [24]$$

$$a_0 = 2\sigma^2 I_1 - k_1 - \left(\frac{I_1 + I_2}{I_2}\right) k_2 \qquad [25]$$

Since ε is small, u_f is possibly a significant disturbance input. Thus, for nonzero Δ there may be a significant steady state error in z_f for some situations using the PD control. This error did not destroy the performance or stability of the control, but its effect, if any, is not analyzed in this paper.

3.6 Singular Perturbation Expansion

The equations describing the slow dynamics, including the slow feedback component of the fast control but neglecting the fast transient disturbances are

$$I_2\ddot{\theta}_2 - z_{IM} = T_2 \qquad [26]$$

$$\varepsilon\ddot{z}_{IM} + \frac{\varepsilon}{I_1} a_1 \dot{z}_{IM} + \left(\frac{\varepsilon k_1 + 1}{I_1} + \frac{1}{I_2} + \frac{a_0\varepsilon}{I_1}\right) z_{IM} + \frac{k_1\phi}{I_1} = \frac{\tilde{T}_1}{I_1} - \left(\frac{1}{I_1} + \frac{1}{I_2}\right) T_2 \qquad [27]$$

The vehicle dynamics are

$$\ddot{\theta}_T - \frac{k_1\phi}{I_T} - \left(\frac{\varepsilon a_1}{I_1}\right)\dot{z} - \frac{\varepsilon(a_0 + k_1)}{I_1} z = \frac{T_D}{I_T} - \frac{\tilde{T}_1}{I_T}$$

[28]

To solve [26] and [27], z_{IM} must be found.

One method of solving for z_{IM} involves expanding z_{IM}, T_1, and T_2 *in power series of* ε.

$$z_{IM} = z_0 + \varepsilon z_1 + \varepsilon^2 z_2 + \ldots \qquad [29]$$

$$\tilde{T}_1 = \tilde{T}_{10} + \varepsilon\tilde{T}_{11} + \varepsilon^2\tilde{T}_{12} + \ldots \qquad [30]$$

$$T_2 = T_{20} + \varepsilon T_{21} + \varepsilon^2 T_{22} + \ldots \qquad [31]$$

Substituting these into [26] and [27], and equating terms of equal power in ε results in:

$$\text{For } \varepsilon^0\text{: } I_2\ddot{\theta}_2 - z_0 = T_{20} \qquad [32]$$

$$\left(\frac{1}{I_1} + \frac{1}{I_2}\right)z_0 + \frac{k_1\phi}{I_1} = \frac{\tilde{T}_{10}}{I_1} - \left(\frac{1}{I_1} + \frac{1}{I_2}\right)T_{20} \qquad [33]$$

$$\text{For } \varepsilon^1\text{: } z_1 = T_{21} \qquad [34]$$

$$\ddot{z}_0 + \frac{a_1}{I_1}\dot{z}_0 + \left(\frac{a_0}{I_1} + \frac{k_1}{I_1}\right)z_0 + \left(\frac{1}{I_1} + \frac{1}{I_2}\right)z_1 = \frac{\tilde{T}_{11}}{I_1} - \left(\frac{1}{I_1} + \frac{1}{I_2}\right)T_{21} \qquad [35]$$

For ε^2: $z_2 = T_{22}$ [36]

$$\ddot{z}_1 + \frac{a_1}{I_1}\dot{z}_1 + \left(\frac{a_0}{I_1} + \frac{k_1}{I_1}\right)z_1 + \left(\frac{1}{I_1} + \frac{1}{I_2}\right)z_2 = \frac{\tilde{T}_{12}}{I_1} - \left(\frac{1}{I_1} + \frac{1}{I_2}\right)T_{22} \quad [37]$$

etc.

For the vehicle dynamics, no singular perturbation expansions are used, since the effect of vehicle motion is regarded only as an exogenous input to the instrument slow dynamics. These equations can be used to determine the desired instrument slow controls, then the vehicle controls.

A Rigidifying or Deformation Suppression control can be found for the instrument if T_2 is not equal to zero. This rigidifying control must drive the instrument deformation (z_{IM}) in a short time to zero and keep it so. This means that the manifold desired is $z_{IM}=z_0 + \varepsilon z_1 + \ldots =0$. After decay of the fast dynamics, this manifold will be reached and the instrument will act as if it were rigid.

An obvious solution to this is $z_0=z_1= \ldots =0$, which forces setting $T_{1i}=T_{2i}=0$ for i=1,2,3,... ;indeed, for this solution, [32] thru [35] become:

For ε^0: $I_2\ddot{\theta}_2 = T_{20}$ [38]

$$0 = \left(\frac{1}{I_1} + \frac{1}{I_2}\right)T_{20} - \frac{1}{I_1}\tilde{T}_{10} + \frac{k_1}{I_1}\phi \quad [39]$$

For ε^1: $0 = T_{21}$ [40]

$$0 = \left(\frac{1}{I_1} + \frac{1}{I_2}\right) T_{21} - \frac{\tilde{T}_{11}}{I_1} \qquad [41]$$

etc.

From these equations, one can design controllers using any means for desired performance, robustness, etc.. This is done in Appendix C. However, deformation suppression can be done only when there are as many controls as modes: all three (T_D, T_1, T_2) controls must be used.

For a Deformation Shaping control, it is not desired to drive the deformations to zero, but rather to shape and use them. For example, if T_2 is not available to directly affect the instrument deformations, the deformations (z) can be shaped to be expressible in terms of the pointing dynamics Θ_2 and achieve the desired response. Since deformations are needed to exist after the fast dynamics have decayed, z_{IM} is not equal to zero. However, by examining the equations [32-37], one notices that with z_i=0 and $T_{1,(i+1)}$=0 (for i>=1), a solution can be found for z_0, T_{10}, T_{11}. The equations are then

$$I_2 \ddot{\Theta}_2 = z_0 \qquad [42]$$

$$\left(\frac{1}{I_1} + \frac{1}{I_2}\right) z_0 + \frac{k_1}{I_1} \phi = \frac{\tilde{T}_{10}}{I_1} \qquad [43]$$

$$\ddot{z}_0 + \frac{a_1}{I_1}\dot{z}_0 + \left(\frac{a_0+k_1}{I_1}\right)z_0 = \frac{\tilde{T}_{11}}{I_1} \qquad [44]$$

3.7 Slow Control Design

Using [24],[25],[30],[42].[43], and [44] we can write (in the frequency domain)

$$\tilde{T}_1(s) = G_1^{-1}(s)\Theta_2(s)+k_1\phi(s) \qquad [45]$$

where

$$G_1(s) = \frac{k_2}{I_1 I_2}\left(\frac{1}{s^2\left(s^2+ 2\sigma s + 2\sigma^2\right)}\right) \qquad [46]$$

To exactly model and control the dynamics, up to fourth derivatives (jerk rate) of Θ_2 would be needed. Since these are unlikely to be available as feedback, a form can be found only requiring higher derivatives of a commanded trajectory. This is done by using the model

$$\tilde{T}_1(s) = G_1^{-1}(s)\Theta_2^{*}(s) + k_1\phi(s) + H_1(s)\left(\Theta_2^{*}(s)-\Theta_2(s)\right) \qquad [47]$$

where $H_1(s)$ is a controller designed below to make Θ_2 follow its commanded trajectory. This model uses commanded feed foward of $G_1^{-1}(s)\Theta_2^{*}(s)$ and the decoupling term $k_1\phi$.

In a fashion similar to that for $T_I(s)$, $T_D(s)$ can be expressed as

$$T_D(s) = I_T s^2 \Theta_T(s) - \left(\frac{I_2}{k_2}\left(a_1 s^3 + (a_0+k_1)s^2\right) - G_1^{-1}(s)\right)\Theta_2^*(s)$$
$$- \left(\frac{I_2}{k_2}(a_1 s + a_0 + k_1)\, s^2 G_1(s) - 1\right) H_1(s)\left(\Theta_2^*(s) - \Theta_2(s)\right)$$
$$+ H_D(s)\left(\Theta_T^*(s) - \Theta_T(s)\right) \qquad [48]$$

where $H_D(s)$ is a controller designed below to make Θ_T follow its commanded trajectory. One major difference between the dynamic models is that the model [47] was free to be chosen, but once this model was picked and the control designed using [47], the model [48] for T_D was completely specified except for $H_D(s)$.

The slow controllers may be designed various ways. The use of classical SISO (single input single output) design can now be done with our new system if care is taken. This will be done for illustrative purposes, but undoubtedly a better control design could be found.

It is desired to have the slow control drive the actual trajectory to the commanded trajectory. The slow control is designed to drive this error to zero. This is not to be confused with the fast control driving the off-manifold dynamics to zero. The deformation dynamics (not error dynamics) resulting from the design of the slow control are the slow manifold.

The model [47] results in the transfer function form given in figure 5.

Figure 5

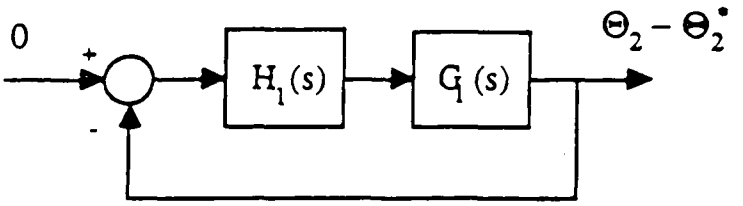

Now a simple regulator design is done to find $H_1(s)$. It was found that the simplest form able to stabilize the system was

$$H_1(s) = \frac{I_1 I_2 K(s^2 + m_1 s + m_0)}{k_2(s+b)} \qquad [49]$$

Once this form was chosen, the parameters were then selected. The final design chosen consisted of $b=m_1=\sigma$, $m_0=\sigma^2/4$. This corresponds to a controller with two zeros at $-\sigma/2$ and a pole at $-\sigma$. K was chosen from the root locus (see figure 6) for good closed loop pole locations. The choices used for K are detailed in Table 2. These situations in Table 2 will be explained in greater detail below. In addition, the effect of K on the time scale separation will also be discussed below.

The design of $H_D(s)$ was done in a similar manner. The same block diagram as figure 5 is used, except the plant was $G_D(s)=I_T(s)/s^2$ and the controller $H_D(s)$ was found to be:

$$H_D(s) = 2I_T c_D\left(s + \frac{c_D}{2}\right) \qquad [50]$$

Figure 6

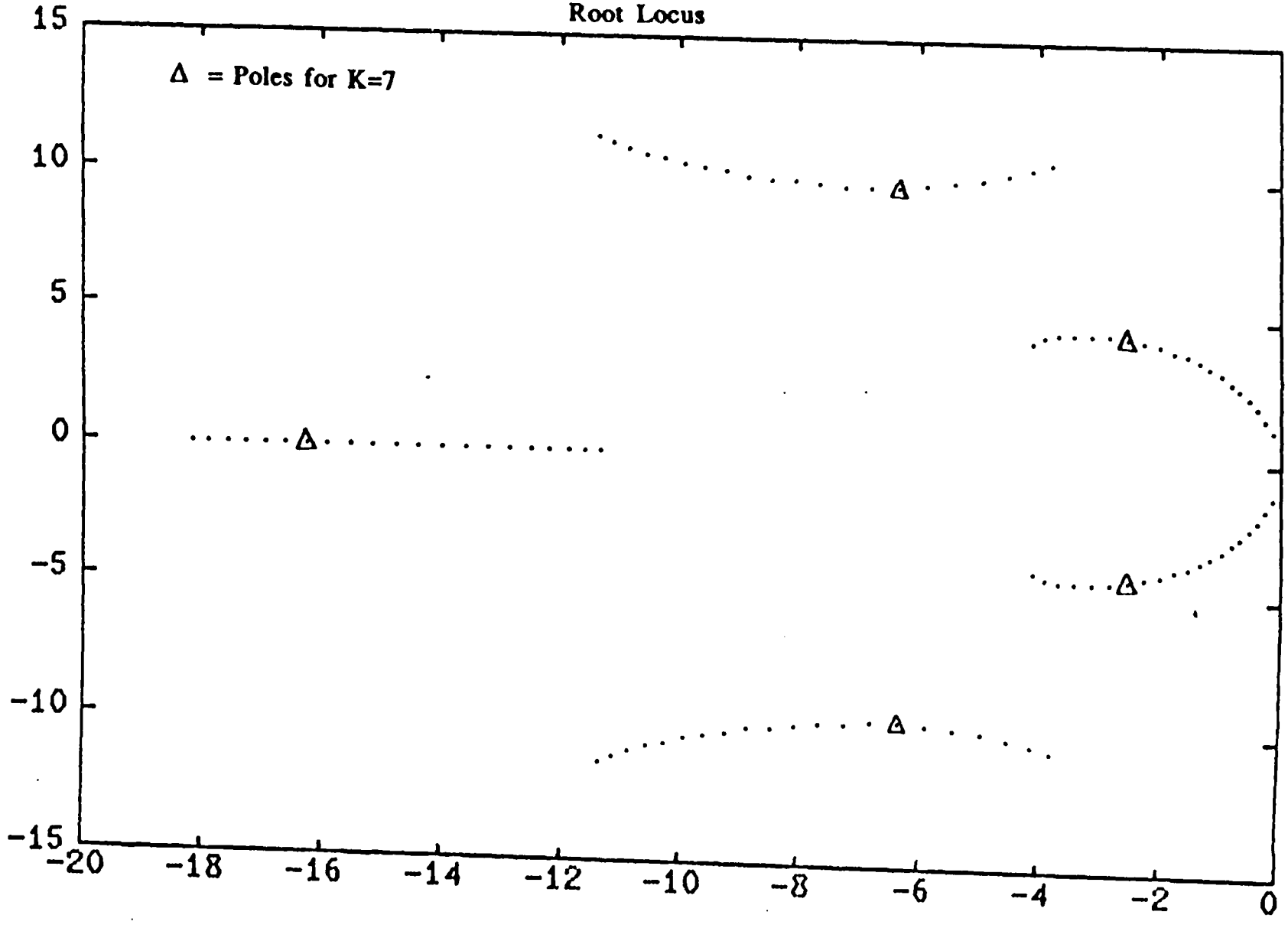

Table 2

Choices used for K

Situation	Choice for K
Low BW	50
High BW	1429
Low BW, larger separation	29
High BW, larger separation	715

The parameter c_D was found to give acceptable performance when it equaled about .28 σ, and good performance when it equaled about σ. Undoubtedly, a better controller could be found, but this one sufficed.

After the control design is done, the resulting controls are:

$$T_1 = a_1\left(\dot{\Theta}_2-\dot{\Theta}_1\right) + a_0\left(\Theta_2-\Theta_1\right) + \frac{I_1 I_2\, d^2}{k_2\, dt^2}\left(\dddot{\Theta}_2^{\bullet} + 2\sigma\ddot{\Theta}_2^{\bullet} + 2\sigma^2\dot{\Theta}_2^{\bullet}\right) + \frac{I_1 I_2 K}{k_2}\left(\ddot{\Theta}_2^{\bullet} - \dot{\Theta}_2 + (m_1-b)\left(\dot{\Theta}_2^{\bullet}-\Theta_2\right) + y_1\right) + k_1\phi \qquad [51]$$

$$T_D = \frac{I_1 I_2}{k_2}\left(\dddot{\Theta}_T^{\bullet} + 2c_D\left(\ddot{\Theta}_T^{\bullet} - \ddot{\Theta}_T\right) + 2c_D{}^2\left(\dot{\Theta}_T^{\bullet} - \dot{\Theta}_T\right)\right) - \frac{I_2\, d}{k_2 dt}\left(a_1\ddot{\Theta}_2^{\bullet} + (k_1+a_0)\,\dot{\Theta}_2^{\bullet}\right) - \frac{I_1 I_2 K}{k_2}\left(\ddot{\Theta}_2^{\bullet} - \dot{\Theta}_2 + c_0\left(\dot{\Theta}_2^{\bullet} - \Theta_2\right) + y_1\right) - \frac{K I_2}{k_2}\left(a_1\left(\dot{\Theta}_2^{\bullet}-\Theta_2\right) + y_2 + y_3\right) \qquad [52]$$

where y_1, y_2, and y_3 are found from

$$\dot{y}_1 = -by_1 + c_1\left(\Theta_2^{\bullet} - \Theta_2\right) \qquad [53]$$

$$\dot{y}_2 = -by_2 + c_2\left(\Theta_2^{\bullet} - \Theta_2\right) \qquad [54]$$

$$\ddot{y}_3 = -2\sigma\dot{y}_3 - 2\sigma^2 y_3 + c_3\left(\dot{\Theta}_2^{\bullet} - \dot{\Theta}_2\right) + c_4\left(\Theta_2^{\bullet} - \Theta_2\right) \qquad [55]$$

and c_0, c_1, c_2, c_3, and c_4 are detailed in Appendix B.

3.8 Scenario B Derivation

The derivation for the scenario in which the deformations of the entire system are shaped is very similar to the derivation for the previous scenario. In this case, however, there are two perturbation variables defined(A perturbation vector).

$$z = \begin{pmatrix} z_1 \\ z_2 \end{pmatrix} = \begin{pmatrix} k_1(\theta_1 - \theta_T) \\ k_2(\theta_2 - \theta_1) \end{pmatrix} \qquad [56]$$

The resulting singular perturbation equations of motion are

$$I_2\ddot{\theta}_2 + z_2 = T_2 \qquad [57]$$

$$\varepsilon I_T \ddot{z}_1 + \left(\frac{I_1 + I_T}{I_1}\right) z_1 - \frac{I_T}{I_1} z_2 = k_1\left(\frac{I_1 + I_T}{I_1}\right) T_1 - \frac{I_T}{I_1} T_2 - T_D \quad [58]$$

$$\varepsilon\delta I_2 \ddot{z}_2 - \frac{I_2}{I_1} z_1 + \left(\frac{I_1 + I_2}{I_1}\right) z_2 = -\frac{I_2}{I_1} T_1 + \left(\frac{I_1 + I_2}{I_1}\right) T_2 \quad [59]$$

where $\delta = k_1/k_2$ and $\varepsilon = 1/k_1$ with $k_1 < k_2$. Using the fast control

$$T_{1_{fast}} = -[k_1 a_{01}\ k_2 a_{02}]\begin{bmatrix} (\theta_1 - \theta_T) \\ (\theta_2 - \theta_1) \end{bmatrix} - [a_{11}\ a_{12}]\begin{bmatrix} (\dot{\theta}_1 - \dot{\theta}_T) \\ (\dot{\theta}_2 - \dot{\theta}_1) \end{bmatrix} \quad [60]$$

results in the fast dynamics having four poles at -w. If a_{01}, a_{02}, a_{11}, and a_{12} are chosen as follows:

$$a_{01} = \frac{w^4 I_1 I_2 I_T}{k_1 k_2 (I_1 + I_2 + I_T)} - 1 \quad [61]$$

$$a_{11} = \frac{4 w^3 I_1 I_2 I_T}{k_2 (I_1 + I_2 + I_T)} \quad [62]$$

$$a_{02} = 1 + \frac{I_1}{I_2} - \frac{6 w^2}{k_2} I_1 + \frac{w^4 I_1 I_2 (I_1 + I_T)}{k_2^2 (I_1 + I_2 + I_T)} \quad [63]$$

$$a_{12} = \frac{4 w^3 I_1 I_2 (I_1 + I_T)}{k_2 (I_1 + I_2 + I_T)} - 2 w I_1 \quad [64]$$

The resulting slow dynamics are again used to solve for the slow manifold through singular perturbation expansions. The expansions used are

$$\underline{z}_{IM} = \underline{z}_0 + \varepsilon \underline{z}_1 + \varepsilon^2 \underline{z}_2 + \ldots \quad [65]$$

$$\tilde{T}_1 = T_{10} + \varepsilon T_{11} + \varepsilon^2 T_{12} + \ldots \quad [66]$$

$$T_2 = T_{20} + \varepsilon T_{21} + \varepsilon^2 T_{22} + \ldots \quad [67]$$

$$T_D = T_{D0} + \varepsilon T_{D1} + \varepsilon^2 T_{D2} + \ldots \quad [68]$$

Substituting these into the slow dynamics equations and equating equal powers in ε results in the equations

$$I_2 \ddot{\theta}_2 + [0\ 1]\underline{z}_0 = T_{20} \quad [69]$$

$$\frac{1}{I_1}\begin{bmatrix} (I_1+I_T)(1+a_{01}) & (I_1+I_T)a_{02}-I_T \\ -I_2(1+a_{01}) & I_1+I_2(1-a_{02}) \end{bmatrix} \underline{z}_0 = \frac{1}{I_1}\begin{pmatrix} I_1+I_T \\ -I_2 \end{pmatrix} T_{10} + \frac{1}{I_1}\begin{pmatrix} -I_T \\ I_1+I_2 \end{pmatrix} T_{20} - \begin{pmatrix} 1 \\ 0 \end{pmatrix} T_{D0} \quad [70]$$

$$[0\ 1]\underline{z}_1 = T_{21} \quad [71]$$

$$\begin{bmatrix} I_T & 0 \\ 0 & \delta I_2 \end{bmatrix}\ddot{z}_0 + \begin{bmatrix} (I_1+I_T)a_{11} & (I_1+I_T)\delta a_{12} \\ -I_2 a_{11} & -I_2\delta a_{12} \end{bmatrix}\dot{z}_0 + \frac{1}{I_1}\begin{bmatrix} (I_1+I_T)(1+a_{01}) & (I_1+I_2)a_{02} - I_T \\ -I_2(1+a_{01}) & I_1+I_2(1-a_{02}) \end{bmatrix} z_1 = \frac{1}{I_1}\begin{bmatrix} I_1+I_T \\ -I_2 \end{bmatrix} T_{11} + \frac{1}{I_1}\begin{bmatrix} -I_T \\ I_1+I_2 \end{bmatrix} T_{21} - \begin{bmatrix} 1 \\ 0 \end{bmatrix} T_{D1} \quad [72]$$

If T_D, T_1, and T_2 were all available, a rigidifying control could be found using a process identical that was used for the previous scenario. However, only the deformation shaping case for $T_2=0$ will be examined for this scenario. With $T_2=0$ a solution can be found is before with $z_i=T_{D,(i+1)}=T_{i,(i+1)}=0$ for $i>=1$. The resulting equations can be written as

$$-[0\ 1]z_0 = I_2\ddot{\theta}_2 \quad [73]$$

$$\frac{1}{I_1}\begin{bmatrix} (I_1+I_T)(1+a_{01}) & (I_1+I_T)a_{02}-I_T \\ -I_2(1+a_{01}) & I_1+I_2(1-a_{02}) \end{bmatrix} z_0 = \frac{1}{I_1}\begin{pmatrix} I_1+I_T \\ -I_2 \end{pmatrix} T_{10} - \begin{pmatrix} 1 \\ 0 \end{pmatrix} T_{D0} \quad [74]$$

$$\begin{bmatrix} I_T & 0 \\ 0 & \delta I_2 \end{bmatrix}\ddot{z}_0 + \begin{bmatrix} (I_1+I_T)a_{11} & (I_1+I_T)\delta a_{12} \\ -I_2 a_{11} & -I_2\delta a_{12} \end{bmatrix}\dot{z}_0 = \frac{1}{I_1}\begin{bmatrix} I_1+I_T \\ -I_2 \end{bmatrix} T_{11} - \begin{bmatrix} 1 \\ 0 \end{bmatrix} T_{D1} \quad [75]$$

3.9 Scenario B Slow Control Design

Proceeding as in Scenario A, [74] is used to substitute in for z_0 into [73] and [75]. Choosing $T_{10}=0$ (otherwise free) , [75] can be solved to find T_{11}, T_{D0}, and T_{D1}. The resulting slow dynamics are:

$$G_D(s)\Theta_2(s) = T_D \qquad [76]$$

$$G_1(s)\Theta_2(s) = \tilde{T}_1 \qquad [77]$$

For the fast control gains used in [61] - [64], the expressions for $G_D(s)$ and $G_1(s)$ are:

$$G_D(s) = \frac{1}{(I_1 + I_2 + I_T)\left(\frac{6}{w^2}s^2 + 1\right)s^2} \qquad [78]$$

$$G_1(s) = \frac{1}{I_1 I_2 (s - 20w)s^3} \qquad [79]$$

Again, a control is sought of the form:

$$T_D(s) = G_D^{-1}(s)\Theta_2^* + H_D(s)\left(\Theta_2^* - \Theta_2\right) \qquad [80]$$

Unlike Scenario A, the use of this control law completely determines the other control law as:

$$\tilde{T}_1(s) = G_1^{-1}(s)\Theta_2^* + G_1^{-1}(s)G_D(s)H_D(s)\left(\Theta_2^* - \Theta_2\right) \qquad [81]$$

The slow control design used in Scenario B differs from Scenario A. Instead of using a root locus, the closed loop poles of the θ_2-θ_2^* error dynamics were placed. The slow control design chosen placed all five poles on the real axis at $-\lambda$. The form of $H_D(s)$ was chosen as the same form as in [49]. To achieve this, the controller parameter values were $b= 5\lambda$, $m_0= \lambda/40$, and

$$m_1 = \sqrt{\frac{1}{64} + \frac{1}{10}} \qquad [82]$$

The parameter $1/\lambda$ represents the time constant of the error dynamics. However, in order to place the poles in this manner λ was found to be related to w by

$$\lambda = \frac{w}{\sqrt{60}} \qquad [83]$$

Thus, the time scale separation was fixed at approximately 7.75 and could not be adjusted as in Scenario A without redesigning the slow control. Consequently, the time scale separation was explicitly stated but for a given fast dynamics speed w, the slow (error) dynamics were much slower (at least twice as slow as Scenario A slow dynamics). This caused the time response for Scenario B to be much worse than the other methods. With a better slow control design this method would perform about as well as Scenario A deformation

shaping. A lesson learned from this is that the slow control design greatly influences the deformation shaping performance.

The controls resulting from the design can be rewritten as

$$T_1 = T_{1fast} + \frac{I_1 I_2}{k_2}\left(\frac{d^2}{dt^2}\left(\dddot{\Theta}_2^* + c_5\ddot{\Theta}_2^*\right) + 40\lambda^3\left(\dot{\Theta}_2 - \dot{\Theta}_2^*\right)\right)$$
$$+\frac{I_1 I_2}{k_2}\left\{40\lambda^3\left((c_5+m_1+b)\left(\Theta_2 - \Theta_2^*\right) + y_4 + y_5\right)\right\} \qquad [84]$$

$$T_D = (I_1+I_2+I_T)\left\{\frac{d^2}{dt^2}\left(\frac{\dddot{\Theta}_2^*}{10\lambda^3} + \Theta_2^*\right) + 4\lambda\left(\dot{\Theta}_2 - \dot{\Theta}_2^*\right)\right\}$$
$$4\lambda(I_1+I_2+I_T)\left\{c_0\left(\dot{\Theta}_2 - \dot{\Theta}_2^*\right) + y_6\right\} \qquad [85]$$

where y_4, y_5, and y_6 are found from solving

$$\dot{y}_4 = -by_4 + c_6\left(\Theta_2 - \Theta_2^*\right) \qquad [86]$$

$$\ddot{y}_5 = -10\lambda^2 y_5 + c_7\left(\dot{\Theta}_2 - \dot{\Theta}_2^*\right) + c_8\left(\Theta_2 - \Theta_2^*\right) \qquad [87]$$

$$\dot{y}_6 = -by_6 + c_1\left(\Theta_2 - \Theta_2^*\right) \qquad [88]$$

and c_1, c_2, c_5, c_6, c_7 and c_8 are functions of various system parameters as detailed in Appendix B. These controls result in a non-minimum phase controller with one zero at $+.233\lambda$.

IV. Simulation

4.1 Simulation Details

The simulation was done on a CDC mainframe computer system. A simulation package called Eclectic Simulation Package (ESP), developed at The Aerospace Corporation, was used. Various ESP commands were converted by the ESP precompiler into Fortran V source code, and then executed. The dynamics were all simulated in state space form with integration performed by a Runge-Kutta Fourth Order fixed step algorithm. The fixed time step used was .001 seconds. The output was produced on an IBM 3820 printer. An example listing of the Fortran V program is listed in Appendix C.

4.2 Results for Scenario A Deformation Shaping

The single deformation shaping case is examined with two types of commanded trajectories θ_2^*. These are

$$\theta_2^* = A(1 - e^{-t/\tau}) \qquad [89]$$

$$\theta_2^* = B\sin(wt) \qquad [90]$$

The commanded trajectories θ_T^* are usually equal to θ_2^*, and A=.087, B=.043, τ=.5, w=2π unless otherwise specified. The variable t is time in seconds, A and B are amplitudes in radians, τ is a time constant in seconds, and w is frequency in rad/sec.

Both the slow and fast control bandwidth can be varied by the choice for σ, the damped natural frequency of the fast dynamics. The

slow control bandwidth can be adjusted through a parameter K, a gain in the slow controller. This K also affects the time scale separation.

The system response and performance varied greatly depending on what bandwidth was chosen. The "low" bandwidth case was for $\sigma = \pi$, with K values of 4 and 7. The "high" bandwidth case was with $\sigma = 3\pi$, with K =100 or K = 200. The K = 4 and K = 100 runs represent time scale separations of about a factor of three; i.e. the fast dynamics are three times as fast as the error dynamics. The K = 7 and K = 200 cases represent the fast dynamics being about twice as fast as the error dynamics.

For an exponential command trajectory as defined above for θ_2^* and θ_T^*, comparisons can be made between different controller bandwidths and different time scale separations for the runs summarized in Table 2. It is evident that the required control effort (peak torque) increases dramatically for a controller bandwidth increase. However, when the time scales are more widely separated, the maximum torque increase is not quite as dramatic. Comparing these torque outputs with the constraints from figure 3, one notices that the high BW controllers require too much torque for the lab (the high BW three times separation case might be possible, but it is pushing the limit of actuator capabilities).

Table 2

Maximum Actual Output Torque

for Exponential Commanded Trajectory

Torque	2X time scaling		3X time scaling	
	Low BW	High BW	Low BW	High BW
T_D	2.1 Nm	24 Nm	1.4 Nm	9 Nm
T_1	5.2 Nm	115 Nm	2.1 Nm	11.5 Nm

Notes

1. Low bandwidth controller uses $\sigma = \pi$
2. High bandwidth controller uses $\sigma = 3\pi$
3. For 2X time scale separation, K=4 (low BW), K=100 (high BW)
4. For 3X time scale separation, K=7 (low BW), K=100 (high BW)
5. All initial conditions equal to zero

Similar runs were made for the sinusoidal commanded trajectory and the control torques are summarized in Table 3. As before, the required control effort was dramatically larger for the higher BW controllers, and required too much torque given the limits of the lab equipment.

Table 3

Actual Output Torque (Nm)

For Sinusoidal Commanded Trajectory

Control	2X time scaling		3X time scaling	
	Low BW	High BW	Low BW	High BW
T_D(max)	3.5 Nm	40 Nm	3.25 Nm	16 Nm
T_D(after transient)	3 Nm	3 Nm	3 Nm	3 Nm
T_1(max)	5 Nm	190 Nm	4 Nm	45 Nm
T_1(after transient)	2.5 Nm	2.5 Nm	2.5 Nm	2.5 Nm

Notes

1. $\sigma=\pi$ for low BW control
2. $\sigma=3\pi$ for high BW control
3. For 2X time scale separation K=4 (low BW), K=100 (high BW)
4. For 3X time scale separation K=7 (low BW), K=200 (high BW)
5. All initial conditions equal to zero

The higher BW controllers cost a lot more control effort, but they gave a faster response, as expected. The approximate 2% settling times for the exponential and sinusoidal commanded trajectories were

Table 4

Deformation Shaping

Time Response

Case	2% Settling time (sec)
low BW, 2X sep.	2
high BW, 2X sep.	0.5
low BW, 3X sep.	4
high BW, 3X sep.	1.5

One reason the response times are longer for the larger separation cases is that the fast dynamics are the same for both time separations, so a larger separation means slower error dynamics. The time response benefits of a higher BW control are evident, but then so are the control effort costs.

The deformation shapes are shown in figures 7 and 8 for the exponential and sinusoidal commanded trajectories, respectively. Both are for $\sigma=3.6\pi$,K=7, $c_D=\pi$, and zero initial conditions. Notice that the deformations never die out for the sinusoidal case, but instead make Θ_2 follow the commanded trajectory.

Figure 7

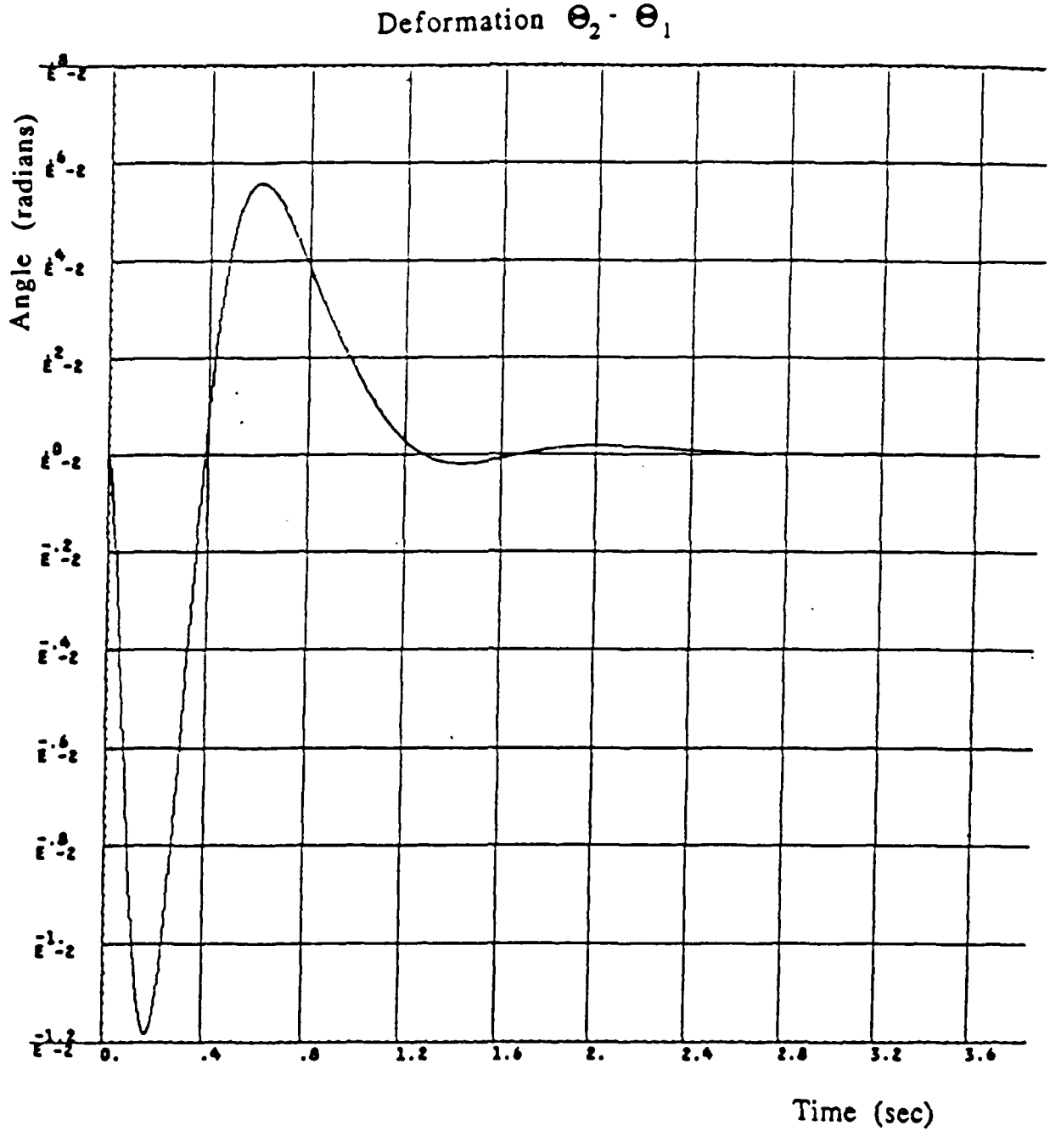
Deformation $\Theta_2 - \Theta_1$
Angle (radians)
0.
.4
.8
1.2
1.6
2.
2.4
2.8
3.2
3.6
Time (sec)

Figure 8

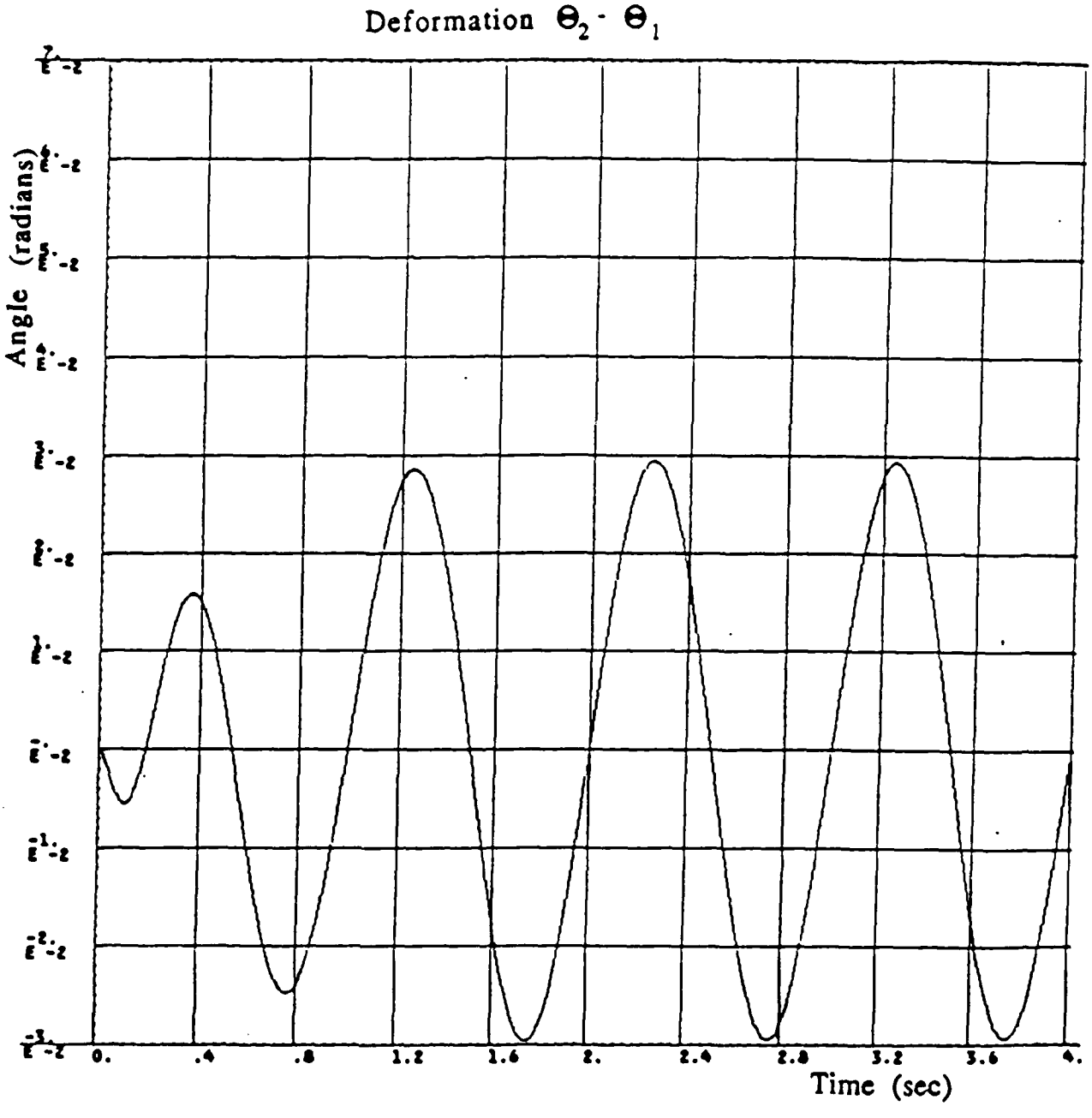
Deformation $\Theta_2 - \Theta_1$
Angle (radians)
0.
.4
.8
1.2
1.6
2.
2.4
2.8
3.2
3.6
4.
Time (sec)

The effect of nonzero initial conditions upon the control was examined. In general, the initial conditions could help or hinder the controller to a significant degree. An example is the case with $\sigma=3.6\pi$, K=7, $c_D=\pi$, an exponential commanded trajectory, and initial condition $\theta_1(0)=.021$. Some of the response characteristics are contained in Table 5.

Table 5

Initial Condition Effect on Response

Category	Response without initial conditions	Response with initial conditions
T_1 (max)	5.2 Nm	1.5 Nm
T_D(max)	2.1 Nm	1.5 Nm
2% settling time	2 seconds	1.5 seconds
Largest $\lvert\theta_1 - \theta_T\rvert$	.035 radians	.115 radians
Max error ($\theta_2 - \theta_2^*$)	.023 radians	.011 radians

This initial condition actually helped the response (for the most part) in this case. However, the $|\theta_1-\theta_T|$ stroke constraint was violated when the initial condition was added. The initial condition caused an increase in the maximum $|\theta_1-\theta_T|$ about four times larger than the case with no initial condition. The solution was to speed up the bottom controller (T_D) to $C_D=3\pi$, reducing the maximum $|\theta_1-\theta_T|$ to .024 radians while raising the required T_D to only 2 Nm. However, it was made evident that an initial condition could have an unexpectedly larger effect upon the performance.

Parameter sensitivity was given only a cursory examination. The effect on the response was observed when the estimated value for I_2 differed from the actual value for I_2. As expected, the response was not as good. The results are summarized in Table 6 for the case of K=4, $\sigma=3.6\pi$, zero initial conditions, and sinusoidal commanded trajectory for θ_2^* and θ_T^*.

The error between the commanded and actual trajectories increased a greater percentage than the error in the parameter estimation, so the controls are relatively sensitive to parameter variations(at least for I_2). The parameter I_2 affects the slow control mainly as a gain. Thus, as long as there is sufficient gain margin in the slow control design the control is stable. However, the feed forward terms using I_2 cause a persistent error for the sinusoidal trajectory. (The correct steady state value is achieved for the exponential trajectory due to the integral part of the control).

Various other parameters may have greater or lesser effects. For example, if the estimate for k_1 varies from the actual value, the

decoupling control terms do not completely decouple the systems, and correction might be required. The parameter sensitivities need to be explored in much greater depth.

Table 6

Effect of Parameter Estimation Error upon Performance

Category	$I_{2act} = I_{2est}$	$I_{2act} = 1.2I_{2est}$	$I_{2act} = .8I_{2est}$
T_I (max)	3 Nm	3 Nm	2.3 Nm
T_D (max)	3.25 Nm	3.8 Nm	3 Nm
Error "after" transient	0	.012 (28%)	.014 (33%)

Next, the effect of sensor noise was studied. Gaussian white noise excitations were added with standard deviations of 1% and 5% of the input signal. The case used was the exponential commanded trajectory for θ_2^* and θ_T^*, $\sigma=3.6\pi$, K=4, and initial condition $\theta_1(0)=.021$. The error $\theta_2-\theta_2^*$ is shown for the two noise levels of 1% and 5% respectively in figures 9 and 10. It is evident that the response is fairly good, the maximum torque magnitudes are still about the same, and the $|\theta_1-\theta_T|$ response was not pronounceably increased. The performance for the depicted runs is summarized in Table 7.

Figure 9

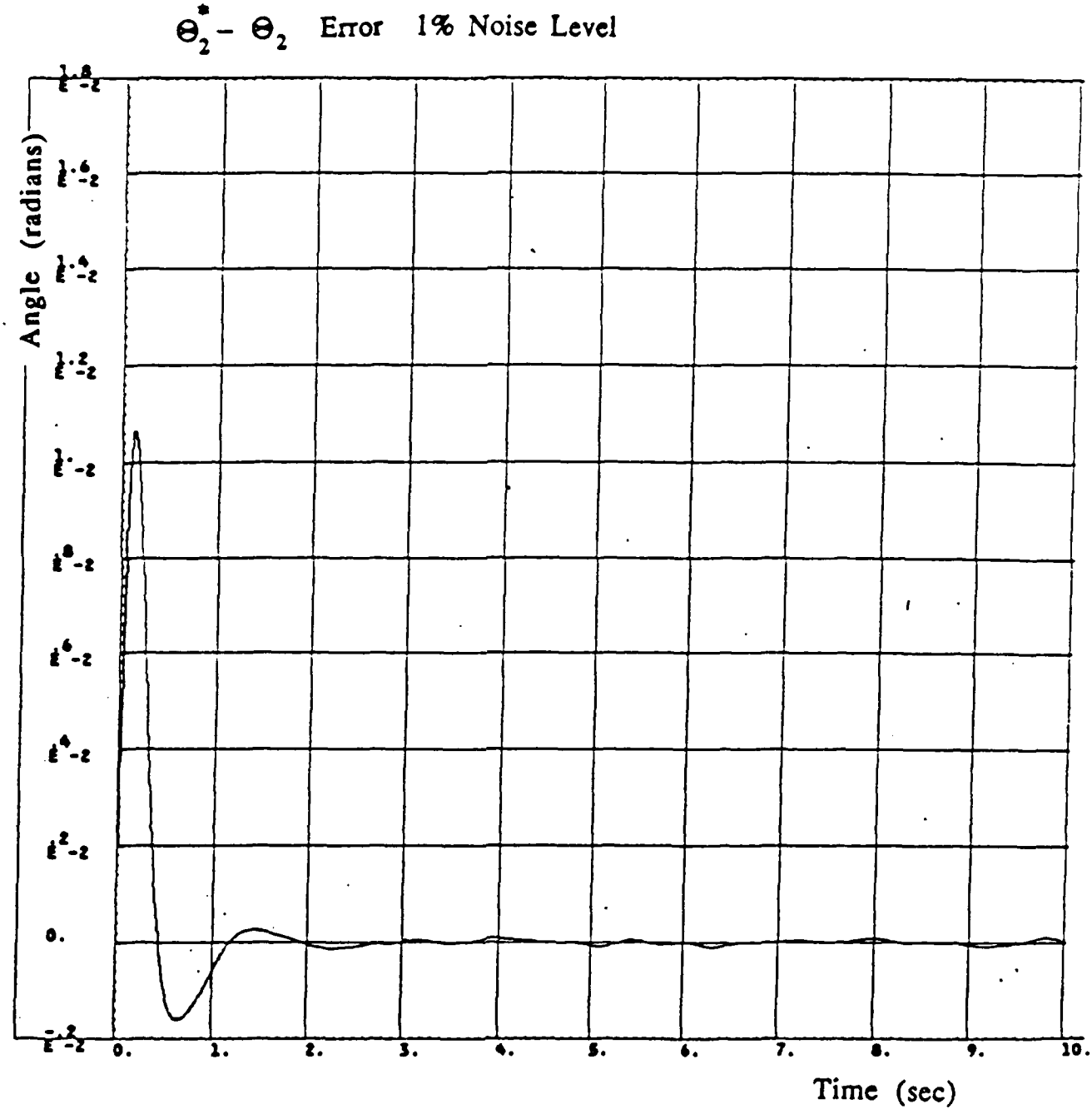
$\Theta_2^* - \Theta_2$ Error 1% Noise Level
Angle (radians)
Time (sec)
0.
1.
2.
3.
4.
5.
6.
7.
8.
9.
10.

Figure 10

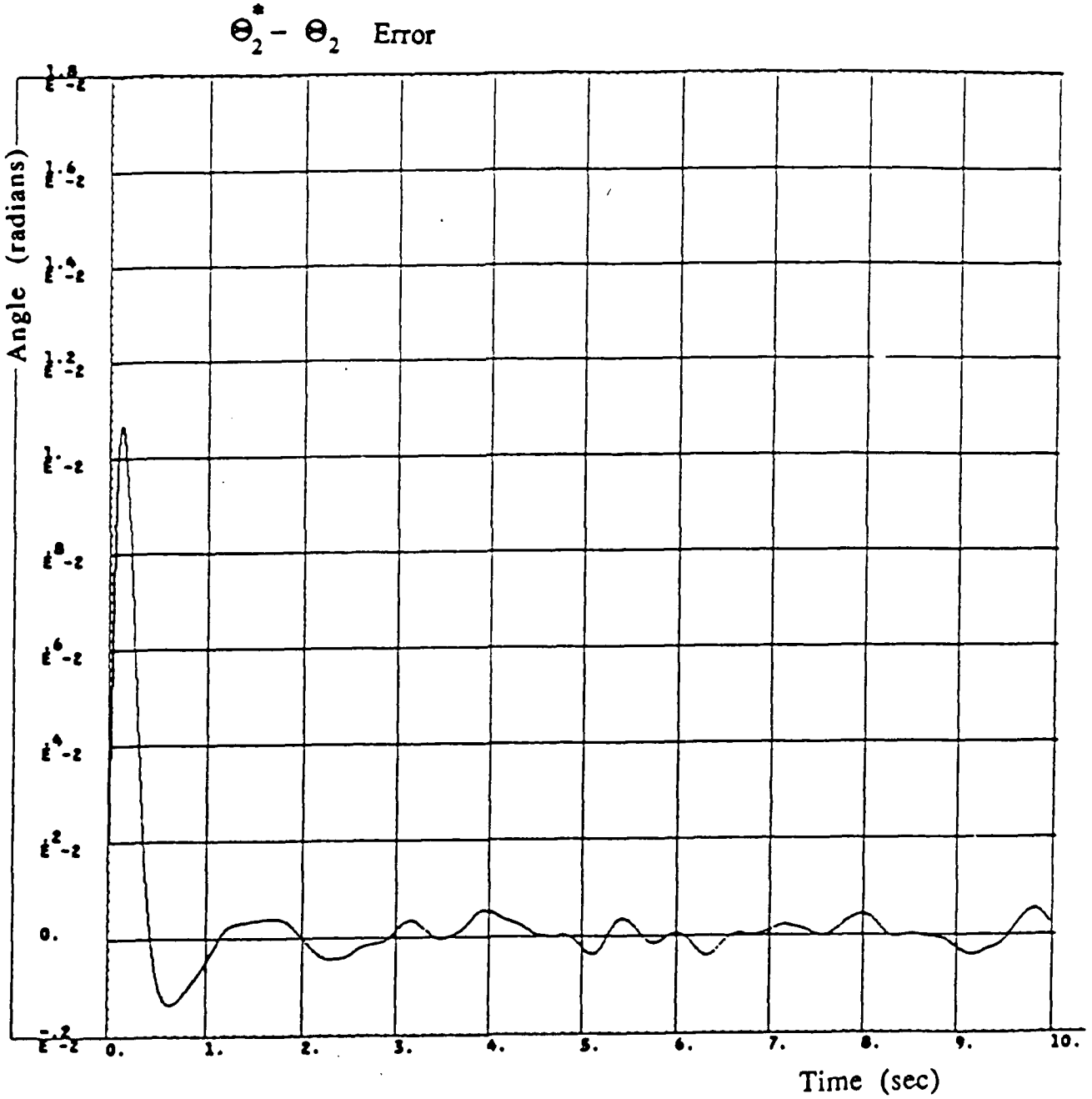
$\Theta_2^* - \Theta_2$ Error
Angle (radians)
1.8E-2
1.6E-2
1.4E-2
1.2E-2
1.E-2
8.E-3
6.E-3
4.E-3
2.E-3
0.
-.2E-2
0.
1.
2.
3.
4.
5.
6.
7.
8.
9.
10.
Time (sec)

Table 7

Effect of Noise upon Performance

Quantity	No Noise	With Noise (σ = 1%)	With Noise (σ = 5%)
T_1 (max)	2.1 Nm	1.5 Nm	1.8 Nm
T_D (max)	1.4 Nm	1.5 Nm	1.5 Nm
Error "after" transient	0	.25 %	.6 %
2% "Settling" Time	1.5 sec	1 sec	1 sec
$\lvert\theta_1 - \theta_T\rvert$ max	.11 rad	.115 rad	.12 rad

Note: The variable σ in the table is the standard deviation of the noise

4.3 Results for Scenario B Deformation Shaping

The deformation shaping Scenario B performance was worse than Scenario A in most respects. Again, this was due to the slow control design, and not any intrinsic flaws of the method. The performance is summarized in Table 8.

Table 8

Scenario B Deformation Shaping

Performance Summary

Category	Low BW	High BW
T_L (max)	11 Nm	5 Nm
T_D ("after" transient)	7 Nm	3 Nm
T_1 (max)	35 Nm	50 Nm
T_1 ("after" transient)	1.5 Nm	1.5 Nm
2% settling time	15 sec	6 sec

These results were with a sinusoidal commanded trajectory. The low bandwidth control used $w=3.1\pi$, and the high bandwidth control used $w=7.75\pi$.

For Scenario B, increasing the dynamics "speed" did not increase the torque cost nearly as much as in Scenario A. The control for T_D actually decreased for the higher BW case. However, this was because the control T_1 for the lower BW case could not keep up with the commanded trajectory as well as the higher BW case, and needed more help from T_D.

V. Comparison of Deformation Shaping with Other Methods

5.1 Introduction to Comparisons

Various other methods of control design were used to obtain solutions for the problem. Most of these solutions, however, used all three controllers while the deformation shaping solutions used only two controllers.

Since the slow control design for Scenario B adversely affected the performance, all comparisons will be made with the deformation shaping solution of Scenario A.

5.2 Deformation Shaping vs. Rigidifying Control

The rigidifying control is detailed in Appendix D. It was examined with the same fast control speed constraints as the deformation shaping control. The rigidifying control low BW case had $w=3.6\pi$, $\lambda=\pi$ and the high BW case had $w=10.8\pi$, $\lambda=3\pi$. The rigidifying control time scale separation was chosen as three for both cases. This is compared to the deformation shaping case with a time scale separation of three.

The maximum torques required are presented in Table 9 for the case with no initial conditions and exponential commanded trajectories.

Table 9

Deformation Shaping vs. Rigidifying

Performance Comparison

Category	Deformation Shaping		Deformation Suppression	
	Low BW	High BW	Low BW	High BW
T_D (max)	1.4 Nm	9 Nm	1.3 Nm	3.3 Nm
T_1 (max)	2.1 Nm	11.5 Nm	18 Nm	6.5 Nm
T_2 (max)	0 Nm	0 Nm	.5 Nm	1.5 Nm
2% settling time	4 sec	1.5 sec	2.5 sec	.5 sec

The required torques for the low BW are very similar, and the settling time isn't even twice as large. The higher BW controllers show more difference in required torques and settling times. However, considering that the deformation shaping is using only two controls while the rigidifying is using all three, the deformation shaping is doing an adequate job of retaining the performance of the rigidifying control. The responses for sinusoidal commanded trajectories also display this trend.

5.3 Deformation Shaping vs. PID Control

A design for PID control was made so that the error dynamics would be no faster than the deformation shaping fast dynamics. The PID control using all three actuators, whose design is detailed in Appendix E, is compared to the deformation shaping control. If the top actuator failed or was unavailable, a stable PID control using the bottom two actuators could not be found. A comparison of the controls for the exponential and sinusoidal commanded trajectories is made in Table 10.

The PID control outperformed the deformation shaping for the exponential commanded trajectory in terms of response time, but it did not do as well for the sinusoidal commanded trajectory. Even though the deformation shaping used only two controls, instead of three, it was able to beat the PID control in this case.

Table 10

Deformation Shaping vs. PID

Performance Comparison

Category	Exponential Trajectory		Sinusoidal Trajectory	
	Deformation Shaping	PID	Deformation Shaping	PID
T_2 (max)	0	3 Nm	0	4.6 Nm
T_1 (max)	5 Nm	40 Nm	3.25 Nm	16 Nm
T_D (max)	3 Nm	3 Nm	3 Nm	3 Nm
2% Settling Time	2 sec	.4 sec	2 sec	-
$\Theta_2 - \Theta_2^*$ error "after" transient	0	$\sim$0	0	.0025 (3%)

5.4 Deformation Shaping vs. LQR Control

Deformation shaping is compared with a "modern" control in the form of an LQR design. The LQR control was designed to have approximately the same maximum required torque magnitudes as the deformation shaping, so the responses could be compared. The LQR design is detailed in Appendix F.

The LQR control performance was comparabl to the deformation shaping control performance.

Table 11

Deformation Shaping vs. LQR Performance Comparison

Category	Deformation Shaping	LQR
T_1 (max)	5.2 Nm	9 Nm
T_D(max)	2.1 Nm	3.5 Nm
2% settling time	2 seconds	1.6 seconds

Table 11 compares the LQR design with the deformation shaping case with $\sigma=3.6\pi$ and K=7 for the exponential commanded trajectory. The LQR design was selected to have comparable control torques, and the required settling time was then found comparable. However, deformation shaping has an advantage, although it didn't apply in

this problem. An LQR design requires full state feedback (feedback of all dynamic state variables) for every control torque, whereas deformation shaping does not require this in general. Only the torques with a fast control component, such as T_1, may require full state feedback (but do not have to). The other torques almost always do not.

5.5 Summary of Comparisons of Results

After comparing the various methods, several observations can be made. In general, it seems that deformation shaping, using only two controls in this problem, can achieve performance about equal to that by PID or LQR methods using all three controls. The price paid for this capability is the need for feed forward of higher derivatives of the commanded trajectory. A summary of the advantages and disadvantages of the various control solutions is presented in figure 11.

Figure 11

Summary of Advantages and Disadvantages

Control	Advantages	Disadvantages
Deformation Shaping	Can get response and required torques nearly same as other methods, but using only 2 controls	Complex, requires feedfoward of commanded higher derivatives
Deformation Suppression	Makes a flexible structure act as a rigid one	Need all 3 actuators
PID	Well understood, simple	Limited capabilities, need all 3 actuators
LQR	"Modern" control, optimal in some sense	Full order compensator control structure needed in general

VI. Future Work

Many unanswered questions remain to be investigated. One unknown is the effect of disturbances to the fast dynamics discussed in 3.5. Also, alternative methods of introducing the fast control are possible, such as introducing the fast control after the slow control has been found. Another question is whether deformation shaping can be used for tracking targets, since it requires higher derivatives of the desired trajectory. A technique of real time interpolation of bearings only data to generate higher rates used in robotics is found in [Ref. 7] , and might be useful. The sensitivities to parameter variations need to be explored. Finally, various schemes, such as treating the slow manifold as a sliding surface for Variable Structure Control, might be added and tested for an increase in the robustness of the control, albeit at the cost of higher required bandwidth.

VII. Conclusions

The deformation shaping method was able to solve the problem using only two controllers instead of all three. It was able to achieve exactly the correct trajectory for the ideal case. The need for a good slow control design was revealed by the Scenario B results. Initial conditions affected only the transient response levels, while the response time remained the same. Parameter estimation error was found to have a significant impact on the response accuracy, and should be investigated further. Sensor noise, on the other hand, had little effect on the accuracy.

The various comparisons with the other methods confirmed that deformation shaping with only two controllers could perform almost as well as the other methods using all three actuators. The price for this capability was the need for higher derivatives of the commanded trajectory, and higher complexity.

The various advantages of deformation shaping make it a method deserving further study.

Actuator Dynamics

The actuators for T_1 and T_2 are standard permanent magnet DC motors and can be found to have the following transfer function [Ref. 8].

$$\frac{K_T R J s}{R J \tau_m s^2 + J s + K_T K_B} \qquad [A.1]$$

The parameters are summarized in table A.1

Table A.1

Actuator Parameter Values

Quantity	Definition	Value for T_1	Value for T_2
R	Coil Resistance	8.76 Ω	2.3 Ω
K_T	Force Constant	3 lb_f /A	.39 lb_f ft/A
τ_m	Electrical Time Constant	4.56 ms	6 ms
J	Inertia or Mass	141 g	.03 lb in sec^2
K_B	Back EMF Constant	3.7 V/ft/sec	.53 V/rad/sec

The actuator dynamics for T_D are not as simple. The dynamics are the result of a complex internal hardware controller. From experimental data, an approximate transfer function was found for it.

$$\frac{20\pi s}{s^2 + 20\pi s + 100\pi^2} \qquad [A.2]$$

Compensation was performed on the motors for two reasons. First, it was desired to have a steady state input command cause a steady state torque output instead of a steady state velocity output. Secondly, certain BW values were needed for the actuators in order for the model to be reasonable.

Through the use of the following integral feedback scheme,

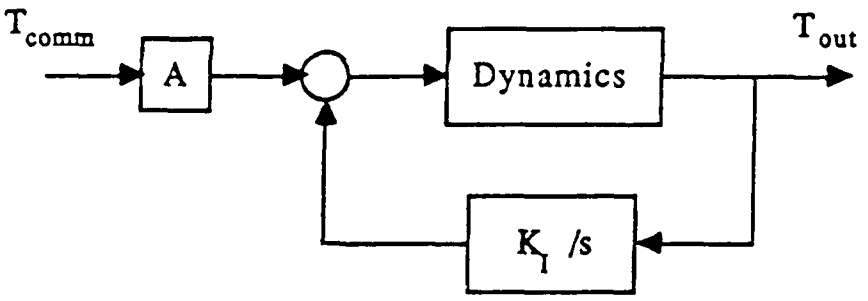

with K_{I1}=11, K_{I2}=6, A_1=12 and A_2=7 the compensated actuator dynamics were achieved. It was also assumed that it was possible to compensate the T_D actuator to its given form [1]. The resulting actuator BW levels were 1.5 Hz for T_D, 30 Hz for T_1, and 8.5 Hz for T_2.

Appendix B

Evaluation of Constants c_i

The constants c_0 to c_8 arise when the controls are rewritten from a transfer function form to a state space form. In general, they are the result of synthetic division and/or partial fraction expansions of the various terms. The constants used in scenario a will be evaluated first, then those from scenario B.

The constants c_0 and c_1 come directly from synthetic division of [47].

$$c_0 = m_1 - b \qquad [B.1]$$

$$c_1 = m_0 - b(m_1 - b) \qquad [B.2]$$

These terms show up in many of the following expressions.

The terms c_2, c_3, and c_4 arise from the partial fraction expansions of the various terms. Intermediate temporary expressions t_1, t_2, and t_3 are used to make the expressions less cumbersome.

$$c_2 = \frac{t_2 - a_1(2\sigma^2 + 2\sigma b) - \left(\frac{t_3}{b} - 2a_1\sigma^2 - b(t_1 - a_1(2\sigma + b))\right)}{\left(2\sigma - \frac{2\sigma^2}{b} - b\right)} \qquad [B.3]$$

$$c_3 = t_1 - a_1(2\sigma + b) - c_2 - I_1 c_1 \qquad [B.4]$$

$$c_4 = \frac{t_3 - 2a_1 b\sigma^2 - 2t_1\sigma^2}{b} \qquad [B.5]$$

where

$$t_1 = a_1 m_1 + a_0 k_1 \qquad [B.6]$$

$$t_2 = a_1 m_0 + m_1(a_0 + k_1) \qquad [B.7]$$

$$t_3 = m_0(a_0 + k_1) \qquad [B.8]$$

The new constants introduced in Scenario B were c_5, c_6, c_7, and c_8. The values for c_0 and c_1 were as above. The constant for c_5 was merely a convenient definition.

$$c_5 = -20\sqrt{60}\,\lambda \qquad [B.9]$$

The others again come from partial fraction expansion and are defined using intermediate expressions for simplicity.

$$c_6 = (bt_4 - bt_5 + t_6) \qquad [B.10]$$

$$c_7 = t_4 - c_6 \qquad [B.11]$$

$$c_8 = -bt_4 + t_5 + bc_6 \qquad [B.12]$$

where

$$t_4 = c_0c_5 + c_1 - 10\lambda^2 \qquad [B.13]$$

$$t_5 = m_0c_5 - 10\lambda^2(m_1 + c_5) \qquad [B.14]$$

$$t_6 = -10b\lambda^2(c_0 + c_5) \qquad [B.15]$$

Appendix C

Program Listing

```
      PROGRAM MAIN(TAPE11, TAPE12, INPUT=TAPE12, OUTPUT)
      EXTERNAL DERIVS,ESPRK4 ,INRKPC
      CALL ESPII(DERIVS,ESPRK4 ,INRKPC )
      END
      SUBROUTINE CONTROL(TS4,TS3,TS2,TS1,TS,Y,TC1,TC2,TD)
      REAL TS4,TS3,TS2,TS1,TS,TC1,TC2,TD,SIG,LAM,A1,A0,K,K1,K2
      REAL M1,M0,B,I1,I2,IT,CD
      REAL Y(100)
      LOGICAL FLAG
      COMMON/THETATS/TTS,TTS1,TTS2
      COMMON/PARAM/SIG,LAM,A1,A0,K,K1,K2,M1,M0,B,I1,I2,IT,CD,AAA,BBB,CCC
      COMMON/FLAGS/FLAG
C
      Y20 = Y(20)
      Y8 = Y(8)
      TC2 = 0.0
      TFAST = A1*Y(6) + A0*Y(5) - A1*Y(4) - A0*Y(3)
      TC1=TFAST+(I1*I2/K2)*(TS4 + 2.0*SIG*TS3 + 2.0*SIG*SIG*TS2)
     1 + (I1*I2*K/K2)*(TS1 - Y(6) + (M1-B)*(TS - Y(5)) + Y8)
     2 + K1*(Y(5) - Y(1))
      TD = (IT*TTS2 + 2.0*IT*CD*(TTS1-Y(2)) + IT*CD*CD*(TTS-Y(1))) -
     1 ( (K*I2/K2)*(A1*(TS-Y(5))+Y20+Y(18))+(I2/K2)*(A1*TS3+(K1+A0)*
     2 TS2)+(-I1*I2*K/K2)*((TS1-Y(6))+(M1-B)*(TS-Y(5))+Y8)
     3 - (I1*I2/K2)*(TS4+2.*SIG*TS3+2.*SIG*SIG*TS2) )
      RETURN
      END
      SUBROUTINE ICCOMP (T,Y)
      DIMENSION Y(100),PAR(100)
      COMMON/SWTCHS/SWTCH(50),SWMEM(50,4),MAXSWS,MAXMEM,NEVENT
      COMMON/PARS/PAR
      REAL SIG,LAM,A1,A0,K,K1,K2,M1,M0,B,I1,I2,IT
      COMMON/PARAM/SIG,LAM,A1,A0,K,K1,K2,M1,M0,B,I1,I2,IT,CD,AAA,BBB,CCC
      COMMON/STPCON/HP,H,FIXSTP,HMIN,HMAX
C
      FIXSTP = 0.001
      LAM = 3.1415927
      CD = 3.1415927
      I1 = 1.627
      I2 = 0.863
      IT = 0.417
      K1=2.27
      K2 = 49.8
      SIG = 0.5*(7.2361)*LAM
      A0 = 2.0*SIG*SIG*I1 - K1 - (I1+I2)*K2/I2
      A1 = 2.0*SIG*I1
      K = 4.*355.92/49.8*K2/(I1*I2)
```

```
      M1=SIG
      M0 = SIG*SIG/4.
      B = SIG
      C1 = A1*M1+A0+K1
      C2 = A1*M0+M1*(A0+K1)
      C3 = M0*(A0+K1)
      AAA = ( C2 - A1*(2.*SIG*SIG+2.*SIG*B) - (C3/B-2.*A1*SIG*SIG)
     1 -B*(C1-A1*(2.*SIG+B)) )/( 2.*SIG-2.*SIG*SIG/B-B)
      BBB = C1 - A1*(2.*SIG+B) - AAA
      CCC = (C3-2.*A1*SIG*SIG*B-2.*SIG*SIG*AAA)/B
      Y(3) = 0.021
      RETURN
      END
      SUBROUTINE DERIVS(T,Y,DY,STOP)
      DIMENSION Y(100), DY(100), PAR(100)
      COMMON/SWTCHS/SWTCH(50),SWMEM(50,4),MAXSWS,MAXMEM,NEVENT
      COMMON/PARS/PAR
      REAL SIG,LAM,A1,A0,K,K1,K2,M1,M0,B,I1,I2,IT
      REAL K11,K12,K21,K22,KI1,KI2,AK,AA,KK,KA
      REAL CD,TTS2,TTS1,TTS
      LOGICAL FLAG
      COMMON/PARAM/SIG,LAM,A1,A0,K,K1,K2,M1,M0,B,I1,I2,IT,CD,AAA,BBB,CCC
      COMMON/TOOUT/TS,TS1,TS2,TS3,TS4,TC1,TC2,TD
      COMMON/THETATS/TTS,TTS1,TTS2
      COMMON/STPCON/HP,H,FIXSTP,HMIN,HMAX
      COMMON/FLAGS/FLAG
      DATA KK,K11,K21,AK,KI1/219.3,219.3,27137.0,20.127,6.47/
      DATA KA,K12,K22,AA,KI2/166.67,166.67,5991.4,7.0,6.0/
      DATA FLAG/.FALSE./
      DATA PI/3.1415927/
      DATA CONST,TAU,TAUD/0.087,.5,.5/
C
      TTS = CONST*(1.0 - EXP(-T/TAUD))
      TTS1 = (CONST/TAUD)*EXP(-T/TAUD)
      TTS2 = -(CONST/(TAUD*TAUD))*EXP(-T/TAUD)
      TS = CONST*(1.0 - EXP(-T/TAU))
      TS1 = (CONST/TAU)*EXP(-T/TAU)
      TS2 = -(CONST/(TAU*TAU))*EXP(-T/TAU)
      TS3 = (CONST/(TAU**3.0))*EXP(-T/TAU)
      TS4 = -(CONST/(TAU**4.0))*EXP(-T/TAU)
```

```
C      TS = TS1 = TS2 = 0.0
C      TS3 = TS4 = 0.0
C
C
       CALL CONTROL(TS4,TS3,TS2,TS1,TS,Y,TC1,TC2,TD)
C
       ERROR = TS - Y(5)
C
       DY(1) = Y(2)
       DY(2) = (1.0/IT)*(TD - TC1 - K1*Y(1) + K1*Y(3))
       DY(3) = Y(4)
       DY(4) = (1.0/I1)*(TC1 - TC2 - K2*(Y(3)-Y(5)) - K1*(Y(3)-Y(1)))
       DY(5) = Y(6)
       DY(6) = (1.0/I2)*(TC2 - K2*(Y(5) - Y(3)))
       DY(7) = -B*Y(7) + K*TS2 + K*M1*TS1 + K*M0*TS
       DY(8) = -B*Y(8) + (M0 - B*M1 + B*B)*(ERROR)
C ***** ACTUATOR INTEGRATORS ******
       DY(9) = Y(10)
       DY(10) = -K11*Y(10) - (K21 + KI1*KK)*Y(9) + AK*KK*KI1*TC1
       DY(11) = Y(12)
       DY(12) = -K12*Y(12) - (K22 + KI2*KA)*Y(11) + AA*KA*KI2*TC2
       DY(13) = Y(14)
       DY(14) = -20.0*PI*Y(14) - (10.0*PI)**2.0*Y(13) +(10.0*PI)**2.0*TD
       DY(15) = Y(16)
       DY(16) = -2.*SIG*Y(16)-2.*SIG*SIG*Y(15)+BBB* TS1 + CCC*TS
       DY(17) = (-B)*Y(17) + AAA*TS
       DY(18) = Y(19)
       DY(19)=-2.*SIG*Y(19)-2.*SIG*SIG*Y(18)+BBB*(TS1-Y(6))+CCC*(ERROR)
       DY(20) = -B*Y(20) + (AAA - I1*(M0 - B*M1 + B*B))*ERROR
       DY(21) = (-B)*Y(21)+(M0-B*(M1-B))*TS
       DY(22) = (-B)*Y(22)+(M0-B*(M1-B))*Y(5)
       DY(15)=DY(16)=DY(17)=0.
       DY(21)=DY(22)=0.
C
       RETURN
       END
       SUBROUTINE SWINPT(VALUES,T,Y)
       DIMENSION VALUES(50), Y(100), PAR(100)
       COMMON/SWTCHS/SWTCH(50),SWMEM(50,4),MAXSWS,MAXMEM,NEVENT
       COMMON/PARS/PAR
       RETURN
       END
       SUBROUTINE SWMEMN(VALUES, T, Y)
       DIMENSION VALUES(50), Y(100), PAR(100)
       COMMON/SWTCHS/SWTCH(50),SWMEM(50,4),MAXSWS,MAXMEM,NEVENT
       COMMON/PARS/PAR
       RETURN
       END
```

```
1440        SUBROUTINE OUTPUT(T,Y,DY,PLOT,PRINT,STOP)
1450        DIMENSION Y(100), PAR(100), PLOT(100), PRINT(60), DY(100)
1460        COMMON/SWTCHS/SWTCH(50),SWMEM(50,4),MAXSWS,MAXMEM,NEVENT
1470        COMMON/PARS/PAR
1480        REAL TS,TS1,TS2,TS3,TS4,TC1,TC2,TD
1490        COMMON/TOOUT/TS,TS1,TS2,TS3,TS4,TC1,TC2,TD
1500        COMMON/THETATS/TTS,TTS1,TTS2
1510        DATA IAN/1/
1520 C
1530        IF(IAN .EQ. 1)THEN
1540          IAN = 0
1550          CALL ANALYZE(T,Y)
1560        ENDIF
1570 C
1580        PRINT( 1)=PLOT(1)=T
1590        PRINT( 2)=PLOT(2)=TS-Y(5)
1600        PRINT( 3)=PLOT(3)=TS1
1610        PRINT( 4)=PLOT(4)=TC1
1620        PRINT( 5)=PLOT(5)=TC2
1630        PRINT( 6)=PLOT(6)=TD
1640        PRINT( 7)=PLOT(7)=Y(1)
1650        PRINT( 8)=PLOT(8)=Y(3)
1660        PRINT( 9)=PLOT(9)=Y(5)
1670        PRINT(10)=PLOT(10)=Y(9)
1680        PRINT(11)=PLOT(11)=Y(11)
1690        PRINT(12)=PLOT(12)=Y(13)
1700        PRINT(13)=PLOT(13)=Y(7)
1710        PRINT(14)=PLOT(14)=Y(8)
1720        PRINT(15)=PLOT(15)=Y(18)
1730        PRINT(16)=PLOT(16)=Y(20)
1740        PRINT(17)=PLOT(17)=TS
1750        PRINT(18)=PLOT(18)=TTS
1760        PRINT(19)=PLOT(19)=Y(5)-Y(3)
1770        PRINT(20)=PLOT(20)=Y(3)-Y(1)
1780        RETURN
1790        END
```

Appendix D

Rigidifying Control Design

The rigidifying or deformation suppression case is just a special case of deformation shaping. It makes the flexible structure behave as a rigid body after the fast dynamics die out. The slow manifold in this case is called the rigid body manifold. Recall the equations resulting from the singular perturbation expansions [38] to [41]. Using these equations, slow controls can be designed similar to what was previously done for the deformation shaping case. The resulting torques are:

$$T_2 = I_2\{\ddot{\theta}^*_2 + 2\lambda(\dot{\theta}^*_2 - \dot{\theta}_2) + \lambda^2(\theta^*_2 - \theta_2)\} \qquad [D.1]$$

$$\tilde{T}_1 = (I_1 + I_2)\{\ddot{\theta}^*_2 + 2\lambda(\dot{\theta}^*_2 - \theta_2) + \lambda^2(\theta^*_2 - \theta_2)\} + k_1(\theta_2 - \theta_T) \qquad [D.2]$$

$$T_1 = \tilde{T}_1 + \{[w^2 I_1 - (k_1\frac{(I_1 + I_2)}{I_2}k_2)](\theta_2 - \theta_1) + 2wI_1(\dot{\theta}_2 - \dot{\theta}_1)\} \qquad [C.3]$$

$$T_D = I_T\{\ddot{\theta}^*_T + 2\mu(\dot{\theta}^*_T - \dot{\theta}_T) + \mu^2(\theta^*_T - \theta_T)\} + (I_1 + I_2)\{\ddot{\theta}^*_2 + 2\lambda(\dot{\theta}^*_2 - \theta_2) + \lambda^2(\theta^*_2 - \theta_2)\} \qquad [D.4]$$

where $1/\lambda$ is the time constant of the θ_2^*-θ_2 error dynamics, $1/\mu$ is the time constant of the θ_T^*-θ_T error dynamics, and $1/w$ is the time constant of the critically damped fast dynamics. Unlike the deformation shaping control, the time scale separation between λ and w can be chosen.

Appendix E

PID Control Design

The PID controller for T_2 was designed to make the angle error from the desired trajectory go to zero. The bottom two controllers were designed to make the angle between the two adjacent bodies go to zero. The controllers for these actuators were designed to treat the bodies above them as a single rigid body. Thus, the T_1 controller treated the pointing mirror and optical bench as one body with inertia I_1+I_2. The T_D controller was designed treating the body as entirely rigid with inertia $I_T+I_1+I_2$.

The resulting parameter gains were:

$$K_{ID}=K_{I1}=K_{I2}=500 \qquad [E.1]$$

$$K_{PD}=K_{P1}=K_{P2}=100 \qquad [E.2]$$

$$K_{DD}=K_{D1}=K_{D2}=5 \qquad [E.3]$$

Of course, a better design is possible, but this one worked well for the given problem.

A similar design using only T_1 and T_D worked adequately for the exponential trajectory, but could not be stabilized for the sinusoidal trajectory. The best that could be achieved with the PID control would be marginally stable.

Appendix F

LQR Control Design

The LQR design was done with the following costs.

Cost for use of T_2 =	1000
Cost for use of T_1 =	1
Cost for use of T_D =	.01
Cost for error in Θ_2 =	10
Cost for error in Θ_1 =	1
Cost for error in Θ_T =	5

These gave reasonable torque levels for the resulting controls, which were of the form:

$$T_2 = K_{2DD}\left(\dot{\Theta}_T - \dot{\Theta}_T^*\right) + K_{2D}\left(\Theta_T - \Theta_T^*\right) + K_{21D}\left(\dot{\Theta}_1 - \dot{\Theta}_1^*\right) + K_{21}\left(\Theta_1 - \Theta_1^*\right) + K_{22D}\left(\dot{\Theta}_2 - \dot{\Theta}_2^*\right) + K_{22}\left(\Theta_2 - \Theta_2^*\right) \quad [E.1]$$

$$T_1 = K_{1DD}\left(\dot{\Theta}_T - \dot{\Theta}_T^*\right) + K_{1D}\left(\Theta_T - \Theta_T^*\right) + K_{11D}\left(\dot{\Theta}_1 - \dot{\Theta}_1^*\right) + K_{11}\left(\Theta_1 - \Theta_1^*\right) + K_{12D}\left(\dot{\Theta}_2 - \dot{\Theta}_2^*\right) + K_{12}\left(\Theta_2 - \Theta_2^*\right) \quad [E.2]$$

$$T_D = K_{DDD}\left(\dot{\Theta}_T - \dot{\Theta}_T^*\right) + K_{DD}\left(\Theta_T - \Theta_T^*\right) + K_{D1D}\left(\dot{\Theta}_1 - \dot{\Theta}_1^*\right) + K_{D1}\left(\Theta_1 - \Theta_1^*\right) + K_{D2D}\left(\dot{\Theta}_2 - \dot{\Theta}_2^*\right) + K_{D2}\left(\Theta_2 - \Theta_2^*\right) \quad [E.3]$$

The values used for Θ_1^* and its derivative were identical to those of Θ_2^* and its derivative. The values for Θ_T^* were given as in Scenario

A. The resulting feedback gains were:

For T_2:	K_{2DD} = 6.5E-05	K_{2D} = 3.9E-03
	K_{21D} = 3.8E-03	K_{21} = .14
	K_{22D} = .03	K_{22} = .096
For T_1:	K_{1DD} = -1.92	K_{1D} = -4.19
	K_{11D} = 31.7	K_{11} = 325
	K_{12D} = 35.8	K_{12} = -44.3
For T_D:	K_{DDD} = 8.43	K_{DD} = 89.7
	K_{D1D} = 25.4	K_{D1} = 183
	K_{D2D} = 14.85	K_{D2} = -43.5

References

[1] J.L. Junkins and J.D. Turner, *Optimal Spacecraft Rotational Maneuvers*, Amsterdam: Elsevier, 1986

[2] P.V. Kokotovic and H. Khalil, Eds., *Singular Perturbations in Systems and Control*. New York: IEEE Press, 1986

[3] M.W. Spong, K. Khorasani, P.V. Kokotovic, "An Integral Manifold Approach to the Feeddback Control of Flexible Joint Robots", *IEEE Journal of Robotics and Automation*, vol. RA-3, August 1987, pp. 291-300

[4] Conversation with Bruce Gardner of The Aerospace Corporation, El Segundo, CA, 6/29/88

[5] V.A. Sobolev, "Integral Manifolds and Decomposition of Singularly Perturbed Systems", *System Control Letters*, vol. 5, pp. 1169-1179, 1984

[6] T.A.W. Dwyer, III , "Slew Induced Deformation Shaping", Proc. *27th IEEE Conference on Decision and Control*, Austin, TX, Dec. 7-9, 1988

[7] P.K. Khosla and T. Kanada, "An Algorithm to Estimate Manipulator Dynamics Parameters", *Int. Journal of Robotics and Automation*, , v. 2, no. 3, 1987, pp. 127-135

[8] B.C. Kuo, *Automatic Control Systems* (Fifth Edition), Englewood Cliffs, NJ: Prentice Hall, 1986